DEVELOPMENT OF ARTIFICIAL CELL CULTURE PLATFORMS USING MICROFLUIDICS

By
HANDE KARAMAHMUTOĞLU

Submitted to the Graduate School of Engineering and Natural Sciences
in partial fulfillment of the requirements for the degree of Master of Science

Sabanci University
July 2019

DEVELOPMENT OF ARTIFICIAL CELL CULTURE PLATFORMS USING MICROFLUIDICS

APPROVED BY

Assoc. Prof. Dr. Meltem Elitaş ..... (Thesis Supervisor)

Assist. Prof. Dr. Murat Kaya Yapıcı .....

Assoc. Prof. Dr. Ali Özhan Aytekin .....

DATE OF APPROVAL: .....

ABSTRACT

DEVELOPMENT OF ARTIFICIAL CELL CULTURE PLATFORMS USING MICROFLUIDICS

HANDE KARAMAHMUTOGLU

Mechatronics Engineering, MSc, Thesis, July 2019

Thesis Supervisor: Assoc. Prof. Dr. Meltem Elitas

Key Words: Cell Culture, Cancer, Microfluidics, Lab-on-a-chip and Single-cell resolution.

Acquiring quantitative data about cells, cell-cell interactions and cellular responses to surrounding environments are crucial for medical diagnostics, treatment and cell biology research. Nowadays, this is possible through microfluidic cell culture platforms. These devices, lab-on-a-chip (LOC), are capable of culturing cells with the feature of mimicking in vivo cellular conditions. Through the control of fluids in small volumes, LOC closely mimics the nature of cells in the tissues compared to conventional cell culturing platforms such as flasks and cell culture plates. On the other hand, existing LOC-based cell culturing platforms are highly complicated to be used in clinics or laboratories without an expert who develops these microfluidic platforms.

Therefore, in this thesis we developed simple and user-friendly microfluidic cell culturing platforms and compared our obtained data with the conventional methods. We performed our research on different human cancer cell lines including liver hepatocellular carcinoma, breast adenocarcinoma, and lymphoma cell lines; both monocytes and monocyte-differentiated macrophages. We examined proliferation rate, morphological and phenotypical differences of the cells in different scales. In addition to cell culturing platform, we developed a microfluidic gradient generator to precisely titrate the concentration of chemicals and observed cellular responses to these stresses. Moreover, we quantitatively inspected the effect of different intravenous fluids on different human cancer cell lines.

Finally, we have developed simple, low-cost and integrable microfluidic platforms, those can be used by untrained people, and perform cell culture experiments in a population at single-cell resolution. Our microfluidic cell culture platforms provide more quantitative and qualitative data compared to traditional batch culture assays.

ÖZET

MIKROAKISKALARIN KULLANIMI ILE YAPAY HÜCRE KÜLTÜRÜ PLATFORMLARININ GELISTIRILMESI

HANDE KARAMAHMUTOĞLU

Mekatronik Mühendisliği Yüksek Lisans Tezi, Temmuz 2019

Tez danışmanı: Dr. Meltem Elitaş

Anahtar Kelimeler: Hücre kültürü, Kanser, Mikro akışkanlar, Çip üstü laboratuvar ve Tek hücre çözünürlüğü

Hücreler, hücre-hücre etkileşimleri ve hücrelerin etraflarını saran ortama verdikleri tepkilerle ilgili nicel bilgi elde etmek, medikal tanı, tedavi ve hücre biyolojisi araştırmaları için oldukça önemlidir. Günümüzde bu mikro akışkan hücre platformları aracılığıyla mümkündür. Bu cihazlar, çip-üstü-laboratuvar (ÇÜL), *in vivo* hücre koşullarını taklit etme özelliği ile hücre kültür etme uygulamaları için kullanılmaktadırlar. Sıvıların küçük hacimlerde kontrolü ile ÇÜL teknolojileri, kültür flask ve şişeleri gibi geleneksel hücre kültür platformlarına kıyasla dokulardaki hücrelerin doğasını yakın bir şekilde taklit ederler. Diğer taraftan var olan ÇÜL tabanlı hücre kültür platformları bu mikroakışkan platformları geliştiren bir uzman olmadan kliniklerde ve laboratuvarlarda kullanılmak için çok karmaşıktır.

Dolayısıyla, bu tezde basit ve kullanıcı dostu mikro akışkan hücre kültür cihazları geliştirdik ve elde ettiğimiz verileri geleneksel metotlar ile kıyasladık. Araştırmamızı karaciğer hepatosellüler karsinom, göğüs adenokarsinom ve lenfoma hücre hatları, monosit ve monositlerden türetilmiş makrofajların ikisini de içeren farklı insan hücre hatları üzerinde gerçekleştirdik. Farklı ölçeklerde hücrelerin çoğalma oranı, morfolojik ve fenotipik farklılıklarını inceledik. Hücre kültür platformuna ek olarak kimyasalların konsantrasyonlarını tam olarak titre etmek için bir mikroakışkan gradyan üretici geliştirdik ve bu streslere verilen hücresel tepkileri gözlemledik. Bundan başka farklı intravenöz sıvıların farklı insan kanser hücre hatlarına olan etkisini nicel olarak inceledik.

Son olarak, eğitilmemiş insanlar tarafından kullanılabilecek olan, basit, düşük maliyetli ve entegre edilebilir mikroakışkan platformlar geliştirdik ve bir popülasyonda tek hücre çözünürlüğünde hücre kültürü deneyleri yaptık. Bizim mikroakışkan hücre kültürü platformlarımız konvansiyonel yöntemlerle yapılan hücre kültürü deneylerine göre daha nicel ve niteliksel veri sağlıyor.

"Do you know what's one mistake we always make? Believing that life's immutable, that once you get on a particular track you have to follow it to the end of the line. But it appears that fate has more imagination than we do. Just when you think you're in a situation you can't escape from, when you've reached the lowest depts of total desperation, everything changes as fast as a gust of wind, everything's overturned; from one second to the next you find you're living a new life."

-Susanna Tamaro

For my beloved mother, Belgin Karamahmutoğlu, father, Bulent Karamahmutoğlu, sister, Elif Çakırlı…

Canım annem, babam ve ablama…

ACKNOWLEDGEMENTS

First of all, I would like to thank and express my sincere gratitude to my thesis advisor, Dr Meltem Elitas. Meeting Dr. Elitas is one of the biggest milestones in my life. After asking about my dreams, she noticed my interest in research and invited me to work in her lab. Ever since that day, she has been a very big inspiration to me. With remarkable support, feedbacks and time she has given to me even before my master studies, I improved noticeably throughout my journey to become a professional academician. My love and respect for her as an idealist, helpful and hardworking professor, dedicating her time for research and caring for her students will always continue.

Besides my advisor, I would like to thank to my jury members, Dr. Murat Kaya Yapıcı and Dr. Ali Özhan Aytekin, for their insight, constructive feedback and valuable time.

My sincere thanks also go to our collaborators, Dr. Tamer Yagci, Dr. Devrim Gozuacik, Dr. Nazim Serdar Turhal, PhD Yunus Akkoc for sharing their equipment, valuable ideas, experience and time, and especially PhD Metin Cetin for always making himself available to help me.

I thank my family, for always believing in and supporting me. My mother, my hero, who encouraged me to learn new things and improve myself not only in school studies but as a human being as well. My father who has shown me how being brave can unlock many roads in life and encouraged me to be more daring in life to follow my dreams. My dear sister, growing up she has been my idol in so many ways, telling me baldly to take better care of myself and not to forget allocating time for the joys of life other than work. And my dear nephew, for bringing happiness to my life and reminding me the importance of imagination.

My lifelong and sincere thanks go to beloved and deeply missed Elvan Kartal Sarı, for all her love and support. I felt acknowledged for my hard work and more motivated to pursue my goals in life thanks to her. She will always be in my heart. May she rest in peace.

I thank to my dear colleagues and friends; Zain Fuad (karaoke buddy), Yagmur Yildizhan (partner in crime and more), Ekin Yagis (confidant) and Buse Bulut (sister) for being there for me in good times and bad times. I will always be grateful for our time together. Also, I thank to Hilal Senuysal, Dogukan Kaygusuz, Sumeyra Vural for all their love and support. Enver Ersen, Ege Can Onal, Yusuf Altun, Fatih Emre Tosun, Mohammed Taleb Zamzam, Zaeema Khan, Sahl Sadeghi, Abdolali Khalili Sadaghiani and all other members and friends of our Biomechatronics family for all the fun. Maria Orlenco, my first assistant as an intern for all the hard work she did during our time together in lab. Likewise, Alara Altay and Umut Gogebakan for sacrificing their eyes for analysis. Elif Taskin for being my jogging buddy. Eray Kurt, the King, for always caring and making me laugh.

Last but not the least, I would like to thank all my besties, especially the dreamer gang for making life outside of work fun as well.

TABLE OF CONTENTS

LIST OF FIGURES

LIST OF TABLES

Chapter 1

INTRODUCTION

1.1 Motivation

Cell culture *in vitro* is essential, for both understanding of cell biology and medical diagnosis and treatment [1]. Through the investigation of cellular behavior in a controlled *in vitro* environment, providing proper media and gas along with appropriate temperature for cell growth and reproduction, experiments can be done with reduced cost and labor in comparison to tissue culture and animal experiments [2]. Thus, for establishing this controlled environment several cell culturing platforms are being used including macroscopic polystyrene dishes, flasks or wells. However, petri dishes and well plates as traditional cell culturing platforms are limited to cell analysis on a population level [3]. Recent studies showed alteration in cell behavior even if cells are identical and in the same microenvironment [4]. Therefore, there is a need to examine large number of cells on a single-cell resolution in a microfluidic environment to have a better insight in cellular function. Conventional cell culturing tools are not adequate for this purpose. To establish a controlled microenvironment and to be able to perform single-cell level analysis, 2D microfluidic cell culturing platforms have been introduced and used [5].

Quantification and accuracy of analyzed data from these platforms are also very important [6]. Therefore, for the microfluidic cell culturing platforms, Polydimethylsiloxane (PDMS), an optically transparent material used for molding that is nontoxic, biocompatible, gas permeable and, thermally and chemically stable, is preferred to obtain data with microscopy imaging from microfluidic chips [7]. Moreover, PDMS based microfluidic chips for cell culture allows researchers to analyze cells as individuals and as cell populations at single-cell resolution depending on their chip designs and experimental protocols [8]. Nevertheless, these platforms are mostly too complex and not adaptable for different applications. Also, 2-dimensional (2D) cell culture platforms are not representative of real cell environment. In this manner, 3-dimensional (3D) cell cultures, introduced by Ross Granville Harrison with the hanging drop method from bacteriology to carry out the first tissue culture increased the interest in 3D cell cultures started to rise due to their potential in drug development since they are considered more realistic compared to 2D cell culturing platforms [9]. Still, most of the 3D culture technologies are costly, bulky and require too much time and effort, therefore, they are still at their crawling period for drug development screening and research. Furthermore, compared to 2D cell culture platforms, imaging and analysis is harder due to their complexity. On the other hand, 2D cell culture systems are less expensive than most systems and they are easier to analyze [10].

As a result, 2D microfluidic cell culturing platforms are preferred more for cell biology research today. They provide laminar flow and large surface-to area-to-volume (SAV) ratio. Various aspects of the cellular microenvironment could be engineered in a precisely controlled manner, creating a cell microenvironment in a controllable and reproducible fashion to test biological questions [11].

1.2 Contributions of the Thesis

This thesis aims to create and test alternative cell culturing platforms that are adaptable, simple and integrable for different purposes including cell analysis in single-cell resolution and under different microenvironments. We propose two microfluidic platforms; one of them aims cell culturing and second one generates gradients of drugs. In these artificial devices breast cancer cells were grown. Then, culturing platforms were connected to a microfluidic gradient generator. Next. Sodium dodecyl sulfate **(**SDS), as a drug representative, was flown through the gradient chip, supplying different gradients of SDS to the microfluidic chip with grown cells to mimic drug effect. Thus, a microfluidic cell culturing platform and a microfluidic gradient generator was established for the investigation of drug concentration in personalize medicine *in vitro* allowing cell culturing in flow, live cell imaging and high-throughput analysis. Then, new chip designs were developed for investigating cell behavior and morphology using cancer and immune system cell lines. This thesis presents novel cell culturing platforms to culture cells for personalized medicine, medical diagnostics and cell biology research.

1.3 Thesis Outline

Chapter 2 presents the literature survey about cellular microenvironment, batch culture and microfluidic cell culture platforms. **Chapter 3** introduces artificial cell culturing platforms, experimental procedures and illustrates setups for cell loading and culturing. Preparation of cells, fabrication of microfluidic devices and image acquisition techniques are also explained. In **Chapter 4**, the results of experiments in conventional culturing devices and in artificial cell culturing platforms are demonstrated along with discussions. Finally, thesis is concluded in **Chapter 5** with possible future applications of microfluidic cell culturing platforms.

1.4 Publications

1.4.1 Manuscripts and papers for peer reviewed journals

- **Karamahmutoglu H**, Altay A, Ozkazanc D, Elitas M. (2018) “Quantitative investigation into the influence of intravenous fluids on human immune and cancer cell lines”, Scientific Reports (Under Review).
- Khan, Z.; **Karamahmutoğlu, H.;** Elitaş, M.; Yüce, M.; Budak, H. THROUGH THE LOOKING GLASS: Real-Time Imaging in Brachypodium Roots and Osmotic Stress Analysis. Plants 2019, 8, 14.
- 2017 Elitaş, Meltem and Sadeghi, Sahl and **Karamahmutoğlu, Hande** and Gözüacık, Devrim and Turhal, Nazım Serdar (2017) "Microfabricated platforms to quantitatively investigate cellular behavior under the influence of chemical gradients", *Biomedical Physics and Engineering Express*, Vol.3, No.3 (SCI)

1.4.2 Peer reviewed conference proceedings

- **Hande Karamahmutoglu**, Metin Cetin, Tamer Yagcı, Meltem Elitas, "Behavior of HepG2 liver cancer cells using microfluidic-microscopy: a preliminary study," **Proc. SPIE 10491**, Microfluidics, BioMEMS, and Medical Microsystems XVI, 104910Y (19 February 2018)

Chapter 2

BACKGROUND/THEORY

Microenvironment of a cell is created by factors that directly determine conditions around a cell or a group of cells, such as; cells, interstitial fluid and extracellular matrix (ECM) including tissue-specific proteins and polysaccharides [12] [13] [14]. They physically, mechanically and biomechanically affect cellular phenotype [15]. Also, they can considerably alter cell behavior and fate by manipulating microenvironmental features [16] [17]. For instance, Satyam et al. demonstrated that with macromolecular crowding in the cell microenvironment the secretion of ECM molecules could be developed for corneal fibroblasts [18]. The changes in the microenvironment of cells influence cell proliferation as well. Generation of new cells is important since it is essential for tissue growth and propagation and is considered as one of the hallmarks of cancer (Figure 2.1) [19] [20].

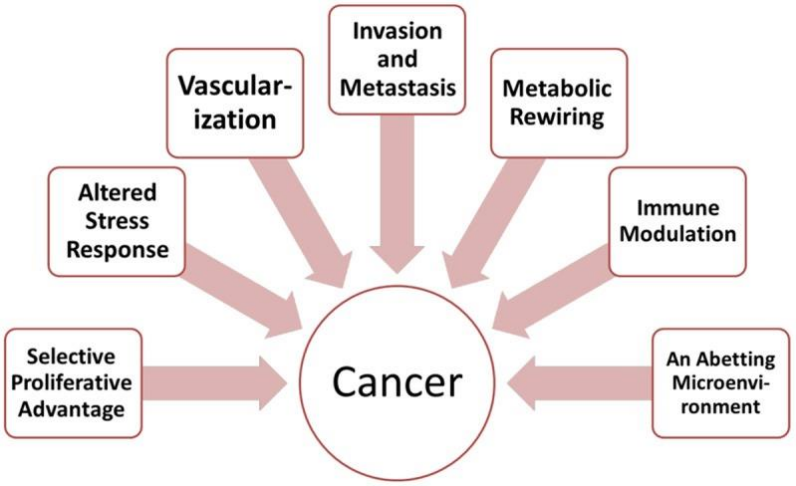

Figure 2.1. The hallmarks of cancer [20].

Surgery, chemotherapy, and radiotherapy have been the most common cancer treatment methods for a long time [21]. These conventional cancer therapies have been considerably beneficial in the elimination of primary tumors. Nevertheless, there is a cancer recurrence issue due to tumor metastases [22]. Furthermore, the number of new cancer cases has become approximately 18.1 million and almost 9.6 million people lost their life due to cancer in 2018 [23]. Thus, new cancer therapies for the eradication of tumor cells have been investigated [24]. Latest research has revealed multiple functions of the tumor microenvironment (TME) in the adjustment of therapeutic efficacy. Even though the effect TME activities have on cancer initiation and metastasis are well known, our insight of the TME's impact on treatment results is still inadequate [25]. Hence, the trend in cancer research has changed from the examination of fatal cancer cells themselves to the investigation of tumor microenvironment and the interactions within [26].

TME consists of resident fibroblasts, endothelial cells, pericytes, leukocytes and extracellular matrix, and causes to the progression of cancer (Figure 2.2.) [27]. It is well established that non-tumor cells are genetically more balanced compared to tumor cells [26] [28]. Therefore, treatments targeting the TME have a very low possibility for generating adaptive mutations and fast metastasis. Still, since cells can both initiate and prevent tumor cell growth, treatments targeting the TME for cancer therapy should be discriminative [26]. Recently, for the investigation of TME, *in vitro* cell culturing techniques are being preferred preliminary for *in vivo* experiments. This is partly because

in vivo tests are very costly and ethical problems due to animal testing [29] [30] [31]. Thus, studies with *in vitro* cell culture models has gained a growing attention [32].

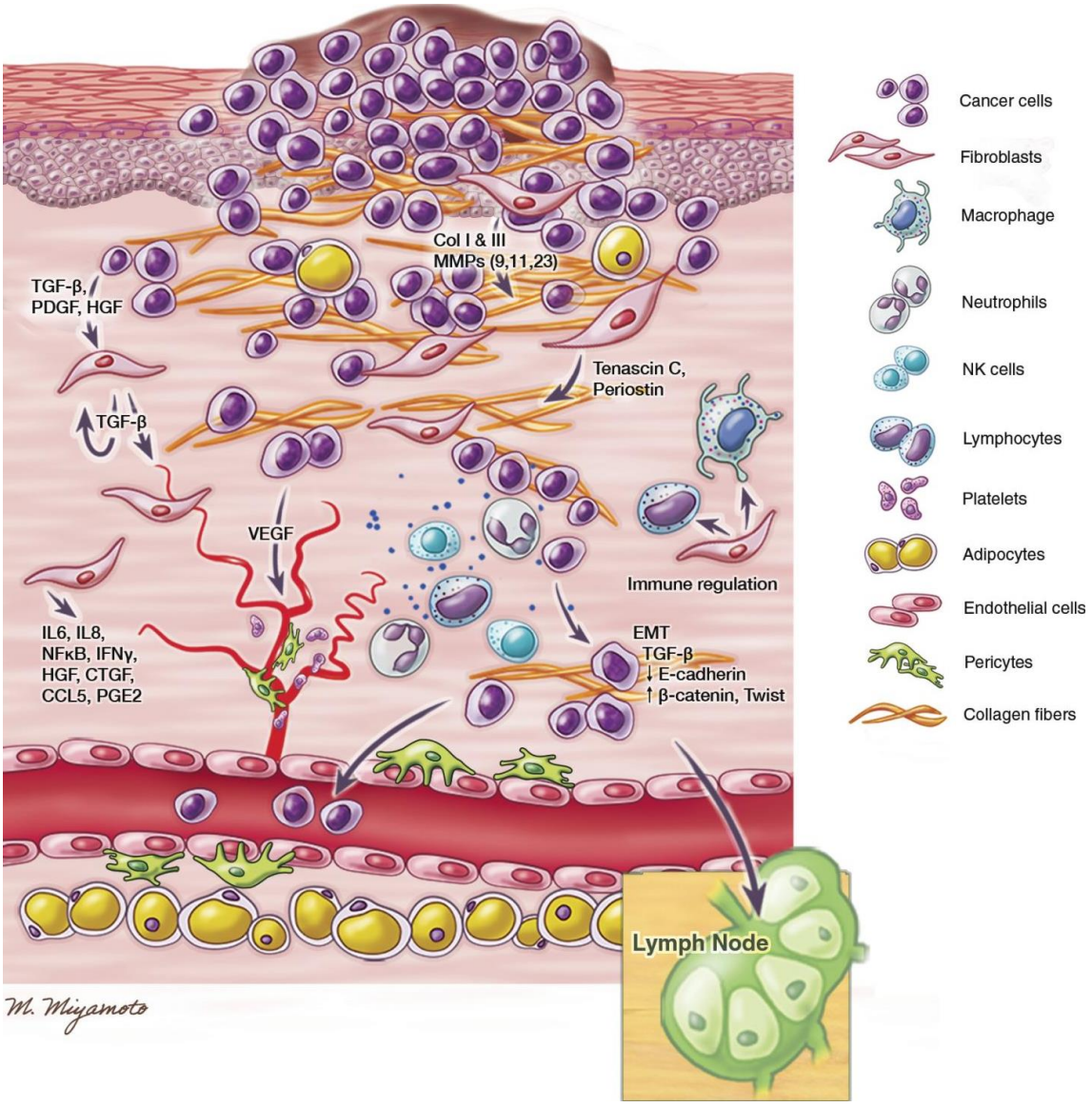

Figure 2.2. Detailed illustration of the tumor microenvironment showing representative cell types, tissues, and signaling factors involved [27].

Conventional cell culture platforms are macroscopic polystyrene dishes, flasks or wells [3]. Using these vessels and novel microfluidic platforms, cells can be cultured *in vitro*. However, researchers accepted failure in reproducibility of their own assays using batch culture and microfluidic cell culture [7] [33]. Different outcomes were obtained after repeating an assay in the same way it was performed before because of the changes

within the cell environment [34]. This inconsistency in conventional and microfluidic platforms is a solvable problem using the right tools [35]. Additionally, in conventional cell culturing platforms cells remain in static condition, yet this is not the case for cells inside human body. This means that the dynamic physiological conditions for cells cannot be monitored in conventional cell culturing vessels with gradients of temperature and CO_2 concentrations that are not optimal [36]. Therefore, it is important to provide sensitive cell culture platforms in which cellular microenvironment can be controlled allowing cell analysis.

Novel *in vitro* cell culturing platforms assists in the examination of various culturing properties that have been investigated with conventional culturing platforms for centuries such as cell proliferation to show drug efficacy in stopping tumor cell proliferation [37]. Investigation of cell proliferation with the likelihood of metastases lead to a better understanding of the influence that culturing elements have on tumor progression [26]. These platforms are microfluidic cell culturing platforms. They allow the manipulation of spatial and temporal gradients and patterns that cannot be obtained and controlled in conventional platforms (Figure 2.3) [38]. Compared to traditional batch culture, microfluidic devices require smaller volumes of materials and thus shorter experiment time due to parallelization and lower cost of assays [39], [40], [41]. Microfluidic cell culture is also proficient for advancing precision medicine focused studies [42]. These works have generated a significant effect on knowledge about cellular activities that is essential in regulating disease features and responses to stimuli [43] [44] [45].

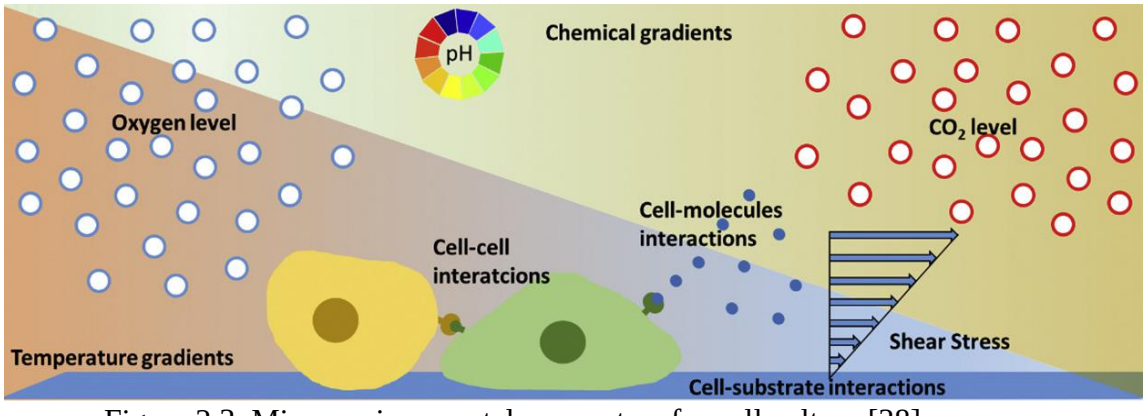

Figure 2.3. Microenvironmental parameters for cell culture [38].

In last decades, through the culturing of cells inside novel microfluidic devices a better insight about the cellular microenvironment was obtained and these platforms were used for various purposes. With the control of the mitotic mechanisms by trapping cells inside a microfluidic platform, it was discovered that the behavior of HeLa cells altered substantially during mitosis due to the entrapment of cells (Figure 2.4). Additionally, researchers observed that new cells produced after the entrapment had different sizes from each other [46] [47]. For trapping nonadherent cells, another microfluidic chip was fabricated in which the immunostaining and labeling of THP-1 cell membranes was shown. This platform allowed cells to be captured without the need for centrifuging and resuspension [48]. In another study, miniaturized fiber-based optical tweezers were used in integration with microfluidic chip for single-cell trapping using red blood cells and colon cancer cells (Figure 2.5). Researchers were able to obtain fluorescence and Raman measurements of single cells [49].

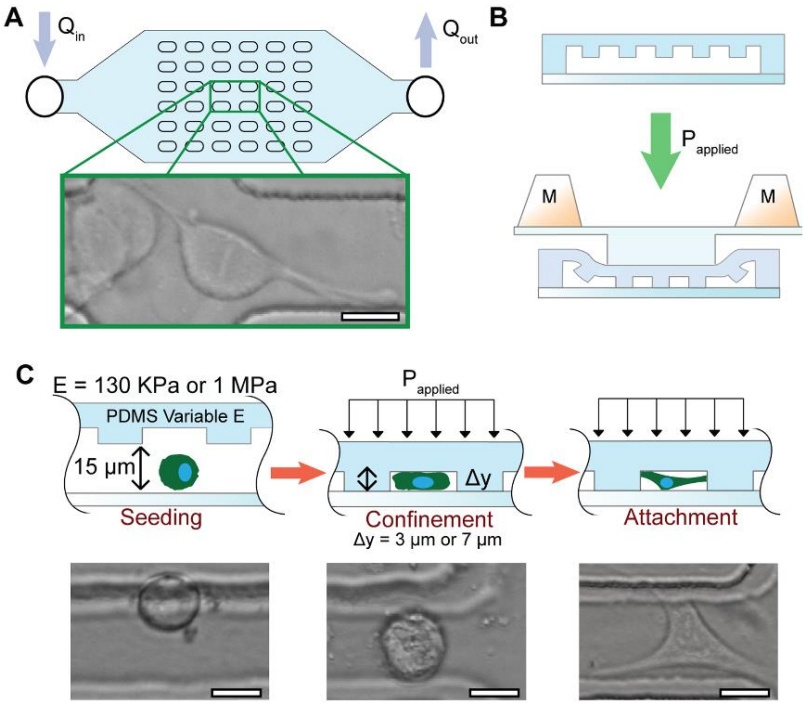

Figure 2.4. The effect of microlevel trapping on the division of HeLa cells. (a) The macroscopic structure of the microfluidic PDMS platform. (b) The cross-section of the microfluidic PDMS platform posts. With the utilization of pressure on the posts, cells can be trapped within the area between the posts. (The distance between the posts is 40 μm). (c) The trapping generated substantial shifts in the behavior of the cells during mitosis and led to the production of new cells with different sizes [46].

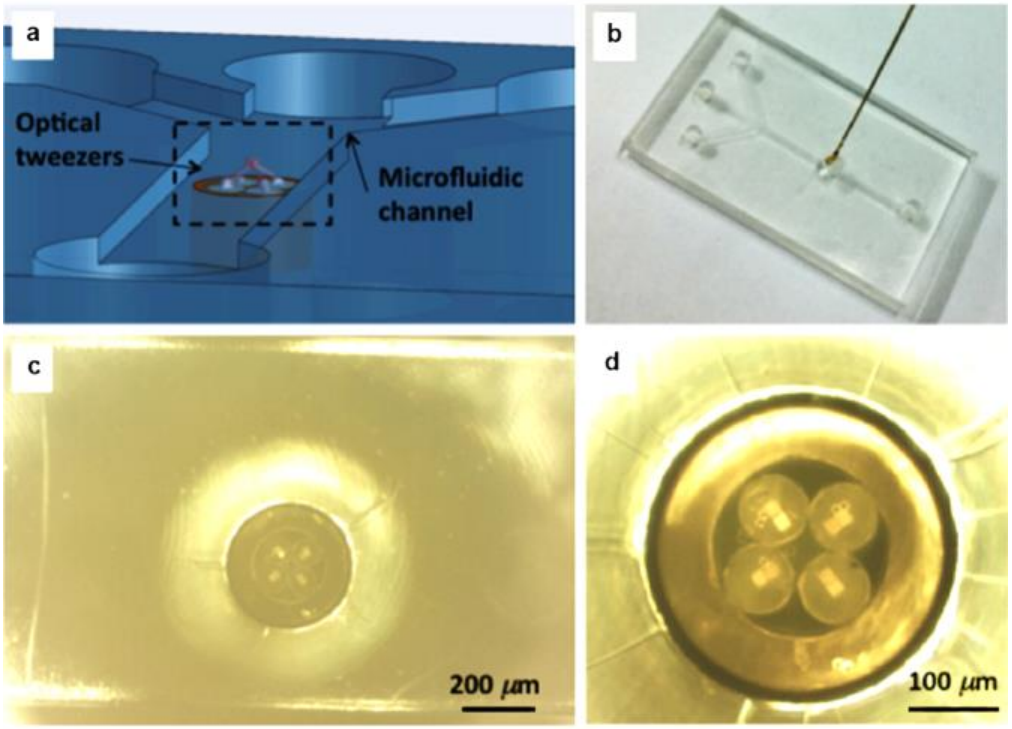

Figure 2.5. Optical micro-tweezer integrated in a microfluidic chip. (a) Isometric view of the optical tweezers integrated in the microfluidic system (b) Top view picture of the device. (c) Enlarged picture of the optical tweezers inside the microfluidic channel (d) Enlarged view of the microprisms on the optical tweezers [49].

There are various microfluidic platforms fabricated for single-cell investigations. For example, Ono *et al.* developed a single-cell and feeder-free culture system for primate pluripotent stem cells. Researchers suggested that monkey embryonic cells cultured in this system can be used for *in vitro* differentiation and gene manipulation [50]. There are various other culturing platforms designed for singe-cell analysis in which cells are isolated, trapped and manipulated in several ways. These isolation and capture methods include droplet-based microfluidics, hydrodynamics, magnetic forces, acoustics, optics and dielectrophoretic traps (Figure 2.6) [51]. For instance, scientists used a droplet-based microfluidic device to separate cells to examine cell growth in a monodisperse nanoliter aqueous droplets surrounded by an immiscible fluorinated oil phase (Figure 2.7). Thus, they were able to obtain high throughput using *Saccharomyces cerevisiae* cells for gene identification [52].

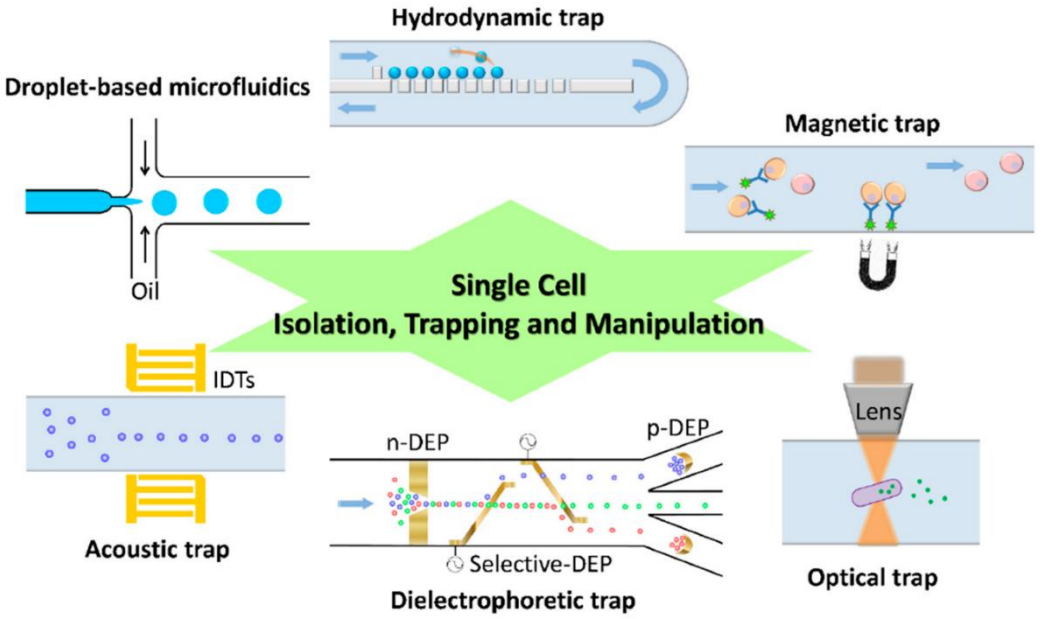

Figure 2.6. Schematic demonstrating various approaches for cell isolation, capture and control of single cells in a microfluidic device [51].

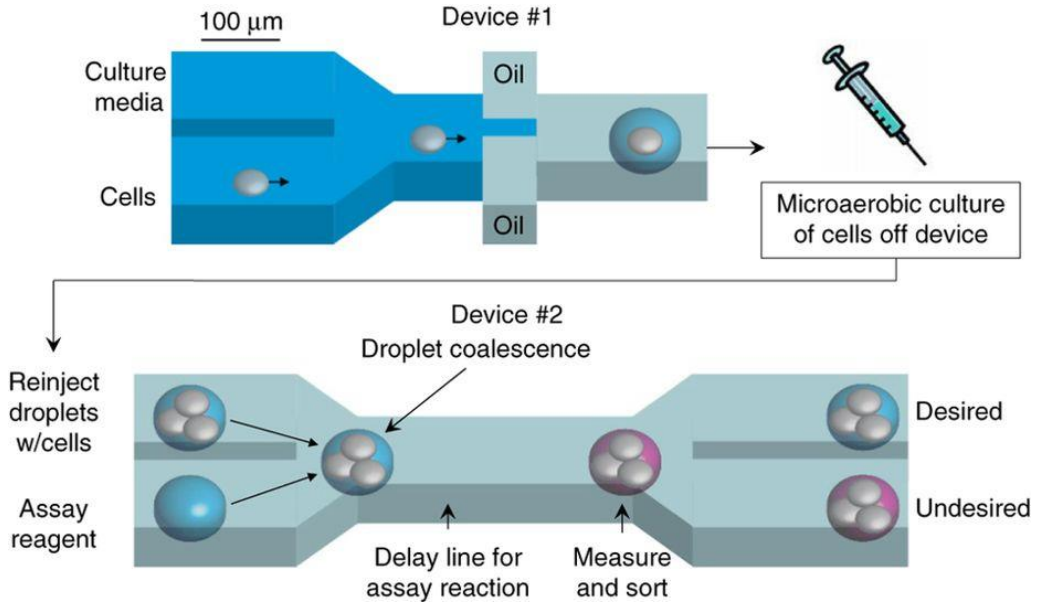

Figure 2.7. Microfluidic high-throughput screening platform. Droplets are obtained through the combination of aqueous stream with two streams including a fluorinated oil and surfactant mixture [52].

Detection of biomarkers is another important application of microfluidic devices. For the detection of biomarkers multiple platforms have been used and tested [53] [54]. Moreover, microfluidic platforms have been used for personalized medicine through drug screening and discovery as well [55] [56]. Figure 2.8 demonstrates a microfluidic chip developed for monitoring of drug screening and cancer research. Scientists used T98G human brain cancer cells inside the microfluidic cell culture platform to investigate cancer cell metabolism [57]. There are a lot of other microfluidic culturing devices used with tumor cells [58] [59], stem cells [60] [61] and other cell types as well [62] [63] [64].

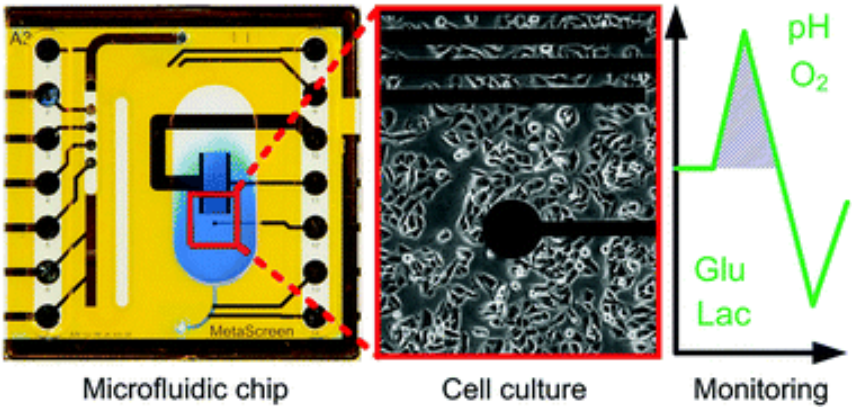

Figure 2.8. A microfluidic chip for monitoring drug screening and cancer research [57].

The cell culture platforms that are mentioned above are mostly 2D cell culturing platforms with short construction time, mimicking the *in vivo* environment. Still, recently some researchers started to suggest the use of 3D cell culturing devices [65]. In 2D microfluidic cell culturing platforms, cell growth occurs on flat surfaces. Cells attach to surface, then start spreading. With 2D culturing chips, cell behaviors can be examined through inexpensive and transparent materials. Also, these systems are expected worldwide. Still these devices have limitations about mimicking culture environment. Because, *in vivo* environment includes cells surrounded by other cells and extracellular matrix (ECM) and 2D cell culture is not enough in mimicking this whole 3D environment. Therefore, cell growth, spreading and migration based research can give misleading results. Yet mostly 2D cell culture outcomes supplies suitable data with *in vivo* studies [66] [38].

Like 2D, establishing a 3D cell culture platform is a rapid process and the homeostasis compatibility of the 3D device with cells provides long-term stability [67]. Nevertheless, despite all advantages 3D culture techniques offer, there are technical problems in microscopy imaging of these devices. Compared to 2D structures, in 3D cultures there can be cases in which live cells cannot be visualized with bright field and phase microscopy. This is because bright field and phase microscopy depends on light transmission through the sample and in 3D cultures the samples may be simply too thick for light passage [68]. Therefore, alternative imaging techniques are required and being developed for 3D cultures. In addition to low throughput in cell imaging in 3D models there is difficulty in maneuverability [69]. Also, due to inconsistencies in between biologically derived matrices, assay outcomes may not be reproducible in 3D culture which is an issue for 2D culture as well [70]. In some 3D constructs, spheroids that differ highly in size are formed, leading to diversity within the same well/flask which is a disadvantage lowering the accuracy of an assay [71]. Another important weakness of 3D culture is that, vasculature, crucial for tumor growth/survival and drug delivery, is deficient in 3D models [72] [73]. Furthermore, 3D cultures are more costly for performing high throughput experiments in comparison to conventional 2D culture [71]. Hence, 2D microfluidic cultures are still being used often. Even though 3D systems are better for mimicking *in-vivo* organisms, they are very complicated while 2D microfluidic devices are simple and acknowledged by a bigger scientific community.

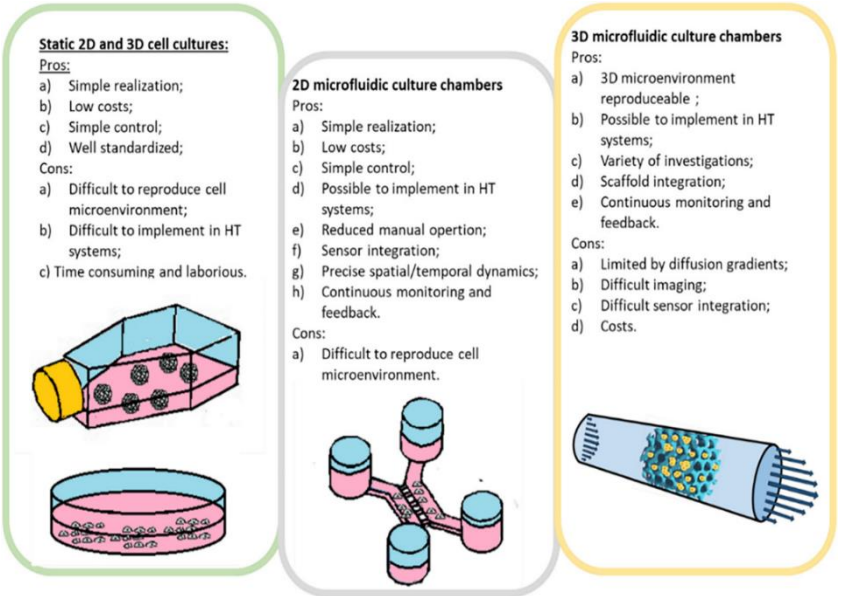

Figure 2.9 Schematic of different cell culture models: Static 2D or 3D cell culture models, 2D microfluidic culture models, 3D microfluidic culture models [38].

Chapter 3

MATERIALS AND METHODS

3.1 Design, simulation and fabrication of microfluidic chip

Microfluidic chips in Figures 3.1 and 3.2 were designed with Layout Editor® and chips in Figures 3.3 and 3.4 were drawn with CleWin Layout Editor®. The microfluidic cell culture chip in Figure 3.1 consists of six identical cell culturing platforms that are independent of each other. These platforms were constructed as flexible designs that can be used for various cell lines. Also, these culturing chambers can be utilized with same type of cells given chemical titration through the microfluidic gradient generator chip in Figure 3.2. The butterfly shaped structures in Figure 3.1 represents pillars and they were placed in order to prevent polydimethylsiloxane (PDMS) collapse. These V-shaped pillars were created with smaller flow passages compared to the diameter of cells. This was done to hold the cells on these designs and to enclose the cells inside the chamber once they enter to the chamber. The bottom of the butterfly structure has passages to prevent the cell movement to outlets as well. Thus, when cells gather at the bottom of the V-shaped pillars,

the flow in the center of the culturing chamber is prevented. As a result, the system pushes surplus cells towards the outlet channel of the chamber.

All culturing platforms on the microfluidic chip in Figure 3.1 consists of a single inlet and a single outlet connected through a channel with a microchamber in between in which cells loaded to the platforms can be grown and observed under microscopy. The diameters of inlet and outlets are 1 mm, the width of the inlet connection channel is 100 µm and the width of the outlet connection channel decreases in width bit by bit to 50 µm. The main culturing chamber in each platform has 530 µm length and 444 µm width (Figure 3.1.b). The minimum gap between the pillars is 10 µm.

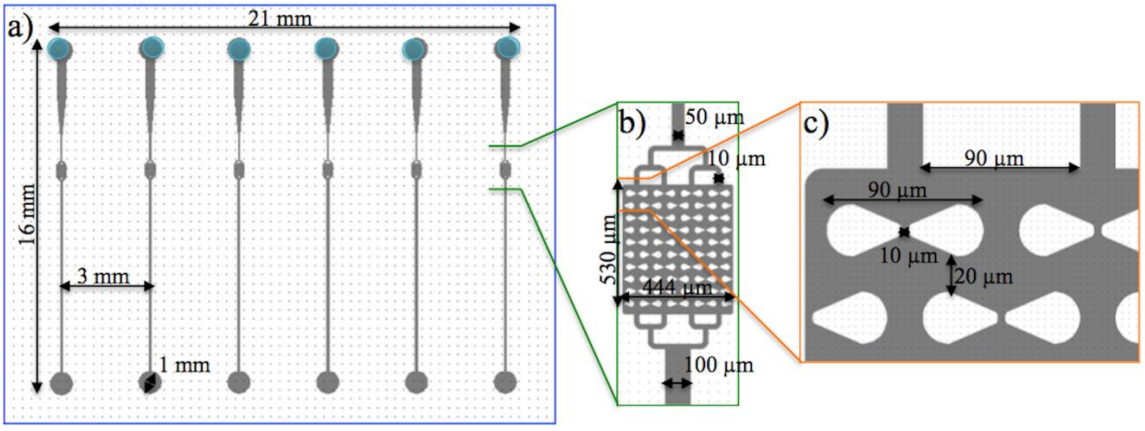

Figure 3.1: Design of the microfluidic cell culture chip in Layout Editor®. (a) Cell culture platforms on a single chip with inlet (gray circles) and outlet (blue circles) diameters as 1 mm, inlet connection channels gradually decreasing in width to 50 μm. Outlet connection channels are 100 μm wide. (b) Magnified view of the microchambers. (c) The white butterfly shaped pillars with 90 μm width to eliminate PDMS collapse [74].

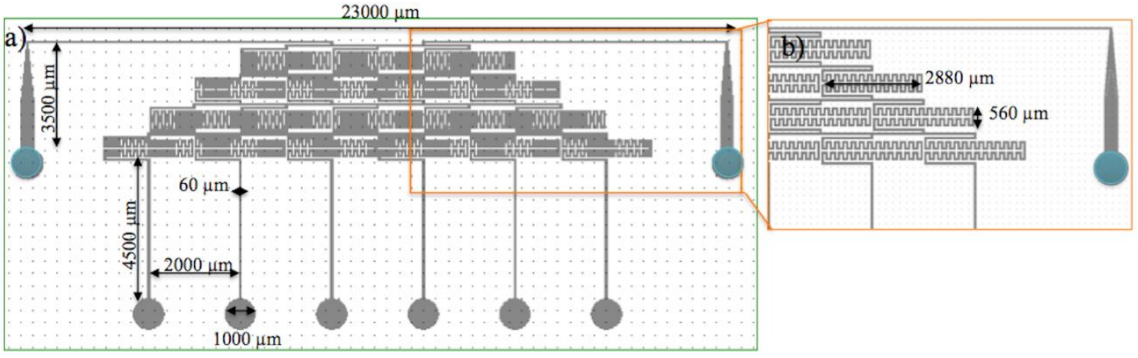

Figure 3.2: The design of the microfluidic gradient generator device in Layout Editor®. a) The complete device with two inlets (blue circles) and six outlets (gray) with 1 mm diameter. b) Magnified view of mixing channels demonstrating the length and width of mixing channels [74].

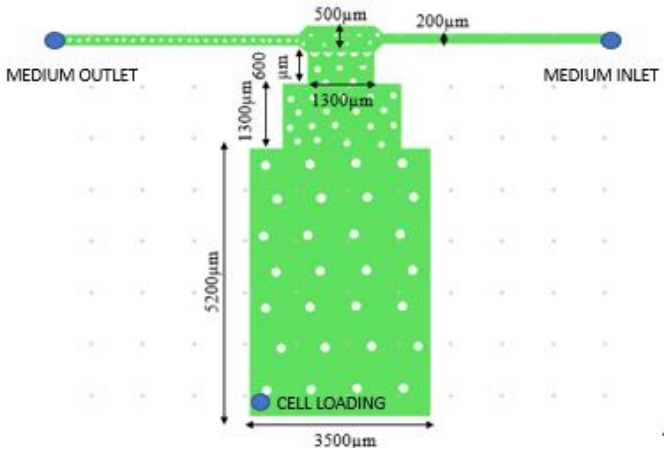

Figure 3.3: Design of the microfluidic cell culturing chip with dimensions. Inlet, outlets and cell loading hole are demonstrated with blue circles. White circles represent pillar structures [75].

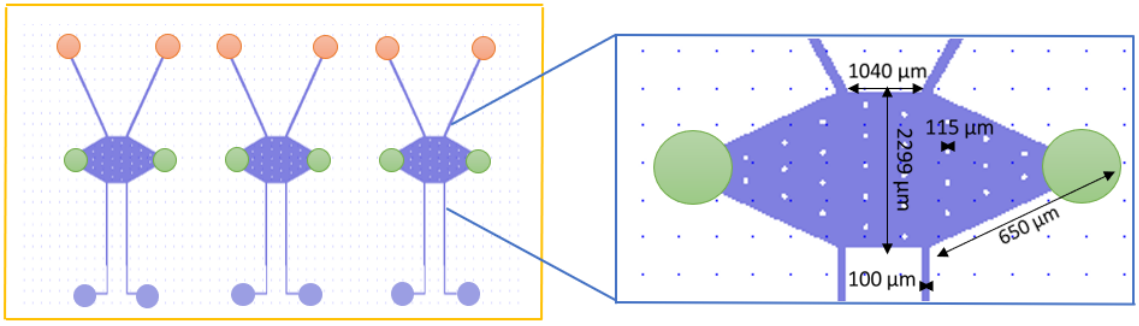

Figure 3.4: Design of the microfluidic co-culture chip with 3 cell culturing platforms. Each platform consists of two inlets (red circles), outlets (blue circles) and cell loading points (green circles). White structures in the design were placed as pillar representatives.

The design for the chemical gradient generator in Figure 3.2, was created based on the "Christmas tree" design, which is a famous design due to its accurate concentration dosing and gradient generation [76]. The gradient generator has two different inlets (blue circles) for obtaining gradients of chemical concentrations from six outlets (gray) with distribution rates of 0 %, 20 %, 40 %, 60 %, 80 % and 100 % (Fig. 3.2.a). With connection to microfluidic cell culturing platforms in Figure 3.1 through tubings the gradient generator was designed to be used for supplying different concentrations of a chemical as a drug representative to an adherent cell line for drug efficacy investigation. Thanks to microchannels being longer than their width, the gradients of the chemical produced

inside the chip are combined well and the chemical concentrations remain stable before being introduced to the cell culturing chip in Figure 3.1 [77, 78, 79, 80]. The diameter of channels is 60 μm in the whole chip to avoid possible inconsistencies in the velocity of the flow inside the chip. Like "Christmas tree" design, every flow given from the inlet divides into two streams, and these two streams join and create an average concentration of both streams. The inlet and outlet diameter of the chip is 1 mm.

The chip design in Figure 3.3 was created as an alternative culturing chip for adherent cell lines. It has a cell loading hole (blue circle) apart from media inlet and outlets (blue circles) (Fig.3.3). In this chip design, media inlet and outlets were separated from cell loading point in order to avoid bubble problems while loading cells prior to experiments. Upon loading, the flow guides cells towards the media outlet and inlet holes. With pillars that were placed to avoid polymer collapse due to surface tension, cells are trapped inside the rectangular chambers. This way, while some cells leave the outlet, the majority of the cells are trapped inside culturing chambers for population level single cell resolution analysis. The rectangular cell growing chambers were arranged to be smaller in size towards the middle chamber in order to increase the number of trapped cells.

The biggest rectangular culturing chamber in the microfluidic chip has 3500 µm width and 5200 µm length. Remaining two rectangles have 2400 µm and 1300 µm width and 1300 and 600 µm length from big to small, respectively. The chamber in between the inlet and outlet channels has 500 µm width and 1300 µm length. The inlet and outlet channel widths were kept the same in this design as 200 µm. Pillars (white circles) were inserted all over the chip design to prevent PDMS collapse (Fig. 3.3).

For investigating the interactions between different cell lines purposes, the design in Figure 3.4 was created. This coculture chip consists of three identical cell culturing platforms that are independent from each other. Each of these platforms have two media inlets, outlets and cell loading holes for the investigation of different cell lines interactions with each other (Fig. 3.4). Through the inlets of a platform different cell types (diseased (cancer) and healthy (immune system)) can be loaded. Hence, two cell lines can be grown together. The geometry of the cell culturing microchambers includes two identical triangles with a rectangle in the middle. This way, upon loading of different cell types from two cell loading points, they will be mixed equally inside the microchamber. The

length of outlet channels is relatively longer then the length of the inlet channels in order to provide high flow resistance and prevent cell flow. Also, pillars (white circles) were placed inside the cell culture chamber to avoid PDMS collapse due to surface forces (Fig. 3.4.).

The edges of the isosceles triangles in the coculture chip design have 650 µm length (Fig. 3.4.). The rectangular culturing chamber in between the triangles have 1040 µm width and 2299 µm length. The width of the inlet channels is 87 µm, the outlet channels is 100 µm, 50 µm and 10 µm in order decreasing towards the outlet to prevent cell escape. The pillar diameter is 115 µm and the distance between pillars is 150 µm.

When the designs of the chips were completed, simulation and fabrication procedures were performed. All chip flow field and velocity distribution simulations in Figures 3.5 and 3.6 were achieved via COMSOL Multiphysics software version 5.1. Simulations in 3.9 and 3.10 were obtained in COMSOL Multiphysics software version 5.3. The flow field simulations were performed to visualize cell passages inside the cell culturing chambers. Velocity distribution was simulated to establish minimum shear stress in the places where cells are trapped. For the chips in Figures 3.5, 3.7 and 3.9, the flow fields inside the platforms were estimated with the Navier-Stokes and Fick's law equations, predefined in COMSOL platform. Stationary, single-phase, incompressible laminar flow was chosen for each simulation condition. In solid walls the flow field and initial values were set as 0 m/s and 0 mol/m^3 in all directions. Non-slip and no flux conditions were defined for cell culturing chambers. The volumetric flow rate was set to 10 $\mu L/hr$ in the inlets of culturing platforms and the outlet pressure was defined as 0 Pa for all chip designs. The fluid chosen as the representative of media was water, with a density of (ρ) of 10^3 kg/m^3 and dynamic viscosity (μ) of 8.9 x 10^{-4} $N.s/m^2$. The inlets and the outlets of the flow were identified.

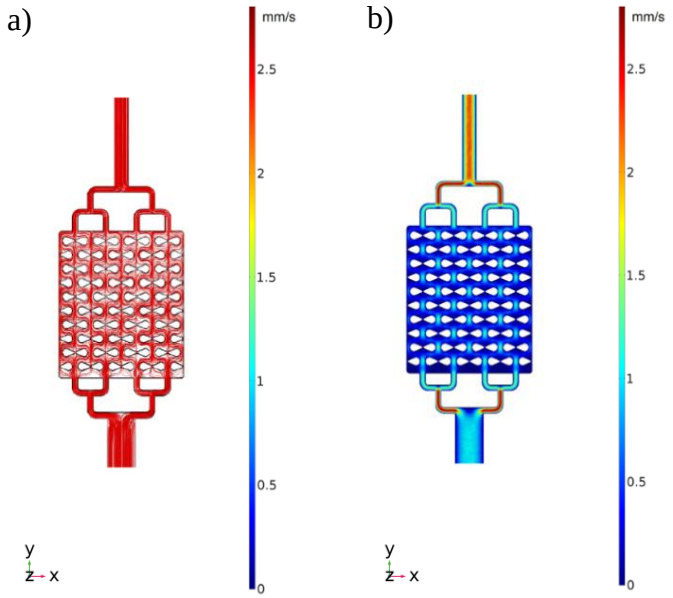

Figure 3.5. Simulation of the cell culturing platforms in Figure 3.1. a) Flow field of micro-chamber designs. Red lines represent the streamlines of the flow. b) Velocity distribution simulation for the chambers. The distribution of the velocity is shown using rainbow colors, red illustrating high velocity and blue low velocity (mm/s).

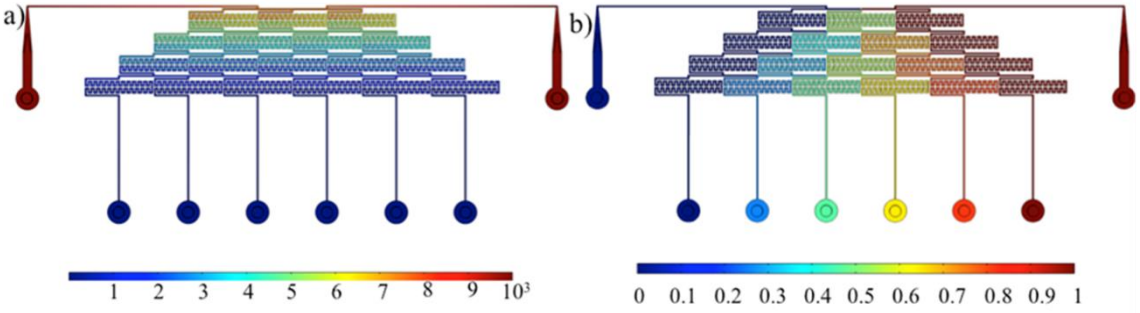

Figure 3.6 a) Pressure (Pa) and b) chemical concentration (mol/m3) simulations depicting uniform distribution through rainbow colors in the microfluidic gradient generator.

Apart from other chip simulations, in the simulation of the gradient generator depicted in Figure 3.6, the inlet pressure was set to 10 *kPa*, and the chemical concentrations were defined as 0 mol/m^3 for inlets. The outlet boundary condition was set as zero static pressure and outflow. The chemical concentrations and the pressure of the gradient generator were simulated using convection and diffusion equations. Rainbow colors were used to show a uniform flow distribution was established in all channels. Thus, diluted chemical concentrations were obtained from the outlets as 0, 0.2, 0.4, 0.6, 0.8 and 1 ($mole/m^3$) (Fig 3.6).

For the simulations of the microfluidic cell culturing chip in Figure 3.9 and the co-culturing platform in Figure 3.10, the designs were first established in three dimensions in Solidworks 2015 edition. Next, the Solidworks three dimensional designs in Figures 3.7 and 3.8 were transferred to COMSOL Multiphysics software version 5.3, where, the simulations were obtained for velocity and pressure distributions.

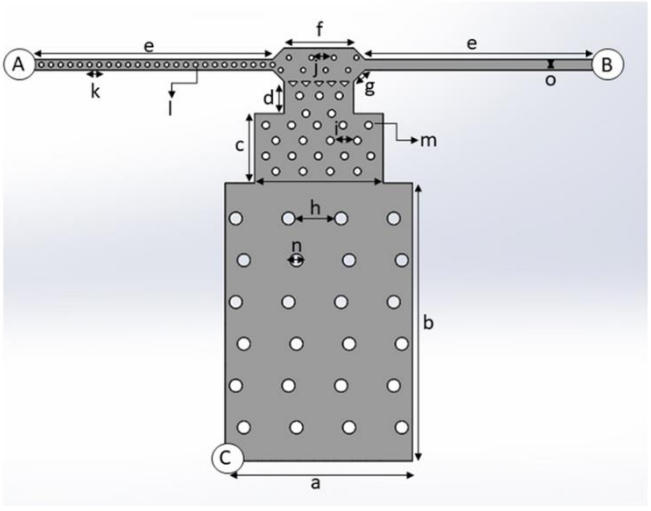

Figure 3.7. The design of the microfluidic cell culture chip in Solidworks. The dimensions in the design are a: 3500 µm b: 5200 µm, c: 1300 µm, d: 600 µm, e: 4500 µm, f: 1300 µm, g: 300 µm, h: µm, i: 350 µm, j: 330µm, k: 90 µm, l: 90 µm, m: 140 µm, n: 240 µm, o: 200 µm . White circles in the design represent pillar structure (A: Medium Outlet, B: Medium Inlet and C: Cell loading point).

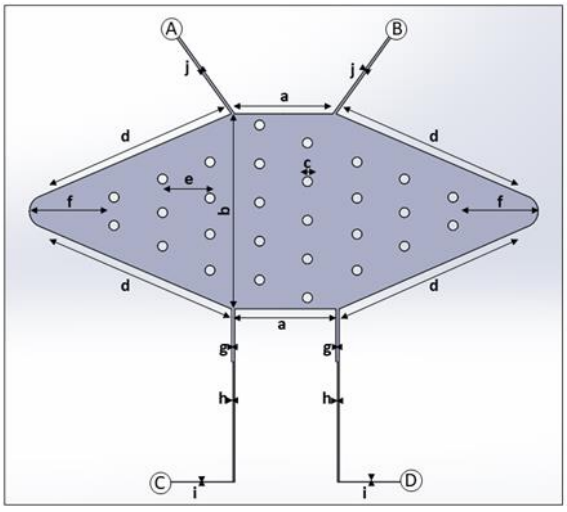

Figure 3.8. The Solidworks design of the co-culture chip. The dimensions in the design are a: 1040 µm b: 2299 µm, c: 115 µm, d: 650 µm, e: 150 µm, f: 250 µm, g: 100 µm, h: 50 µm, i: 10 µm, j: 100 µm. White circles in the design represent pillar structures.

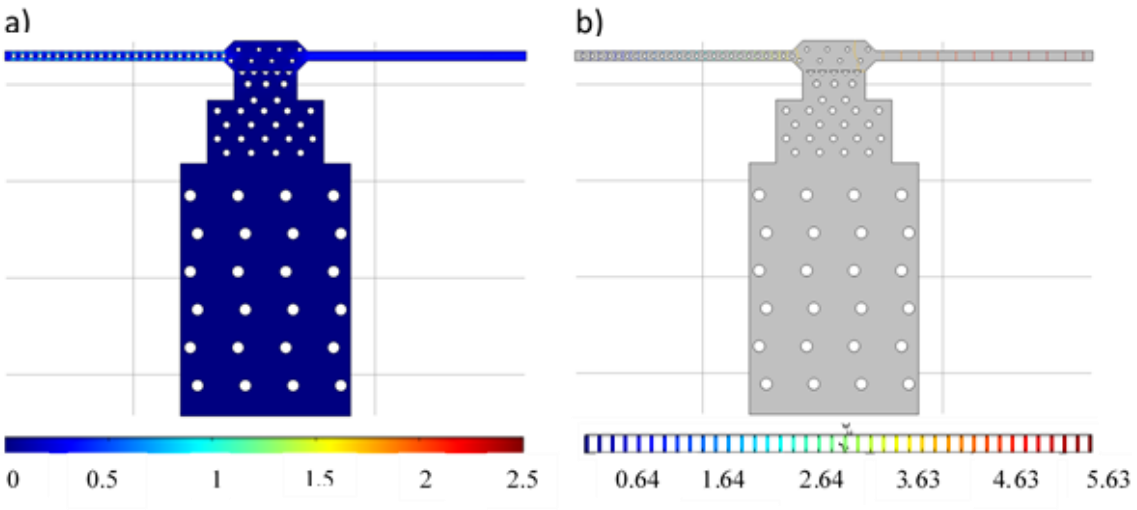

Figure 3.9. Simulation of the cell culturing platforms. a) Velocity distribution simulation for the chambers (x 10^5 µm/s). b) Pressure distribution simulation for the chambers (x 10^3 Pa). The distributions are shown using rainbow colors, red illustrating high velocity, pressure and blue low velocity, pressure.

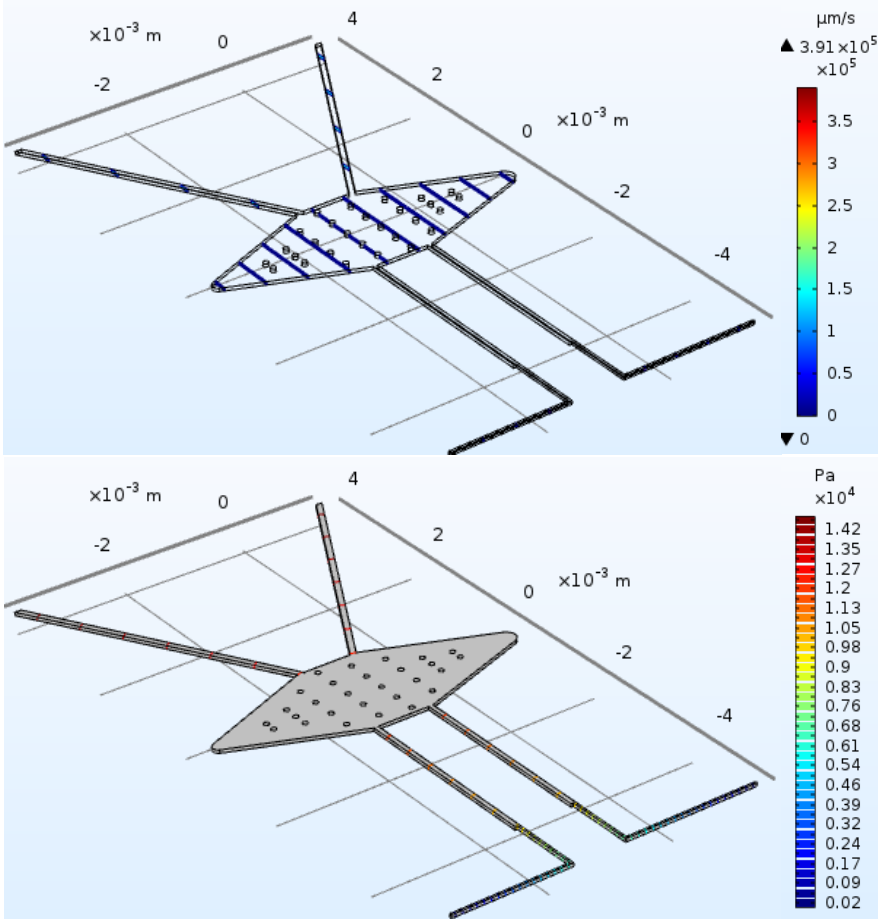

Figure 3.10. The a) velocity (µm/s) and b) pressure (Pa) simulations for the co-culture chip.

When the simulation results confirmed for the designed chips, their fabrication was performed. The mask designs were patterned on a thin film chromium deposited photo mask (Cr-blank) using a Vistec/ EBPG5000plusES Electron Beam Lithography system. For the chips in Figures 3.1 and 3.2, SU-8 2025(SU-8®2025, MicroChem) was spin coated on a 4-inches silicon wafer to obtain structures of height 40 μm. Next, the photoresist-coated wafers were soft baked at 65°C for 3 minutes and at 95°C for 5 minutes. For the platforms in Figures 3.3 and 3.4, SU-8 3050 (SU-8® 3050, MicroChem) was spin coated on a 4-inches silicon wafer to obtain structures of height 50 μm. Afterwards, all wafers were exposed to UV light 160 mJ/cm^{-2} using e-beam written masks by a Midas/MDA-60MS mask aligner. After two consecutive post-baking process at 65°C for 1 min and at 95°C for 5 min, they were developed for 5 min using MicroChem's SU-8 developer. Later they were rinsed with isopropanol. The obtained wafers were used as molds for the elastomeric polymer, Polydimethylsiloxane, PDMS (Sylgard® 184, Dow Corning, Midland, MI, USA) [81]. The PDMS base and curing reagents were mixed at a ratio of 10:1. Then, the mixture was poured to the wafer. Upon bubble removal through vacuuming, the wafer with PDMS was baked at 75°C for 60 min. Finally, PDMS mold of the structures was removed. Chip designs were cut, and device inlet and outlet ports were punched. PDMS chips were bonded on glass slides utilizing the Corona system (BD20-AC, Electro-Technic Products Inc.) [82].

3.2 Cell Culture and staining using conventional methods

For different applications, various types of human cancer cell lines were cultured both using tissue culture techniques and microfluidic cell culturing platforms. All cells were kept inside a 5 % CO2 – 95 % air atmosphere in a humidified incubator (Nuve, Ankara, Turkey). Cell counting during culturing and experiments were performed using the Trypan blue dye (Sigma-Aldrich) with a hemocytometer (Marienfeld-Superior, Lauda-Knigshofen, Germany). The following cell lines have been cultured according to ATCC (LGG Standards, Middlesex, UK) protocols:

- U937 monocytes (the human myeloid leukemia) cell line (ATCC®CRL-1593.2™)

Monocytes were obtained from ATCC (American Type Culture Collection, Manassas, VA, USA). For culturing U937 monocytes, RPMI-1640 complete medium (PAN-Biotech, Aidenbach, Germany) supplemented with 10% fetal bovine serum (FBS; PAN-Biotech, Aidenbach, Germany) and 1% Penicillin-Streptomycin solution (PAN-Biotech, Aidenbach, Germany) was used. Before each experiment, cells were spun down at 3000 rpm (MERCK, Darmstadt, Germany) for 5 minutes and resuspended in fresh media or appropriate intravenous fluid (IVF) according to experiment purpose.

- U937 macrophages

Macrophages were prepared by the differentiation of the U937 monocytes (5×10^5 cells/mL) were seeded in a petri dish with complete medium including 2.5 µL of 10 ng/mL phorbol myristate acetate (PMA)/DMSO (PAN-Biotech, Aidenbach, Germany) solution for 5 days. In day 3 and 4, nonattached cells were removed by aspiration, and the adherent cells were washed with a complete medium. In day 5, after aspiration of the nonattached cells, differentiated macrophages were washed first with PBS (PAN-Biotech, Aidenbach, Germany) and then incubated for 10 minutes inside 1 mL pre-warmed trypsin solution (PAN-Biotech, Aidenbach, Germany). Detached macrophages were spun down at 3000 rpm for 5 minutes to remove residual media. Finally, cells were resuspended in fresh media or appropriate intravenous fluid (IVF) according to experiment purpose.

- MCF7 human breast adenocarcinoma cell line (ATCC® HTB-22™)

For the creation of RFP-expressing MCF7 (MCF7-RFP) cells, lentiviruses were produced by the transfection of pRSI9-U6-UbiC-TagRFP-2A-Puro plasmid (Addgene plasmid no. 28289) together with its helper plasmids psPAX2 and pMD2.G (Addgene plasmids 12260 and 12259) into HEK293T cells. Supernatants of cells were harvested

after 48 hours and 72 hours upon the transfection. The mixtures of collected supernatants were stored at −80 °C and used to infect the cells. MCF7 cells were infected at a 60 % confluence for 24 hours with lentiviral supernatants diluted 1:1 with full Dulbecco's modified Eagles' medium (DMEM; Sigma-Aldrich) culture medium supplemented with 5 μg mL^{-1} polybrene (Sigma-Aldrich, H9268). Twenty-four hours after infection, the medium was altered with fresh medium. MCF7 cells expressing RFP vector were chosen with 1 μg mL^{-1} puromycin in DMEM supplemented with 10 % fetal bovine serum (FBS; Sigma-Aldrich), 1 % penicillin–streptomycin (Pen/Strep; Sigma-Aldrich) and 1 % L-glutamine (Sigma-Aldrich) for a month. No additional stain was used.

MCF7 cells expressing RFP vector were taken from Sabanci University Molecular Biology, Genetics and Bioengineering Department. MCF7-RFP cells were cultured in DMEM supplemented with 10% FBS, 1% Pen/Strep, 1% L-glutamine both in 75 cm2 flasks (Corning® T-75 flasks) and in the microfluidic platforms inside the incubator. Trypsin-EDTA (Sigma-Aldrich) solution was used to detach the cells from the flask and to load those cells into the microfluidic chips. Cells were cultured inside 96-well plates prior to loading inside the chips until their cell counts reached 3.5 x 10^4 cells/mL.

- HepG2 human liver hepatocellular carcinoma epithelial cell line (ATCC®HB-8065™)

HepG2 cells were taken from Gebze Technical University Molecular Biology and Genetics department, were used to demonstrate the utility of the microfluidic cell culture platform. For culturing cells, DMEM (PAN-Biotech) supplemented with 10 % FBS (Sigma-Aldrich) was used both in 75cm2-flasks (Corning® T-75 flasks) and in the microfluidic chips inside the incubator. Trypsin-EDTA solution (Sigma-Aldrich) was used to detach the cells from the flask and to load those cells into the microfluidic chips.

- U87 human brain glioblastoma epithelial cell line (ATCC® HTB-14™)

U87 cells were taken from Yeditepe University Molecular Biology and Genetics department, were used to demonstrate the utility of the microfluidic cell culture platform. For culturing cells, DMEM (PAN-Biotech) supplemented with 10 % FBS (Sigma-Aldrich) was used both in 75cm2-flasks (Corning® T-75 flasks) and in the microfluidic chips inside the incubator. Trypsin-EDTA solution (Sigma-Aldrich) was used to detach the cells from the flask and to load those cells into the microfluidic chips.

In experiments with intravenous fluids, U937 monocytes, macrophages and MCF7 and HepG2 cells were stained separately with 0.128 mM Hoechst (Life Technologies) and 0.0111 mM Propodium Iodide (PI) (Sigma Aldrich) solutions for end-point staining. Cells were kept in solutions for 20 minutes in the incubator using 1 µL of dyes from the working solutions of Hoechst (10 mg/L in water) and Propidium Iodide (1 mg/L in water).

Inside the microfluidic chips, for the heterogeneity analysis of the HepG2 cells no stain was used. For co-culturing purposes, U87 cells with red cell tracker (1 µM) and U937 macrophages were stained with green cell tracker (2 µM) inside 6-well plates.

After cells were grown inside conventional cell culturing platforms, prior to loading the cells into the microfluidic devices we cleaned and prepared the chips. The cell culturing chip and the gradient generator in Figures 3.12 and 3.13 were cleaned using 70 % aqueous ethanol. Next, the devices were washed in phosphate buffered saline (PBS; Sigma-Aldrich) in order to remove the remaining ethanol from the channels. The Tygon tubing (Tube Tygon s54HL.02X.06 500, Andwin Scientific) and metal couplers were autoclaved (Hirmaya HMC HV-85L). Then, metal couplers were attached to the inlet ports prior to sample loading into the microfluidic devices. Before usage, the media and PBS were warmed in a 37 °C water bath. Finally, 1000–10 000 cells/mL were loaded into the device using a 100 μL Hamilton syringe (Hamilton, 100 μl SYR, no. 84884). Both the inlet and the outlet channels of the cell culturing platforms were filled using prewarmed media with a height difference (h) to establish a flow in between inlet and outlet channels (Figure 3.11). The cells were collected at the chambers with single-cell resolution through the designed cell trapping mechanism. Upon examination of the cells in the microfluidic

cell culture platform on a table top microscope (Carl Zeiss, Primovert Model Trinocular Inverted Microscope), the device was placed into the incubator overnight to allow cell attachment to surface with an average medium flow rate of 4 μL/h. PBS-wetted tissue were placed inside the Becher glass, next to the chips to avoid media evaporation from the PDMS device (Figure 3.12).

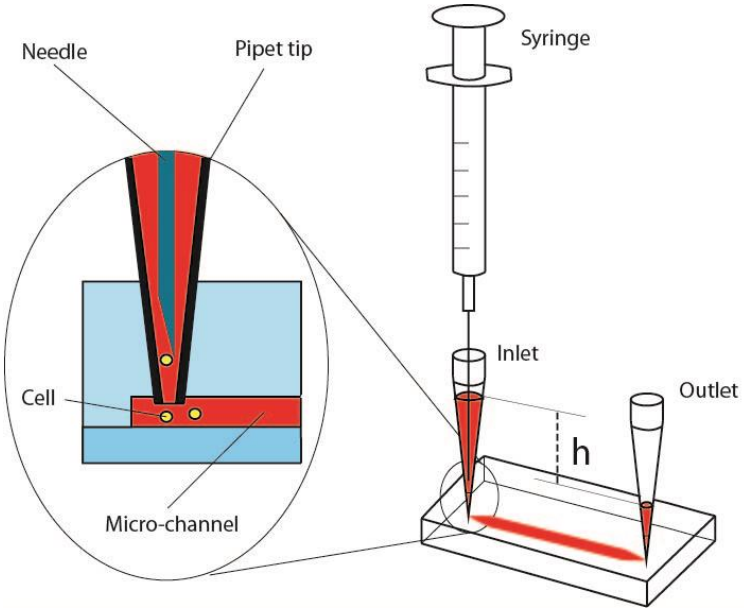

Figure 3.11. Schematic of cell loading procedure in a microfluidic PDMS device (cells are depicted as yellow circles) [83].

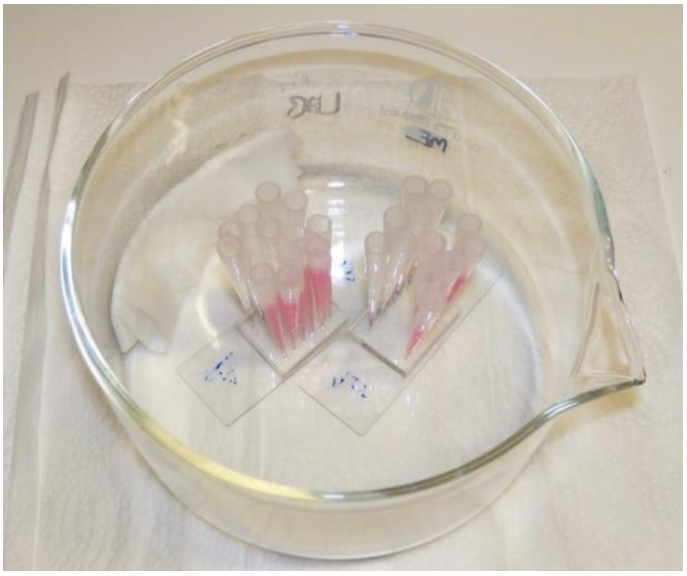

Figure 3.12. The PDMS devices loaded with MCF7 cells.

The gradient generator was tested initially with yellow and blue food dyes (Herco, no.156819593) through loading with gravity-driven flow. The image of this tested chip giving the mixed concentrations of the dyes can be found in the results section in Figure 3.13. After, ensuring the chip is working both with simulations and experiments using food dyes, 1 mg/mL of fluorescein isothiocyanate (FITC; fluorescein5(6)-isothiocyanate, Sigma-Aldrich) solution in carbonate–bicarbonate buffer (lot no. RC233804, Thermo Scientific) was prepared with pH value 9. This solution was given from the first inlet, while introducing the carbonate–bicarbonate buffer without FITC via the second inlet using two syringes mounted on a syringe pump (New Era Pump Systems, NE-1000). The flow rate was initially set as 300 μL/h. Upon achieving a steady chemical gradient, the flow rate was reduced to 10 μL/h.

After initial checks with dyes were completed, MCF7 breast cancer cells stably expressing RFP vector were grown inside 96-well plates (TPP). These cells were removed from the surface with Trypsin (3X, Pan Biotech) when their density reached 3.5 x 10^4 cells/mL. An SDS concentration range of 0 % to 0.005 % gives the sensitivity and precision of the microfluidic gradient generator in Figure 3.13. Hence, the detached cells were cultured in Dulbecco's phosphate buffered saline (PBS, Pan Biotech) supplemented with 0.005 %, 0.01 %, 0.025 %, 0.05 %, 0.075 % and 0.1 % sodium dodecyl sulfate (w/v) (SDS; MP Biomedicals, LLC, cat. No. 194831) and in PBS for 10 minutes inside the incubator (NUVE) to test the effective concentrations. Experiments were utilized in triplicate. Next, the well images were captured and the number of intact cells (excluding Trypan Blue solution; Sigma-Aldrich) were counted with a hemocytometer. SDS from one of the gradient generator inlets and PBS from the other one separately. Cell viability in 96-well plate after exposure to SDS was plotted using Gradpad Prism based on the hemocytometer counting (Fig. 4.1.4). Thus, according to our experiment we proved the effective SDS concentrations as PBS supplemented with 0.005 %, 0.01 %, 0.025 %, 0.05 %, 0.075 % and 0.1 % SDS (w/v).

After the preliminary tests for both the microfluidic cell culture chip and the gradient generator, first, MCF7-RFP cells were cultured and grown inside the six microchambers of the microfluidic cell culture array. Their microscopy images were taken with the inverted microscope for 3 days and their growth curve based on their fluorescent intensities was obtained in Gradpad Prism (Fig. 4.2.2 and Fig. 4.2.3). Second, the microfluidic gradient generator was integrated to the microfluidic cell culture platform through tubings (Fig. 4.3.3). Next, the gradient chip produced the SDS solution gradients for the concentrations of 0.005 %, 0.004 %, 0.003 %, 0.002 %, 0.001 % and 0 %, with PBS. Then, cells inside the chambers were exposed to SDS for 30 minutes with a flow rate of 10 µL/h. The images of cells before and after SDS exposure are depicted in the results section in Figure 4.3.4 along with their viability plots obtained in Gradpad Prism based on fluorescent intensities in Figure 4.5.

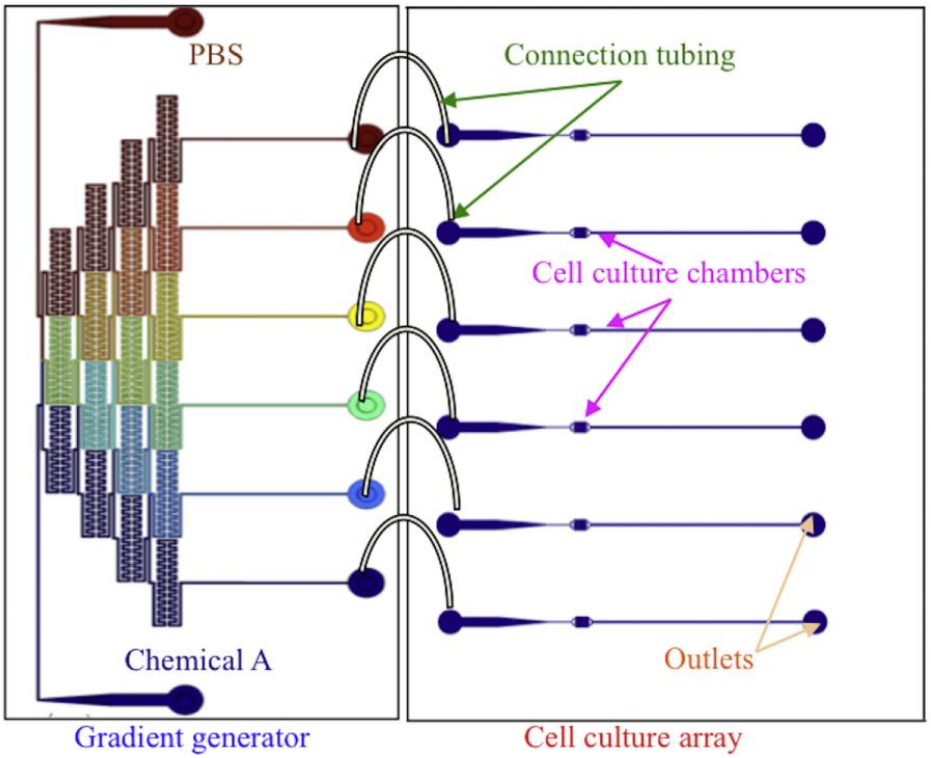

Figure 3.13. a) Schematic view of the gradient generator and cell culture array [74].

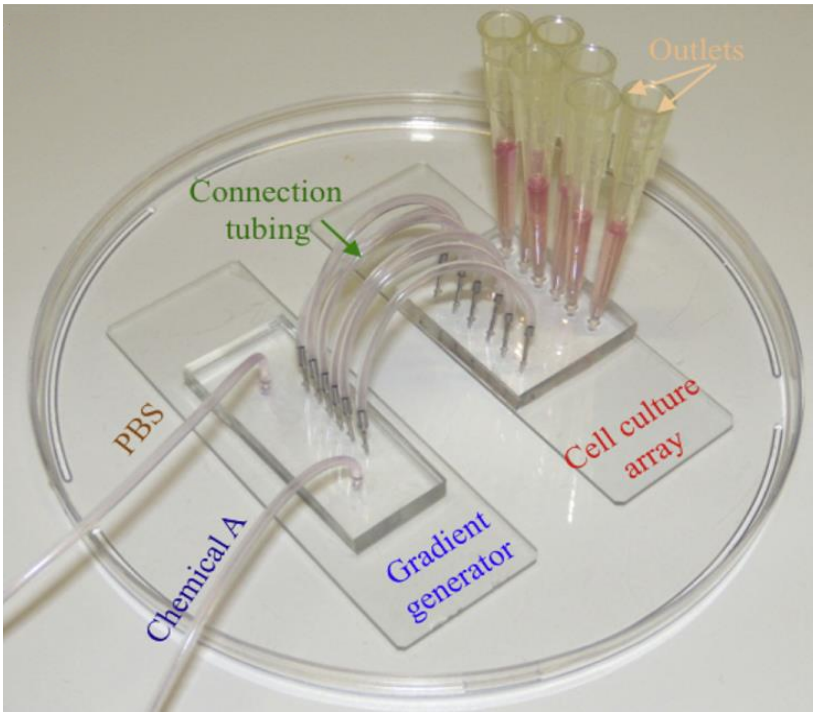

Figure 3.14. Integration of the gradient generator with the cell culture array using the connection tubing [74].

The chip in Figure 3.3 was tested experimentally for cell culturing with HepG2 cells. Prior to cell loading into the microfluidic devices, cell culture platform, metal couplers and tips couplers were autoclaved (Hirmaya (HMC) HV-85L) and tips were connected to medium inlet and outlet ports. The medium was prewarmed at 37 °C water bath. HepG2 cells were centrifuged at 1800 rpm for 10 minutes in 15 mL falcons. Next, the supernatant was removed, and the pellet was completed to 1 mL including fresh DMEM with %10 FBS. Then, the cells were counted with hemocytometer and loaded into the device by a pipetman, connected to a blunt needle with a modified tip, with approximately 10^5 cells/mL. The chambers were filled with cells through the cell trapping mechanism in single cell resolution. The microfluidic platform was placed into an autoclaved glass beaker with tissues wetted with phosphate buffered saline (PBS, Sigma-Aldrich) to avoid medium evaporation from the PDMS device. After microscopy inspection (Carl Zeiss, Primovert Model Trinocular Inverted Microscope) of the cells in the microfluidic cell culture platform, the device was transferred into the incubator overnight.

3.3 Fluorescent Imaging and Image Analysis

Images of the devices in Figure 3.12 tested with MCF7 cells, we acquired images with a 10X objective combining phase and DsRed fluorescent channels using a Carl Zeiss, Axio Observer Z1 motorized stage equipped with the AxioCam Mrc5 camera. The total fluorescent intensity of the cells within the microchambers were measured to quantify cellular growth using ImageJ software. To observe fluorescent intensity changes in the gradient generator, the imaging was done with green fluorescent filter with an exposure time of 400 ms. The composite image of the whole gradient generator was obtained via tiled images using Zen Pro microscopy software (Carl Zeiss). The fluorescent intensities obtained as 2.5D image (pseudo-3D image) through the same software. Upon FITC application to the chips resulting images were tiled together and their fluorescent intensities estimated via ZEN Pro 2 software (Zeiss). The images of the chambers after the SDS exposure were obtained using the DsRed fluorescent channel with an exposure time of 500 ms. The SDS effect was correlated with the fluorescent intensity values by measuring the total fluorescence intensity in the microchambers.

During the growth of HepG2 cells inside the microfluidic cell culturing chip in Figure 3.14, images of the individual chambers in the device were obtained using 10X objective and a Carl Zeiss, Axio Observer Z1 motorized stage equipped with the AxioCam Mrc5 camera. Cell images were captured using 12.5 ms exposure under transparent light. After imaging, cells with and without pseupodium were counted.

Upon introducing the cells into microchambers in the cell culturing chips, cells attached to the glass surface of the microfluidic chip overnight. Upon cell attachment due to the height difference between the inlet tip and outlet tips of the devices, gravity-driven medium flow fed the cells inside the microchambers. Cell growth was captured for 6, 18, 48 and 72 hours using both phase and red fluorescent channels. Obtained images were quantified to determine the growth of the cells in the microfluidic cell culture array. With Gradpad Prism software, using the measured raw fluorescent intensities of the microchambers, intensity versus time plots were created for 6, 18, 48 and 72 hours.

The obtained chip images were used as a dataset and adaptive thresholding was performed to several images of the chips using Matlab. For cell counting Hough transform was applied, isolating features of a shape within an image. Since it needs target features to be specified in some parametric form, the typical Hough transform is generally used for detecting regular curves such as lines and circles for this case [84]. By defining cell nucleus in DAPI images as circle, cells were detected and counted directly from the images. For this the Hough transform algorithm was set to detect circles and draw a line around circles within the range of minimum radius 10 µm and maximum radius of 50 µm. Also, it was arranged to give the number of lines that are drawn to get the cell count information.

3.4 Flow Cytometry (FACS) and Analysis

In preliminary tests using IVFs, flowcytometry experiments were performed using the BD LSR Fortessa FACS analyzer (BD Biosciences, Franklin Lakes, NJ, USA). For high throughput, cell number was arranged to 2.5 x 10^5 cells/mL. Cells were kept inside IVF for 15 minutes. One sample group was exposed to PBS and stained with PI, while the other samples were exposed to IVFs (Dextrose, NaCl, Ringer) and stained with PI. The intact cells were determined according to their forward scatter (cell size) versus side scatter (cell granularity) profiles using blue (488 nm) excitation laser. The data was examined using the FlowJo v10 software (TreeStar, Inc., OR, USA). Double cell discrimination was done by plotting the height against the area for forward scatter. While double cells have roughly the same height with single cells, they have double the area values of single cells. Thus, we identified and excluded double cells based on disproportions between height and area [85]. Then, we separated live cells from debris and dead cells by gating on the area values of cells for forwards scatter versus side scatter plots. Events found at the bottom left corner of the density plots in gating were excluded to separate debris and dead cells with lower level of forward scatter [86] [87].

Chapter 4

RESULTS AND DISCUSSION

4.1 Cell culture in conventional growth environment

- U937 monocytes (the human myeloid leukemia) cell line (ATCC®CRL-1593.2™)

U937 monocytes that were used for obtaining macrophages via differentiation through PMA were grown for viability confirmation using a 96-well plate. Cells were counted with a hemocytometer for 3 days in triplicates. The resulting graph plotted in Gradpad Prism using cell numbers per day can be seen in Figure 4.1.1

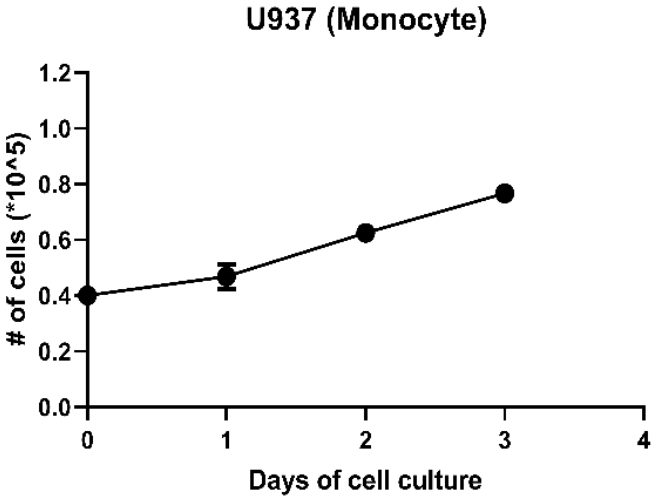

Figure 4.1.1. The plot for the growth of U937 monocytes in 96-well plates. The points on the growth line depicts the average value for cell growth and standard deviation of the growth.

- U937 macrophages

Upon differentiation of U937 monocytes into macrophages in petri dishes with 21 cm^2 growth area, macrophages were grown and ready to be used on day 5. The image of grown macrophages inside petri dishes can be seen in Figure 4.1.2

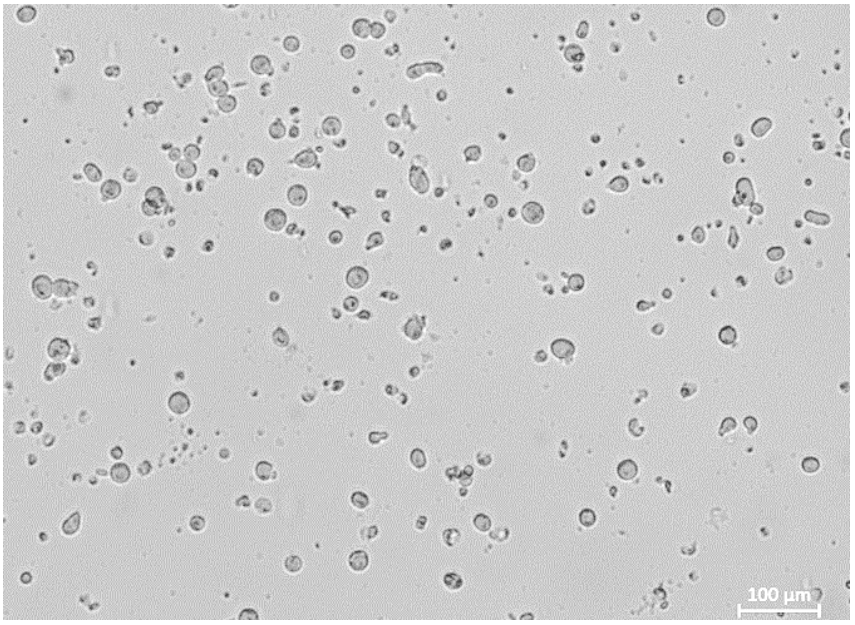

Figure 4.1.2. The plot for the growth of U937 macrophages in 96-well plates.

- MCF7 human breast adenocarcinoma cell line (ATCC® HTB-22™)

MCF7 cells that were being used in microfluidic devices were also cultured inside conventional platforms for validation of growth with a 96-well plate [88]. Cell counting was established with a hemocytometer for 3 days in triplicates.

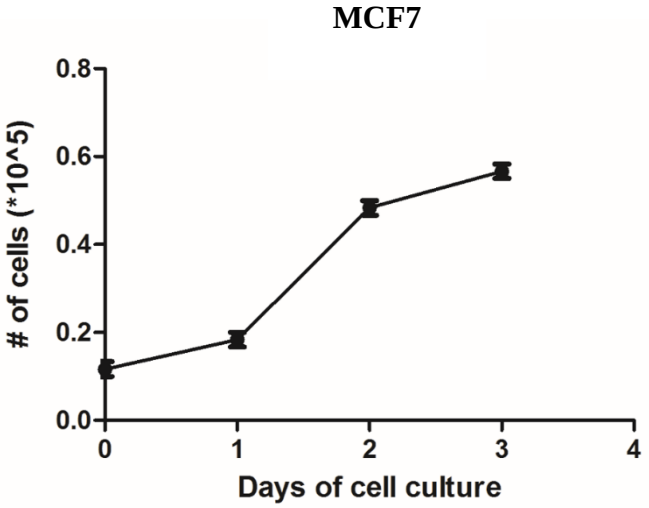

Figure 4.1.3. The plot for the growth of MCF7 cells in 96-well plates. The points on the growth line depicts the average value for cell growth and standard deviation of the growth [74].

From the testing of MCF7-RFP cells in PBS solutions with 0.005 %, 0.01 %, 0.025 %, 0.05 %, 0.075 % and 0.1 % SDS (w/v) inside 96-well plates with hemocytometer-based counting of intact cells a viability graph demonstrating the number of live cells versus SDS concentration was obtained (Fig. 4.1.4). This graph displays a correlation between the cell viability and SDS concentrations. According to Figure 4.1.4. cell viability goes down as the concentration of SDS in PBS solutions increases. As a consequence, the SDS concentrations in the range of 0 % to 0.005 % was confirmed to provide the sensitivity and accuracy of our microfluidic concentration generator.

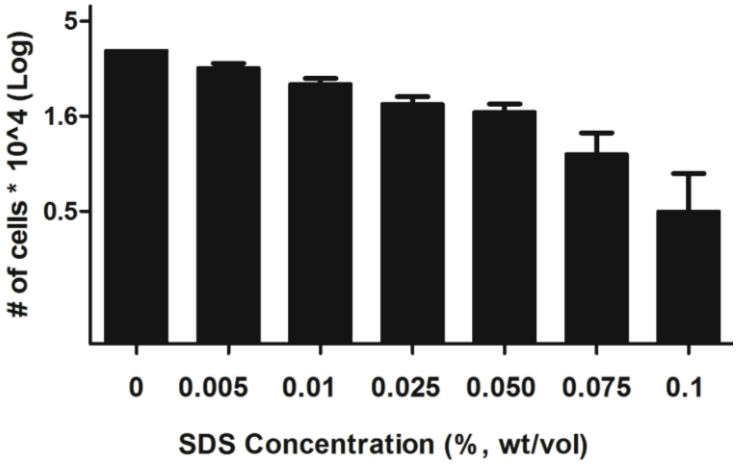

Figure 4.1.4. Cell viability plot for MCF7 cells upon exposure to SDS in 96-well plate. and then exposed to SDS for 10 min in the incubator. The bars represent the average number of live cells shown with their standard deviations [74].

- HepG2 human liver hepatocellular carcinoma epithelial cell line (ATCC®HB-8065™)

HepG2 cells were grown inside a 96-well plate in addition to microfluidic platforms for the validation of cell growth. Upon daily cell counting with hemocytometer in triplicates the graph in Figure 4.1.4 was acquired using Gradpad Prism.

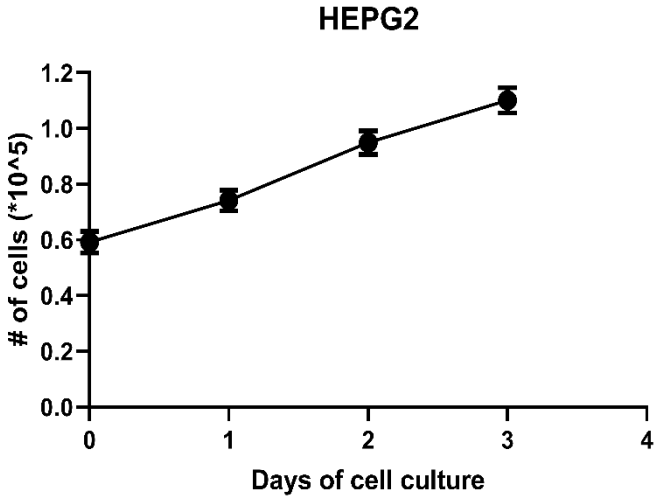

Figure 4.1.5. The plot for the growth of HepG2 cells in 96 well plates. The points on the growth line depicts the average value for cell growth.

Growth of the hepatocellular carcinoma cell line was also observed at population-level using petri dish with 21 cm^2 growth area. Figure 4.1.6 is the image of hepatocellular cells overnight inside the petri dish taken with inverted microscope. For the investigation of cell heterogeneity, the number of cells that grow pseupodium and the number of cells that did not have pseupodium were plotted based on single-cell level analysis in Figure 4.1.7.

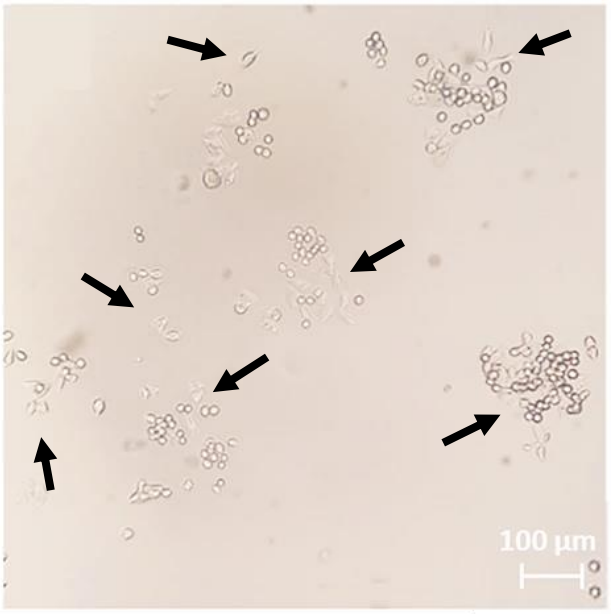

Figure 4.1.6. Microscopy image of HepG2 cells in tissue culture petri dish overnight at 37 °C. The areas with pseupodium are denoted with black arrows [75].

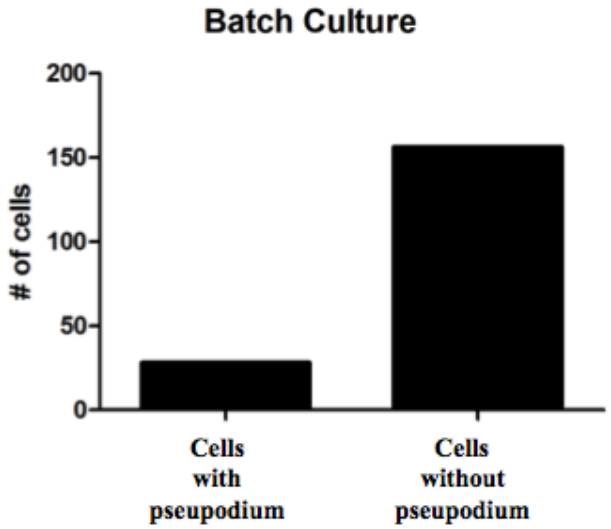

Figure 4.1.7. Plot of liver cancer cells in the batch culture with and without pseupodium based on single-cell analysis [75].

- U87 human brain glioblastoma epithelial cell line (ATCC® HTB-14™)

Prior to their usage in co-culture platforms, U87 cell were cultured in a 96-well plate for growth confirmation. After counting cells daily with a hemocytometer in triplicates the graph in Figure 4.1.8 was acquired using Gradpad Prism.

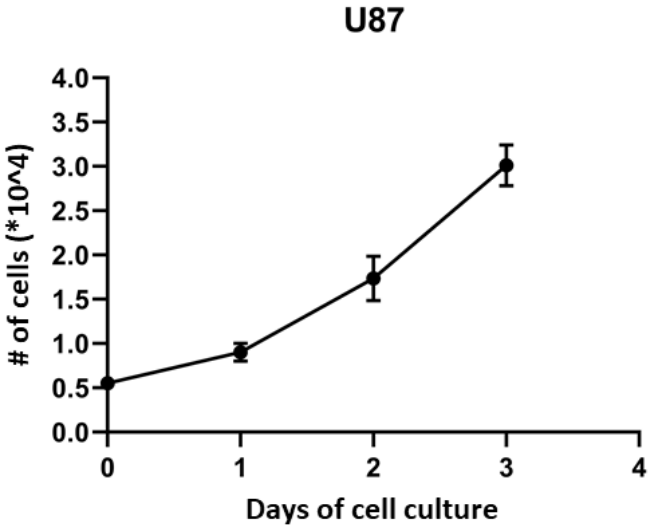

Figure 4.1.8 The growth of U87 cells in 96 well plates

4.2. Cell culture in the artificial microfluidic platforms

After growing cells inside conventional platforms, cells were cultured in PDMS based microfluidic platforms.

- U937 macrophages

Grown macrophages were removed from the petri dishes using Trypsin solution (3X).

- MCF7 human breast adenocarcinoma cell line (ATCC® HTB-22™)

After transferring MCF7 cells into the microfluidic cell culturing platform in Figure 3.13b, the cells were incubated overnight for cells attachment to the glass surface. Next, upon the adherence of cells to the surface, gravity-driven medium flow fed the cells inside the microfluidic chip. Images of grown cells inside the culturing chambers were captured with an inverted fluorescent microscope using phase and red fluorescent channels for 6, 18, 48 and 72 hours (Fig. 4.2.1) [89]. The microscopy images were quantified measured raw fluorescent intensities of the microfluidic culturing chambers obtained with Image J for 6, 18, 48 and 72 hours in order to determine the growth rate of the cells inside the platforms (Fig. 4.2.2). Additionally, image processing was performed on the fluorescent microscopy images of Hoechst stained MCF7 cells to be able to modify images for further investigations and to be able to interpret experiment results accurately. Figure 4.2.3 represents the fluorescent microscopy images of the stained MCF7 cells taken with DAPI channel before and after image processing in MATLAB. Also, as an alternative to hemocytometer, a Hough Transform algorithm for circles was offered for counting cell automatically from fluorescent microscopy images [90]. Cells were detected with the definition of cell nucleus in DAPI images as a circle and circle boundaries with a radius range from 10 to 50 using Hough Transform (Fig. 4.2.3.c). Finally, hemocytometry based cell counting was compared with automated cell counting via Hough Transform for circle boundaries and the results were plotted with a graph in Figure 4.2.4 [91].

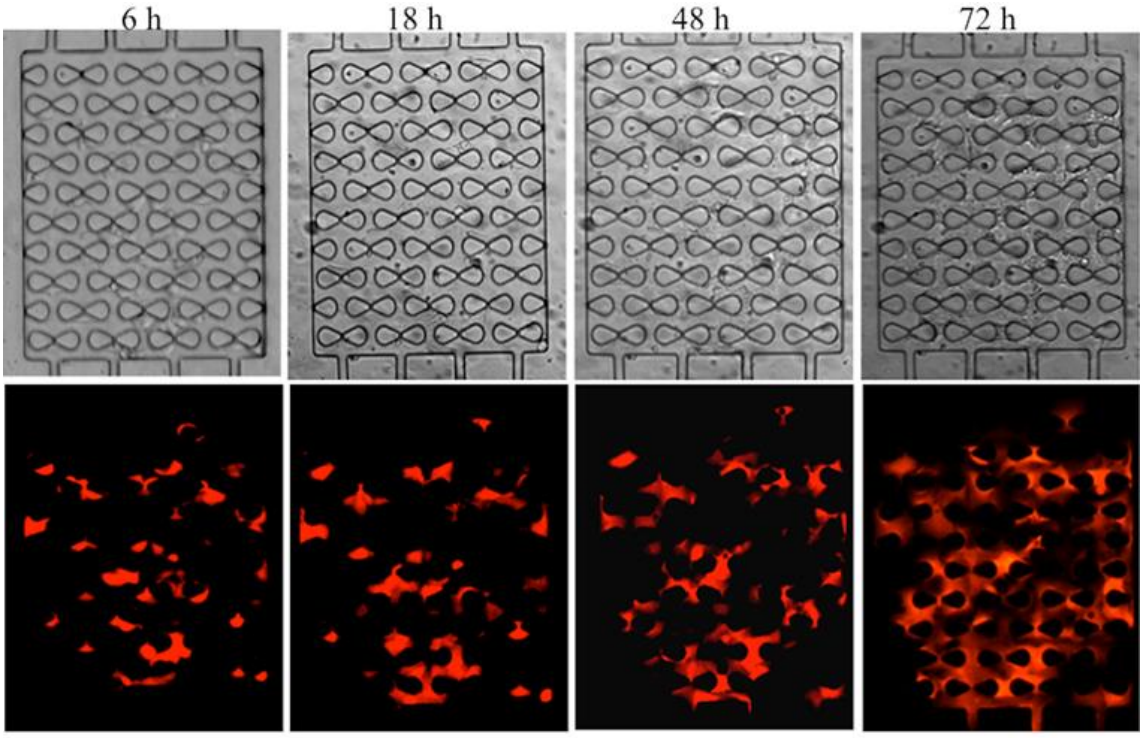

Figure 4.2.1. Cellular growth of MCF7 cells inside the microfluidic culturing chambers [74].

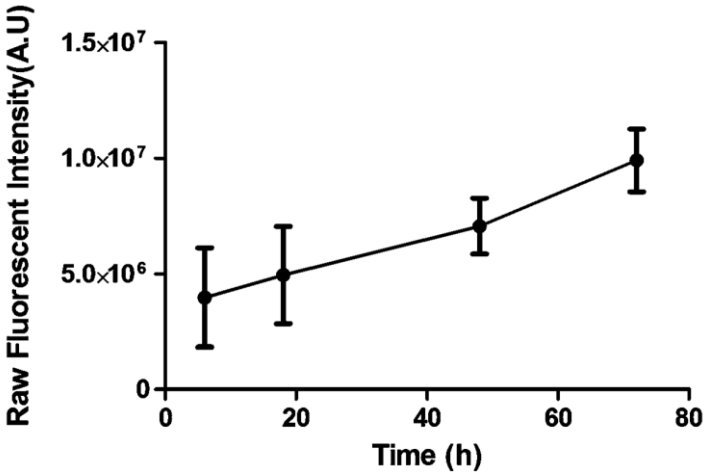

Figure 4.2.2. The plot demonstrating the cell growth inside the microfluidic chambers in terms of raw fluorescent intensities. Points depict the average raw fluorescent intensity density measurement of three different microchambers. Error bars represent the standard deviation [74].

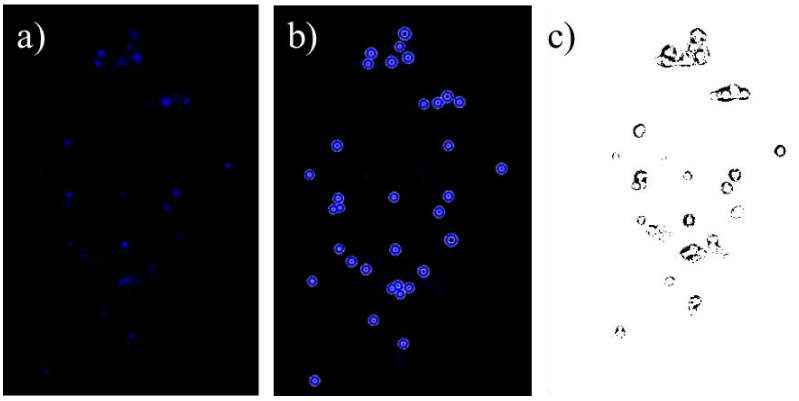

Figure 4.2.3. The DAPI image of MCF7 cells inside a cell culturing chamber a) before and b) after Hough Transform and c) Adaptive Thresholding, respectively.

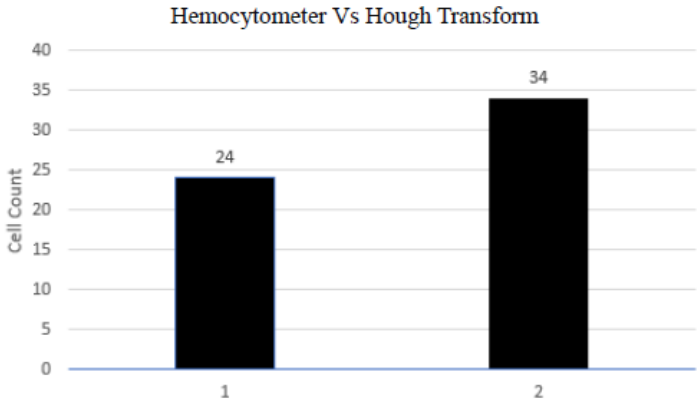

Figure 4.2.4. Cell counting with hemocytometer (1) vs. Hough Transform (2) for circle boundaries with radius range of [10,50].

According to analysis results of image processing, Circle Hough Transform could detect more cells compared to counting done with hemocytometer, thus, demonstrated itself as a more accurate alternative than hemocytometer for cell counting. However, this algorithm was used only in Hoechst stained MCF7 cell images inside the microfluidic chip. In order to prove that this algorithm is more effective then hemocytometer-based counting further tests with a large data bank existing of cell images inside the microfluidic devices should be used [92]. Also, even though the algorithm was successful for the images used, it requires cell staining. Instead, a K-means algorithm combined with Hough Transform could be developed as a future solution which could allow the knowledge of cell count from microscopy images without staining cells [91]. This can decrease photo-bleaching and phototoxicity during the fluorescence imaging.

- HepG2 human liver hepatocellular carcinoma epithelial cell line (ATCC®HB-8065™)

HepG2 cells were grown inside the microfluidic platform depicted in Figure 4.2.5 at single-cell level overnight. Cell images inside the culturing chamber were taken for morphology analysis upon incubation of cells overnight in the incubator (Figure 4.2.5.b).

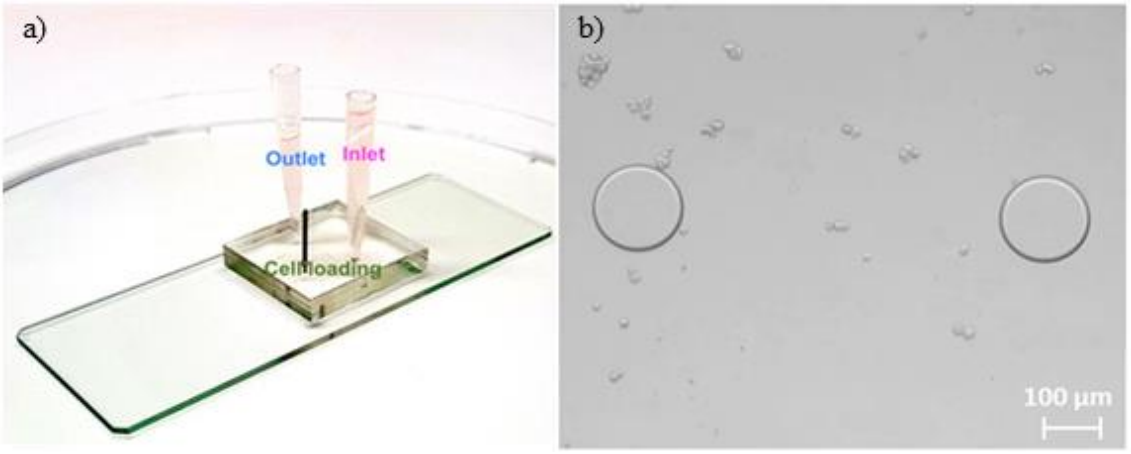

Figure 4.2.5. a) Microfluidic cell culturing platform for HepG2 cell morphology analysis. The chip consists of one inlet and one outlet for media flow. Cell loading hole was closed upon cell flow inside the culture chamber with a both ends closed metal pin. b) Microscopy image of the HepG2 cells inside the PDMS based microfluidic device overnight at 37 °C [75].

As expected, images of cells displayed cell heterogeneity [93]. Some cells developed cellular pseupodium while others remained circular. These cells either grew pseupodium in later phase of their inoculation or they never generated one. Figure 4.2.6 demonstrates the count of single cells that grew pseupodium upon overnight incubation inside the microfluidic culturing chip.

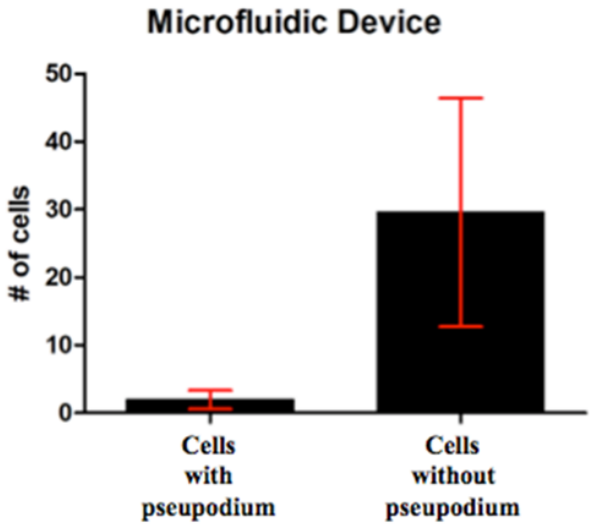

Figure 4.2.6. Plot of liver cancer cells in the microfluidic cell culturing platform with and without pseupodium based on single-cell analysis [75].

Our preliminary result presents the morphological difference in between liver cancer cell lines grown inside the tissue-culture petri dish and in the microfluidic device. As it can be seen from Figure 4.2.5, the HepG2 cells did not generate any pseupodium when they were cultured in the PDMS based microfluidic device. Still, in conventional culturing platform, we observed cells with pseupodium upon overnight incubation (Fig. 4.1.5). When we quantified the microscopy images of these two culturing platforms, two graphs showing the number of cells with and without pseupodium in our culturing platforms were obtained (Fig. 4.1.6, Fig. 4.2.6). These plots confirmed our observations quantitatively based on single-cell analysis data. The outcomes of this research are backing Xiaohui et al. who similarly deduced that growth of live liver cancer cells is less feasible on silicon wafer upon investigation of liver cells under scanning probe acoustic microscope (SPAM) [94]. When the cells did not develop pseupodium inside our microfluidic device, they could not adhere to the surface of the glass and grow. They remained alive only for a few days with the spherical morphology. Additionally, they formed cellular clusters. Therefore, we stained these clusters with Hoechst and PI since they are commonly used dyes for cell-based research for the separation of live and dead cells [95] [96] [97]. According to our examination, most of the cells were dead. In order to develop better immune therapies or molecularly targeted treatments it is important to increase our knowledge of the variations in the microenvironment and the dynamic relation between

the microenvironment and tumor ecosystem [98].Consequently, researchers must be careful about the restraints of microfluidic technologies when these devices are being developed. Because, not carrying a cautious investigation about the limitations of the microfluidic platforms might mislead us into contemplating about on-chip liver cancer spheroids with PDMS based microfluidic chip on a glass surface.

4.3 Cell culture and gradient generator using microfluidic platforms

Starting with the growth of MCF7 cells inside the microfluidic platforms of our cell culture device, we investigated the effects of chemical concentrations to these cells. For this study, we decided to develop a gradient generator chip to supply gradients of chemicals into our microfluidic cell culturing device through tubings (Figure 3.13). Usage of microfluidic gradient generator for medical research has become common since it provides researchers the tools to examine gradient-driven mechanisms that are essential for important biological processes at a cellular level [99]. In batch culture, sensitive flow concentrations and blood flow cannot be modelled and tested. In addition to generating mixtures of chemicals, our microfluidic gradient generator allows cells to be examined in flow mimicking *in vivo* cell environment which is an advantage of advanced cell culturing platforms while this is a drag for the conventional culturing platforms [38] [100].

The gradient chip platform allows the dilution of a chemical compound (Drug A) with PBS or the mixture of two different chemical agents (Drug A and Drug B) (Figure 3.13). Prior to experimenting with the cell culture device, we tested the gradient generator with dyes for performance check using blue and yellow food dyes. We supplied these dyes to the devices through tubings with a gravity-driven flow. Figure 4.3.1 shows the outcome of experiments with each outlet port giving the specific concentration of the dye mixture.

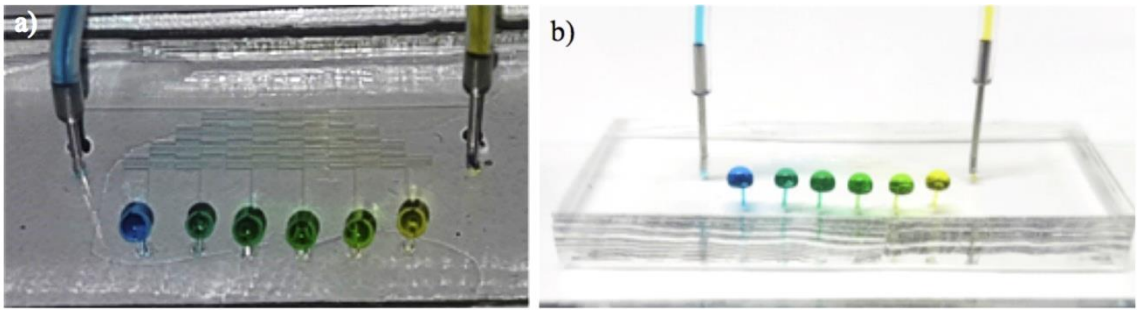

Figure 4.3.1. Images of the microfluidic gradient generator after testing with the blue and yellow food dyes [74].

Next, FITC solution was fed through the first inlet as explained in the methods section. In Figure 4.3.2 represents the image of the microfluidic gradient generator with the FITC dye. The light intensity increased linearly from left (0% FITC) to right (100% FITC) as shown in Figure 4.3.2c.

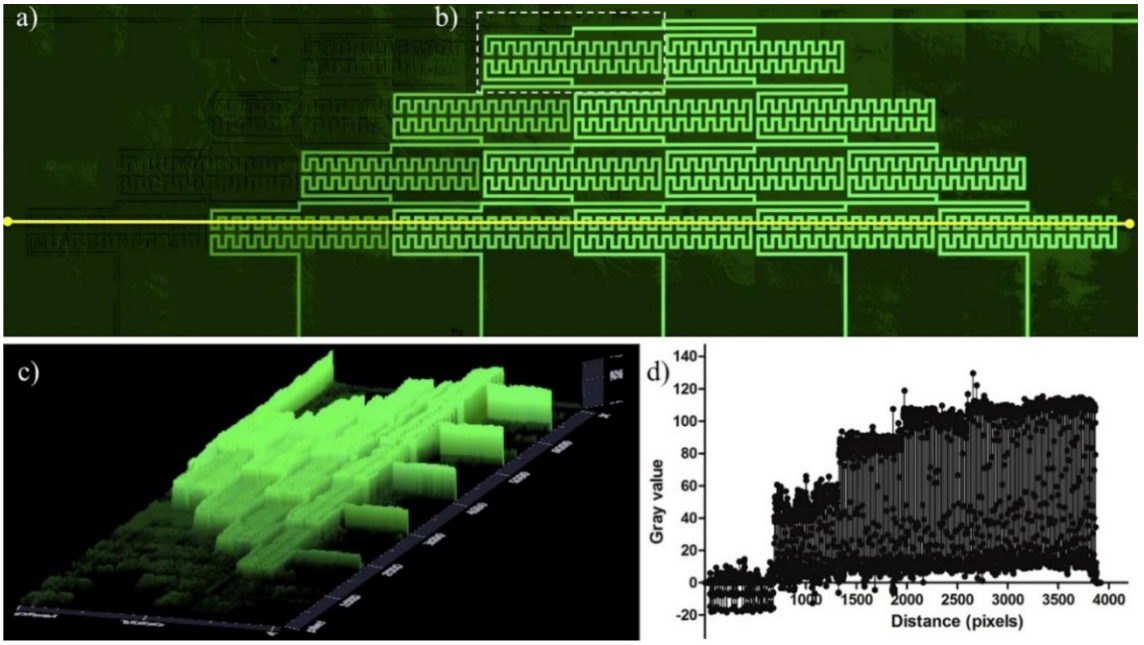

Figure 4.3.2. The microfluidic gradient generator with the FITC dye. (a) The tiled image of the gradient generator under steady-state flow (10 μL/h). (b) The diffusion of FITC and non-fluorescent buffer solutions in the microfluidic channel. Two solutions completely diffused together using a flow rate of 300 μL/h before bifurcation to produce 50 % FITC concentration. (c) The normalized 2.5D fluorescent intensity map of the gradient generator generated by ZEN 2 microscope software (Zeiss). (d) The gray value intensity alters along the yellow line illustrated in (a) show the stable distribution of FITC dye concentration in the concentration gradient generator [74].

After performing initial assays with dyes, first, we waited for our MCF7 cells to grow in the six microchambers of our microfluidic cell culture array. Then, we integrated the microfluidic gradient generator to the microfluidic cell culture platform through tubings (Figure 4.3.3). As a drug representative we delivered SDS solution to the gradient generator for acquiring the following concentrations, 0.005 %, 0.004 %, 0.003 %, 0.002 %, 0.001 % and 0 %, with PBS given from the other inlet. Figure 4.3.4 demonstrates the cells before and after SDS exposure. We quantified these images according to intensities to obtain the correlating graph in Figure 4.3.5. Thus, we presented the SDS concentration-dependent cell death in the microchambers.

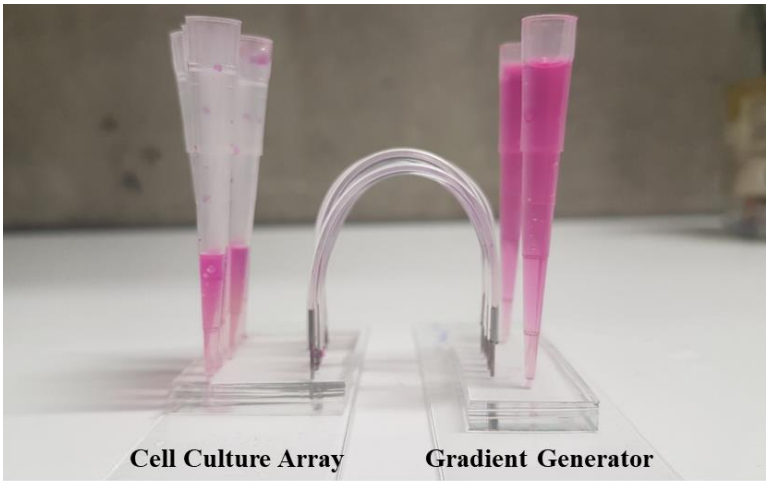

Figure 4.3.3. The image of the connected microfluidic cell culturing chip and gradient generator.

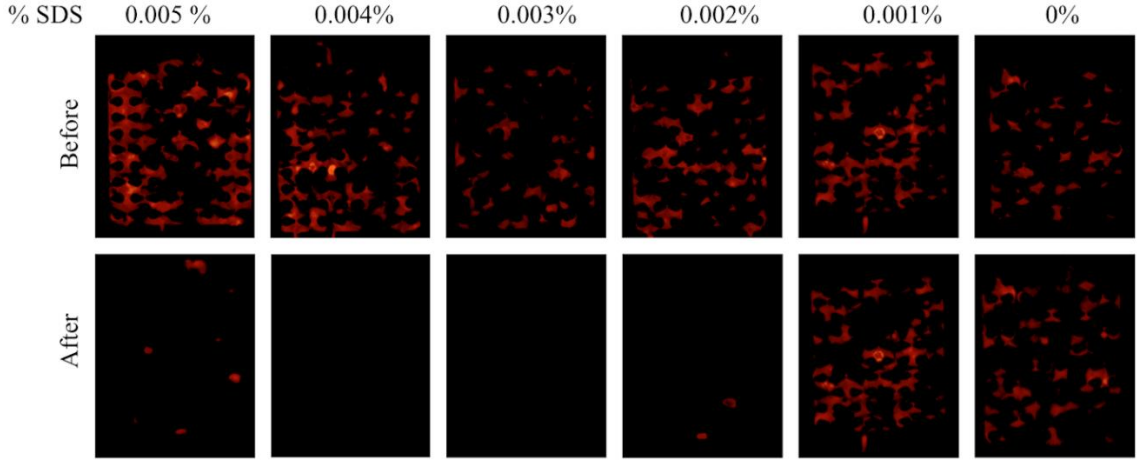

Figure 4.3.4. SDS exposure in the microfluidic platform. The images present the change in fluorescent intensity for pre- and post-SDS exposure for 0, 0.001%, 0,002%, 0.003%, 0.004%, and 0.005% SDS (wt/vol) [74].

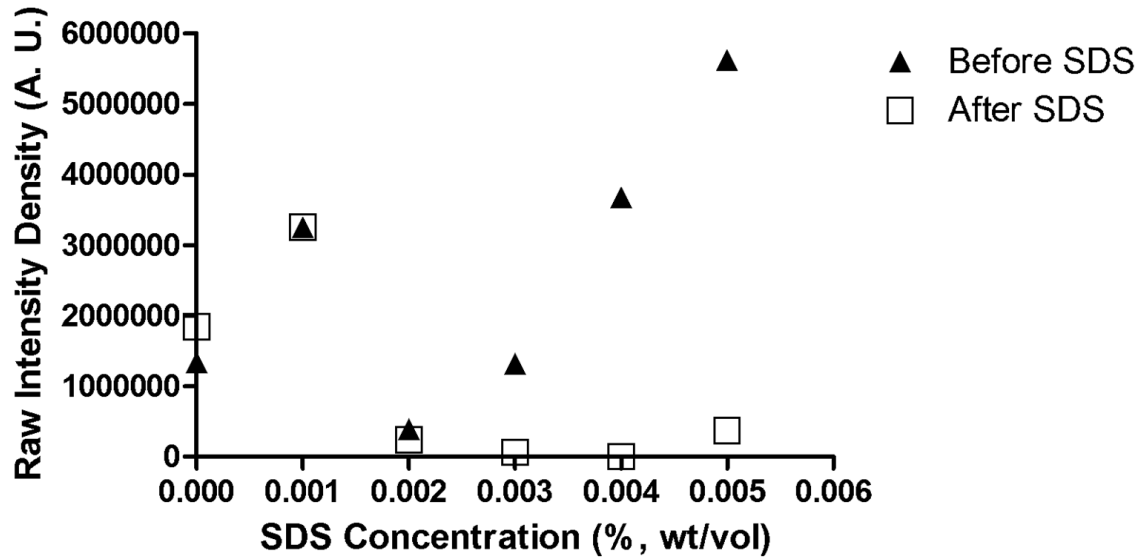

Figure 4.3.5. Raw fluorescent intensity densities of cells before and after SDS exposure in the microfluidic platform. The raw fluorescent intensity density prior to SDS exposure is illustrated with triangles. Squares show the fluorescent intensity densities post-SDS exposure [74].

The cell culture chip and the gradient generator chip introduced above can also be used separately from each other for different purposes. In the cell culture device with 6 independent platforms, six different cell types can be grown at the same time while 6 different concentrations of a chemical are being supplement to them via the gradient generator. Moreover, these controlled microenvironments can be observed with microscope thus allowing automated quantification of cell images.

Here, we created a microfluidic platform with relatively simple fabrication and operation concerns compared to previously reported devices [Table 4.1]. Our chips can be utilized for culturing cells, generating gradients of a chemical and inducing chemical stress into grown cells in their microchambers. Furthermore, because of their simplicities, these microfluidic devices minimize experimental deviations and accomplishes practical automation.

Application		Parallelization (chambers or wells)	Automation	Sensor integration
Cell culture	a. Cancer Cells	384 [39], 96 [101,[102], [103], [104]] 64 [105], 24 [106,107,108], 16 [109], 12 [45,110], 1 [111,112,113]	Data acquisition Fluid handling Environmental control	Pressure sensor pH sensor Thermal sensor
	b. Stem Cells	96 [114,115], 75 [116], 10 [117], 6 [50], 3 [60], 1 [112,118,119]	Data acquisition Fluid handling Environmental control	Thermal sensor pH sensor Pressure sensor
	c. Organ-on-chip	6 [120,121], 4 [122], 2 [123], 1 [124,125,[126], [127], [128], 129]	Data acquisition Environmental control Fluid handling	Fiber Optic sensors (O_2) Temperature sensor & controller pH, DO, CO_2sensor
	d. Body-on-chip	2 [130], 1 [131]	Data acquisition Fluid handling	Optical sensors
	e. other cells	96 [132], 6 [133], 3 [62], 2 [134]	Data acquisition fluid Handling Environmental control	Pressure sensor pH sensor Thermal sensor
Drug screening		32 [135] 8 [136], 4 [137,138], 5 [139], 7 [108], 2 [129], 1 [[140], [141], [142]]	Data acquisition fluid Handling, motion tracking system, Image acquisition	–
Cryopreservation of cells		96 [143], 1 [144]	Data analysis	–

Table 4.1. Examples of microfluidic devices used for specific applications at different parallelization, automation and sensor integration levels [36].

Within our knowledge, pure cell cultures were grown *in vitro* firstly more than 100 years ago [145]. Hung *et al* introduced the first continuous perfusion microfluidic cell culture array to grow and monitor cells for long periods of time in 2004 [146]. Today, researchers are still producing novel tools to acquire more realistic physiochemical growth conditions for the cells, and automated quantification methods for their analysis [150-153]. Our technique supplies a simple and cost-effective way for cell culturing and economical way to culture cells and to add a gradient of a chemical into these cells when they were close to their natural microenvironment due to the small scale of the microchambers. Also, all our presented microdevices were compatible for gravity-based and syringe pump-produced flows. Cell mediums could be given through gravity-based continuous flow. Thus, thank to this flow, syringe-pump-free assays could be performed and transferred to the incubator easily. Therefore, our microfluidic chips might be suitable for most of research and clinical laboratories. Additionally, microfluidic concentration gradient generators have made an important contribution to biological operations for quantitative researches of chemotaxis, growth factor experiments and migration studies [153].

We designed a SDS concentration gradient utilizing a Christmas tree type gradient generator, created by Jeon *et al* in 2000 [154]. This gradient generator has been studied broadly; Toh *et al* stated its typical operating feaurures for gradient stabilization in an outstanding review article [155]. Hence, we targeted the utilization of this platform rather than its characterization in our experiments. As Beta and Bodenschatz reviewed, the most common use of this platform is in investigating cellular chemotaxis. Hence, it was convenient for single-cell research, which involved a well-controlled spatiotemporal microenvironment and short experiment time, such as following cellular responses to fast switches of chemical gradients [156]. As mentioned above, Hung *et al* demonstrated the utilization of a 2D concentration gradient that was very similar to our work, where they directly connected the cell culture microchambers to microchannels of the gradient mixer [152]. This study was one of the pioneering works that implemented by Jeon and co-workers for high-throughput cell-based experiments. Nevertheless, our proposed gradient generator chip is more practical in terms of fabrication and operation. The future trend of these technologies would focus more on translational research for clinical applications, such as Berthier and co-workers' arrayed high-content chemotaxis assay for patient

diagnostics [157]. From a broader perspective, we anticipate that microfluidic platforms would be rapidly developed and modified for simple applications, high sensitivity, high accuracy and high throughput automation to achieve a noteworthy contribution to bench-to-bedside researches.

4.4 Integration of IV fluids using conventional growth environment

Evey year, a large number of patients are treated with intravenous fluids (IVFs). Lately, scientists have been focusing on recent cell-based medication approaches in which IVFs are essential to a large extent. Accordingly, the effect of IVFs on patients has been examined in referring to critical care practice [158, 159, 160, 161, 162]. Most of the investigations on IVFs have addressed to disclosing their influence on treatment stability, compatibility and administration [163]. Until now, there have been minor quantitative *in vitro* studies concerning the effect of IVFs on cellular level (Table 4.4.1). In our study, leaning towards the cell-based strategies, we presented the responses of U937 monocytes, U937-differentiated macrophages, HepG2 liver cancer and MCF7 breast cancer cells when they were exposed to IVFs.

IVF	Cell line	Method	Result	Raised Question	Ref.
Hyperton ic saline (HTS)	Human colon cancer cells (LS174T), Human umbilical vein endothelial cells (HUVECS)	In vitro: Flow cytometry, fluorescence microscopy	HTS reduces adhesion molecule and laminin expression. HTS did not alter cell viability.	How does hypertonic saline contribute metastasis?	163
Plasma-activated lactated Ringer (PAL)	Human pancreatic cancer cells (Capan-2, BxPC-2, AsPC-1/CMV-Luc, MIA PaCa-2)	In vitro: Microscopy, Absorbance. In vivo: Mouse model (BALB/c Slc-nu/nu mice)	PAL induces apoptosis in pancreatic cancer cells	Is PAL convenient to be used as a therapeutic for peritoneal metastasis?	164
Hyperton ic saline (HTS)	Brain endothelial cells (bEnd.3)	In vitro: Flow cytometry, RNA-seq, Quantitative real-time polymerase chain reaction, western blot, enzyme-linked immunosorbent assay	40 mmol/L NaCl HTS enhances cell viability and attenuates cell apoptosis.	How do the levels of IL-1β and EGFR is correlated to the performance of HTS and apoptosis?	165
Hyperton ic saline (HTS)	HeLa cells	In vitro: Biochemical analysis, hemocytometry , microscopy	Increasing NaCl concentration more than 130 mM decreases growth rate, increases protein levels, and cell volume.	Ionic and osmotic effects of HTS in the metabolism of HeLa cells	166
Hyperton ic sucrose (HTSu)	Human leukemia cells(U937)	In vitro: Percoll gradient, ion concentration measurement, microscopy	U937 cells developed apoptosis thanks to regulatory volume increase in HTSu.	Are U937 cells capable of being a model organism to study cellular volume regulation?	167

IVF	Cell line	Method	Result	Raised Question	Ref.
Hyperton ic D-glucose (HTD-g)	Human breast cancer cells (MCF7)	In vitro: MTT assay, Comet assay, flow cytometry	HTD-g reduces the viability, increases the apoptosis and DNA damage of the MCF7 cells	Does HTD-g induce cytotoxic, genotoxic, and apoptotic effects in tumor cells?	168

Table 4.4.1. Comparison of *in vitro* studies for IVF.

First, we quantified the number of live and dead cells using hemocytometry and fluorescent microscopy imaging data for the U937 monocytes, U937-derived macrophages, MCF7, and HepG2 cancer cell lines after incubating cells in IVFs for 15 minutes. Upon 15-minute incubation, cell viability of the U937 monocyte cells significantly decreased in IVFs while they were preserved in PBS (Fig. 4.4.1a and Fig. 4.4.1b). We evaluated the differences in the changes of surface area and cell nuclei based on the microscopy images of the U937 cells in IVFs and PBS (Fig. 4.4.1c, Fig.4.4.1d, Fig. 4.4.2a). Next, we used flow cytometry to examine a larger number of cells to confirm single-cell analysis data obtained with hemocytometer and microscopy images [169]. We separated dead cells from live cells through PI staining [95]. We investigated cell morphologies via forward scatter and side scatter data (Fig. 4.4.2, Fig. 4.4.3, Tables 4.4 and 4.5) [170]. Then, we performed the same experiments and analyses for U937-derived macrophages, MCF7, and HepG2 cancer cell lines as well in triplicates.

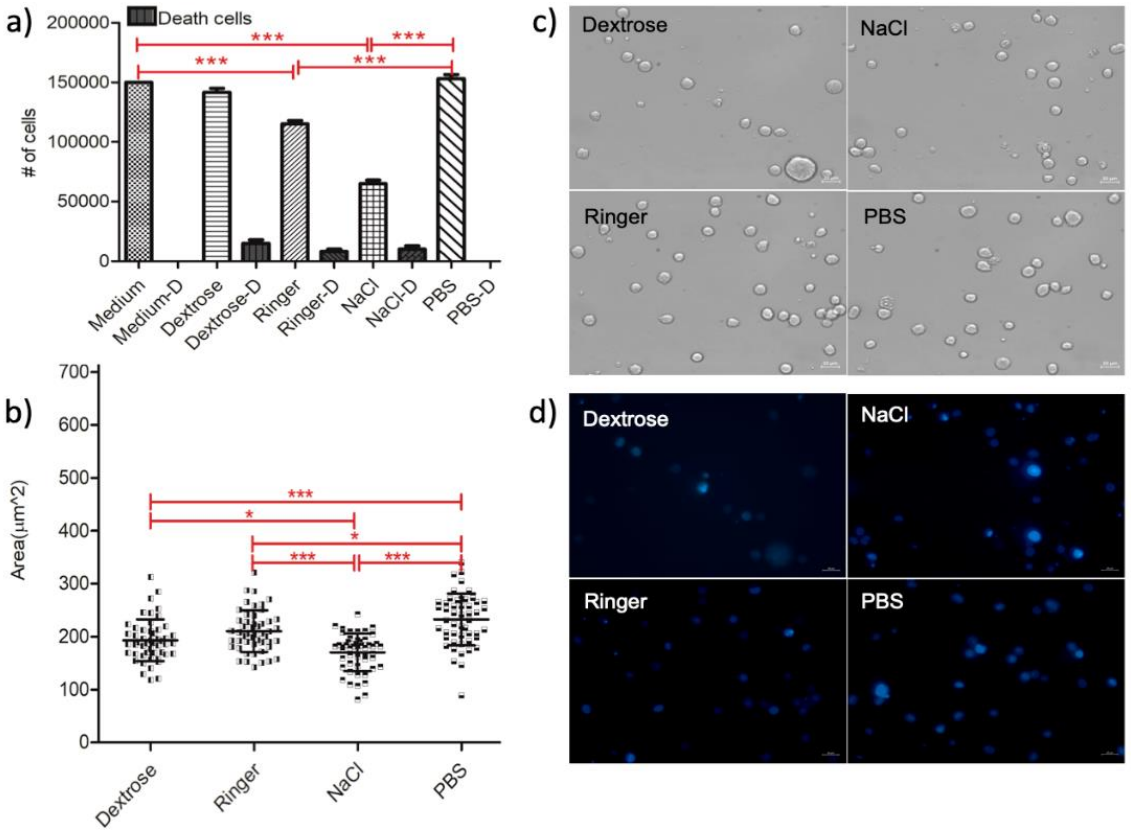

Figure 4.4.1. Plots and correlating microscopy images showing cell viability and cellular area of the U937 monocyte cells. a) Cell viability graph of U937 monocytes showing the number of cells after incubation in IVF, medium and PBS for 15 minutes. One-way ANOVA Tukey's Multiple Comparison Test is applied, $p < 0.05$ is significant. b) Surface area measurements of the U937 monocytes presented upon IVF treatment, medium and PBS incubations for 15 minutes. One-way ANOVA Tukey's Multiple Comparison Test is applied, $p < 0.05$ is significant. c) The phase images of the U937 monocytes are obtained by the inverted fluorescent microscope after 15 minutes incubation in PBS, Dextrose, Ringer and NaCl solutions with 12,5 ms exposure time. d) Fluorescence microscopy images of the DAPI stained U937 monocytes, exposure time: 300 ms. The scale bar shows 20 µm. Data are representative of three independent experiments and the values are expressed in mean ± s.d.

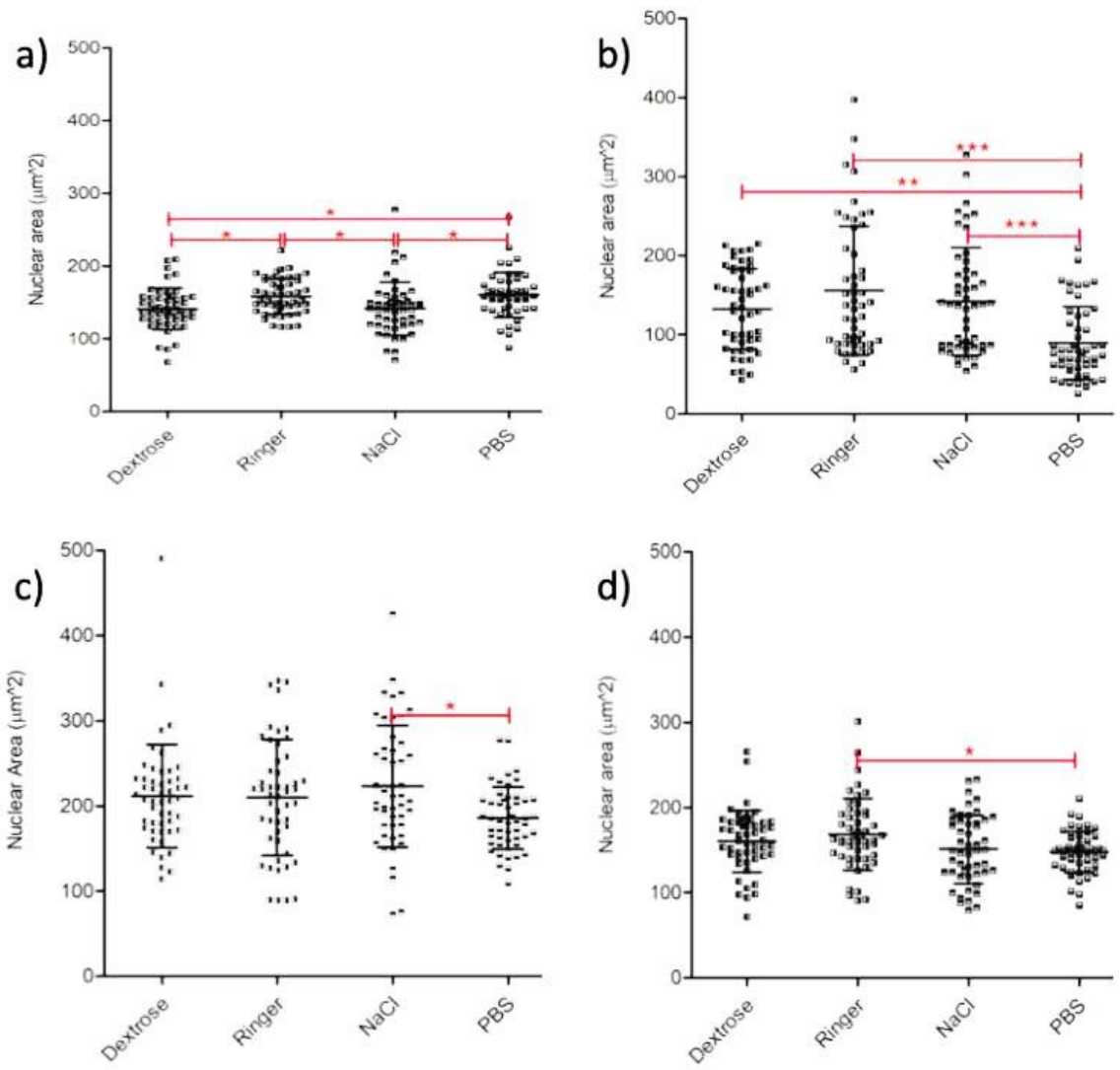

Figure 4.4.2. Nucleus size of the IVF-treated cell lines. a) U937 monocytes, b) U937-differentiated macrophages, c) HepG2, d) MCF7 cells. Analysis of the nucleus size with mean and standard deviations after 15 minutes incubation in Dextrose, NaCl, Ringer and PBS. One-way ANOVA Tukey's Multiple Comparison Test was performed, $p < 0.05$ is significant. Three independent experiments were performed.

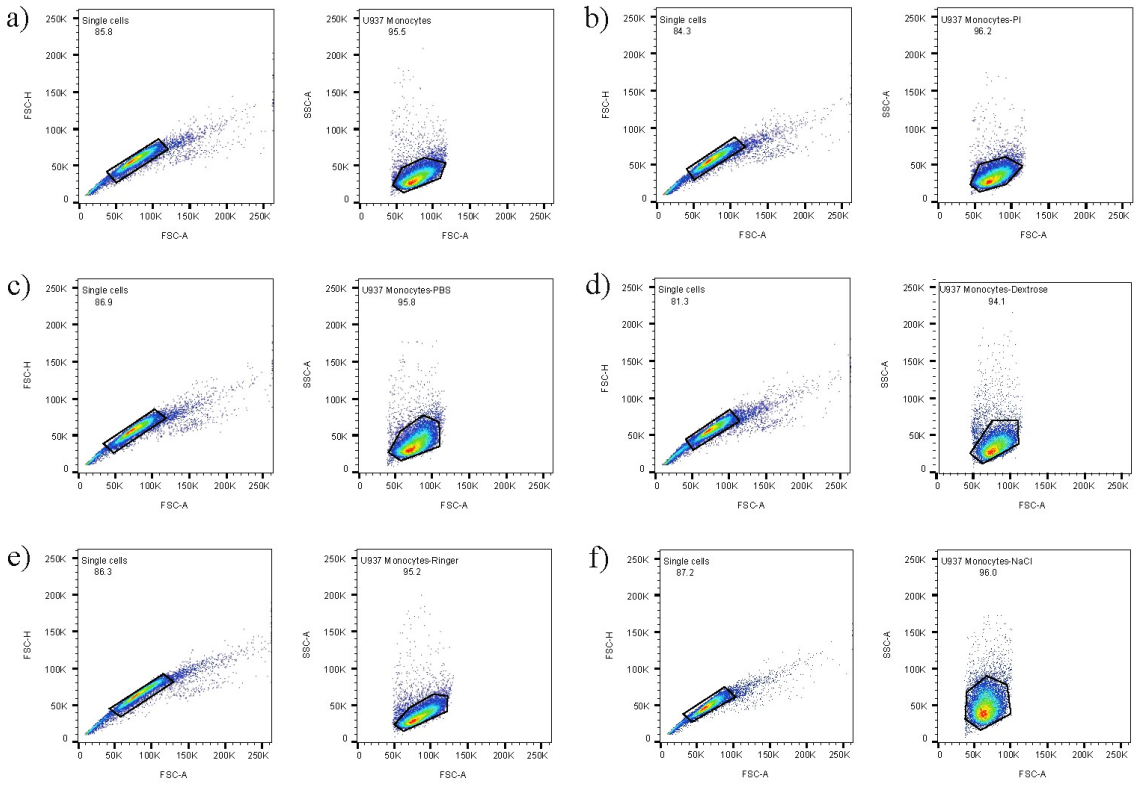

Figure 4.4.3. Forward scatter (FCS) vs. side scatter (SSC) data are illustrated in the dot display mode, and the core population of the U937 cells is surrounded by a gate for confirming cell morphology changes in IVFs. (a) The U937 monocytes without staining with PI and incubation in IVFs. (b) U937 monocytes with PI staining and without incubation in IVFs. U937 monocytes with PI staining and 15 minutes incubation in (c) PBS, (d) Dextrose, (e) Ringer, (f) NaCl.

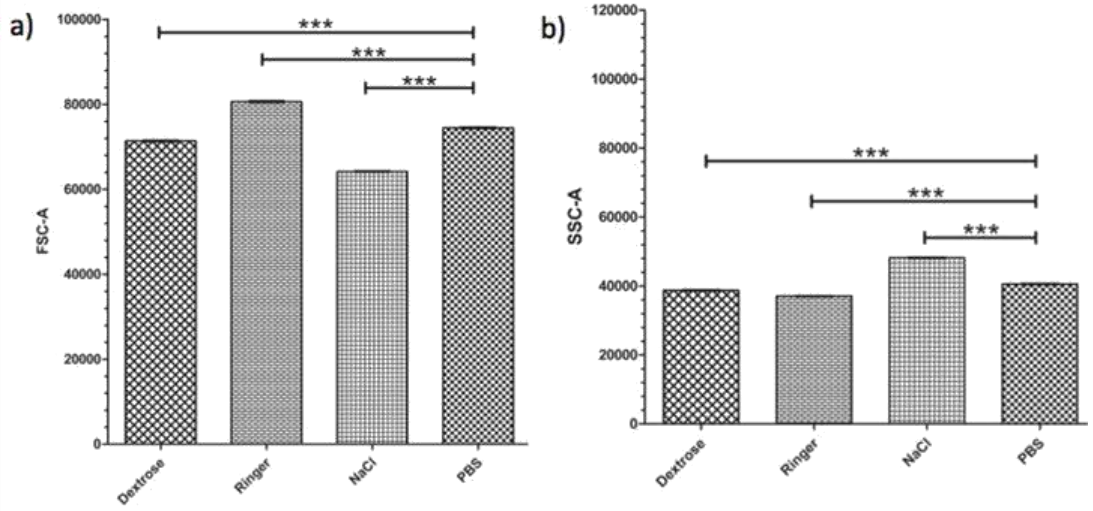

Figure 4.4.4. Statistical t-test analysis for the U937 monocyte data obtained in S2 Figure, (a) Forward scatter, (b) Side Scatter.

After incubating in IVFs, viability of the U937-differentiated macrophages significantly decreased, and their cellular area increased in IVF solutions (Fig. 4.4.5). The alterations in the area of nucleus size and the results of the flow cytometry analyses can be found in Figures 4.4.2, Figure 4.4.6 and Figure 4.4.7.

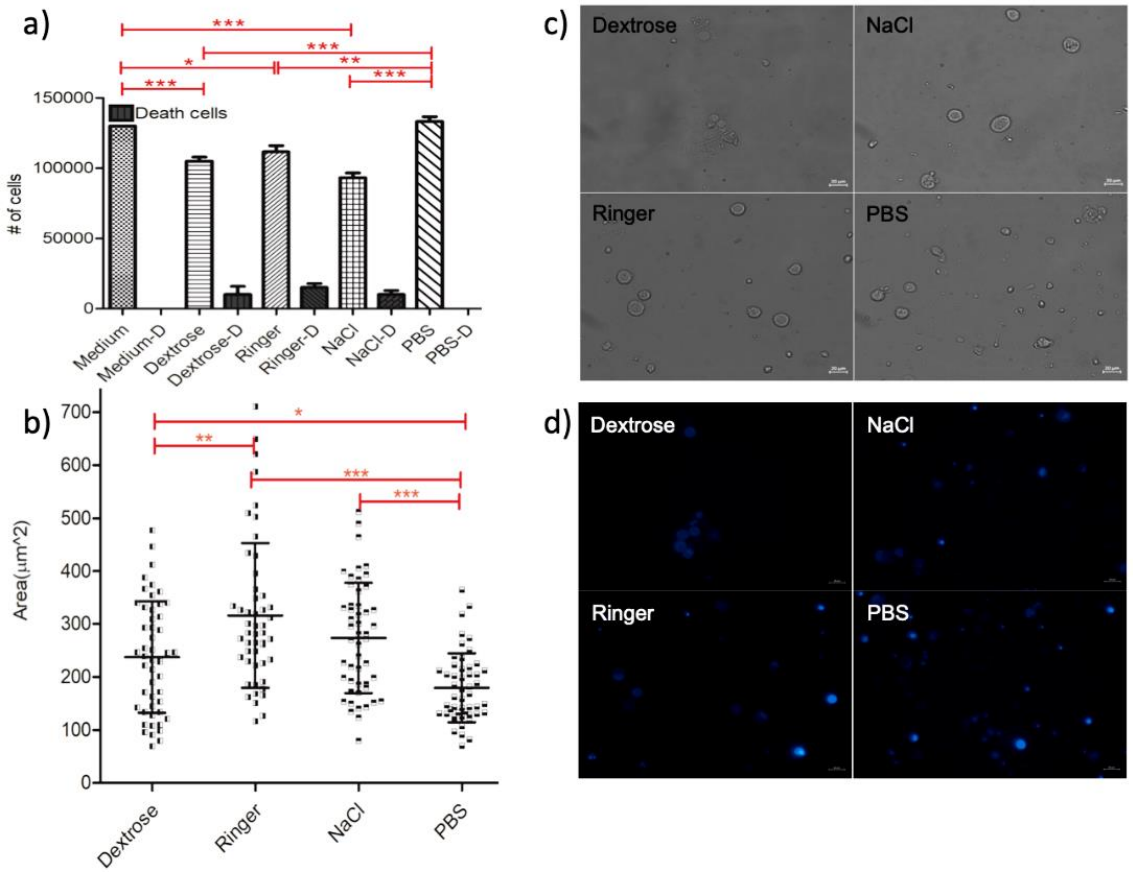

Figure 4.4.5. Plots and correlating microscopy images showing cell viability and cellular area of the U937-differentiated macrophages. a) Cell viability graph of the macrophages showing the number of live and dead cells after incubation in IVF, medium and PBS for 15 minutes. One-way ANOVA Tukey's Multiple Comparison Test is applied; $p < 0.05$ is significant. b) Surface area measurements of the macrophages presented upon IVF, medium and PBS incubations for 15 minutes. One-way ANOVA Tukey's Multiple Comparison Test is applied; $p < 0.05$ is significant. c) The phase images of macrophages are taken by inverted fluorescent microscopy after 15-minute incubation in PBS, Dextrose, Ringer and NaCl with 12,5 ms exposure time. d) Fluorescence microscopy images of the DAPI stained U937-differentiated macrophages, exposure time: 300 ms. The scale bar shows 20 µm. Data are representative of three independent experiments and the values are expressed in mean ± s.d.

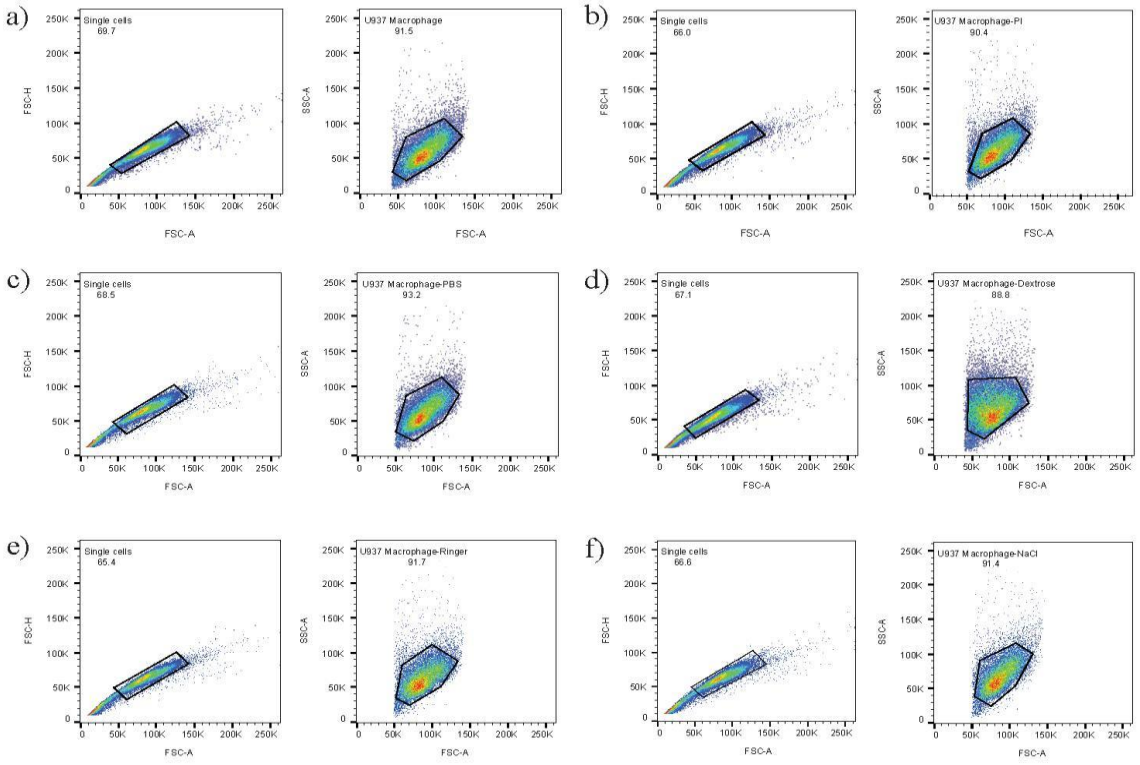

Figure 4.4.6. Forward scatter (FCS) vs. side scatter (SSC) data are depicted in the dot display mode, and the core population of the U937-differentiated macrophages is surrounded by a gate for confirming cell morphology changes in IVF. (a) The U937-differentiated macrophages without staining with PI and incubation in IV fluids. (b) U937 monocytes with PI staining and without incubation in IVF. Macrophages with PI staining and 15 minutes incubation in PBS (c), in Dextrose (d), in Ringer (e), in NaCl (f).

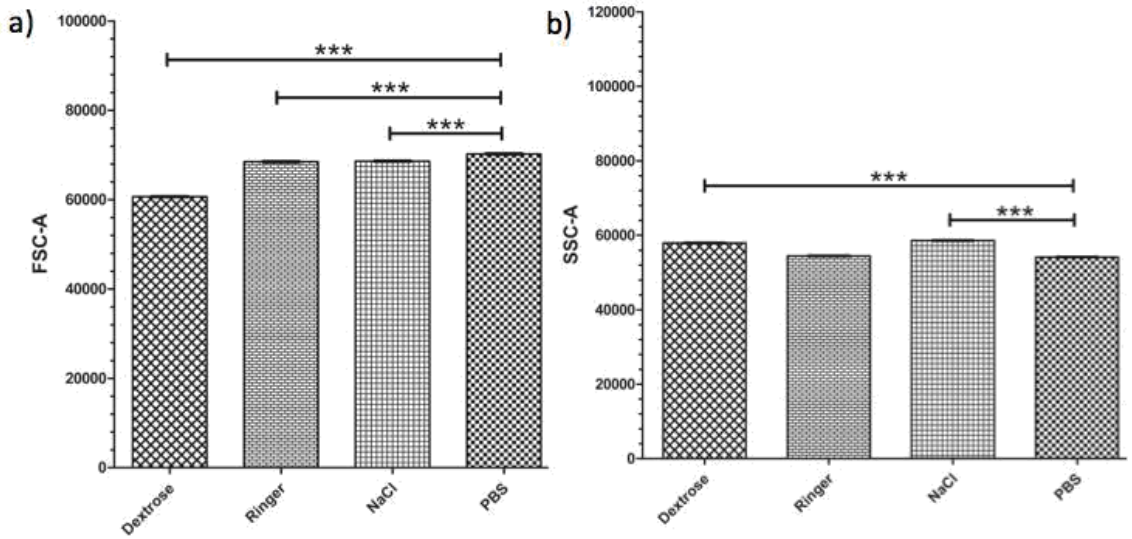

Figure 4.4.7. Statistical t-test analysis for the U937-differentiated macrophage data obtained in Figure S5, (a) Forward scatter, (b) Side Scatter.

Upon exposure to IVFs for 15 minutes, NaCl significantly decreased the viability of the HepG2 cells and their cellular area compared to other solutions (Figure 4.4.8). The analysis of the changes in the nucleus-size of HepG2 cells in IVFs and the flow cytometry data can be found in Figure 4.4.2, Figure 4.4.9 and Figure 4.4.10.

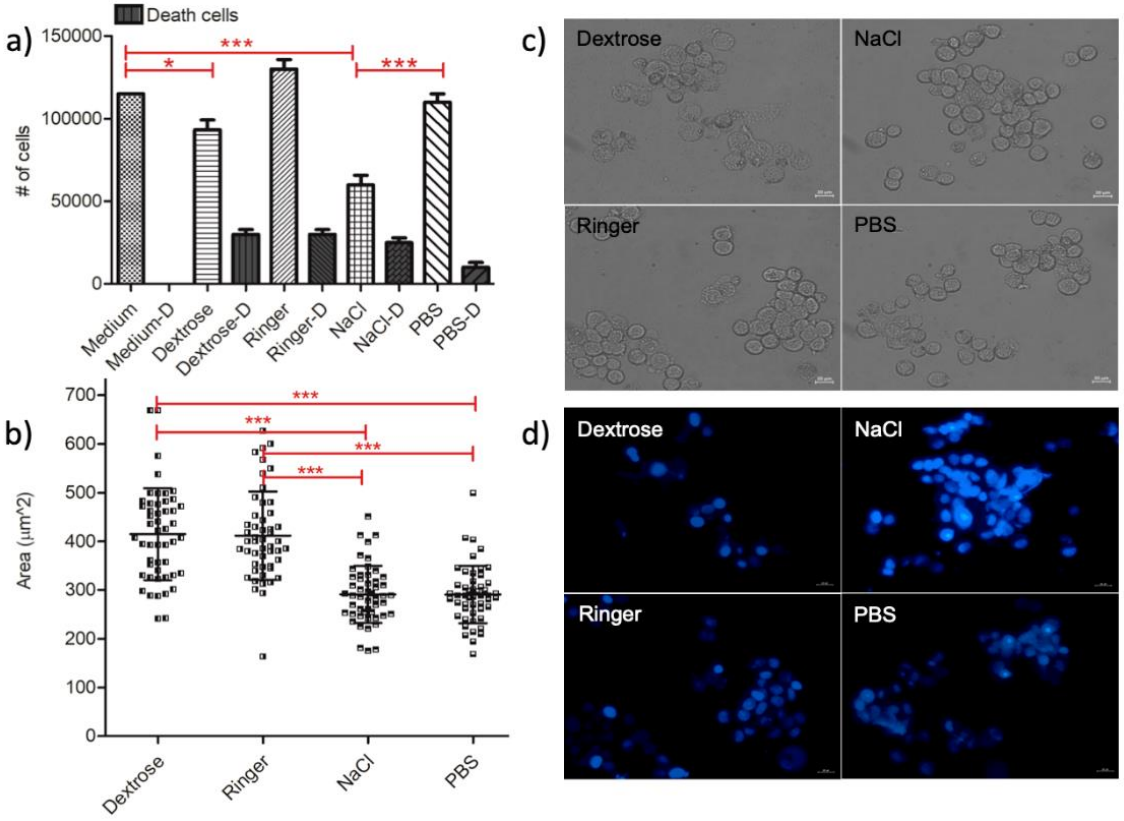

Figure 4.4.8. Plots and correlating microscopy images showing cell viability and cellular area of the HepG2 cells. a) Cell viability graph of the macrophages showing the number of live and dead cells after incubation in IVF, medium and PBS for 15 minutes. One-way ANOVA Tukey's Multiple Comparison Test is applied; $p < 0.05$ is significant. b) Surface area measurements of the HepG2 after IVF, medium and PBS incubations for 15 minutes. One-way ANOVA Tukey's Multiple Comparison Test is applied; $p < 0.05$ is significant. c) The phase images of macrophages are taken by inverted fluorescent microscopy after 15-minute incubation in PBS, Dextrose, Ringer and NaCl with 12,5 ms exposure time. d) Fluorescence microscopy images of the DAPI stained HepG2 cells, exposure time: 300 ms. The scale bar shows 20 µm. Data are representative of three independent experiments and the values are expressed in mean ± s.d.

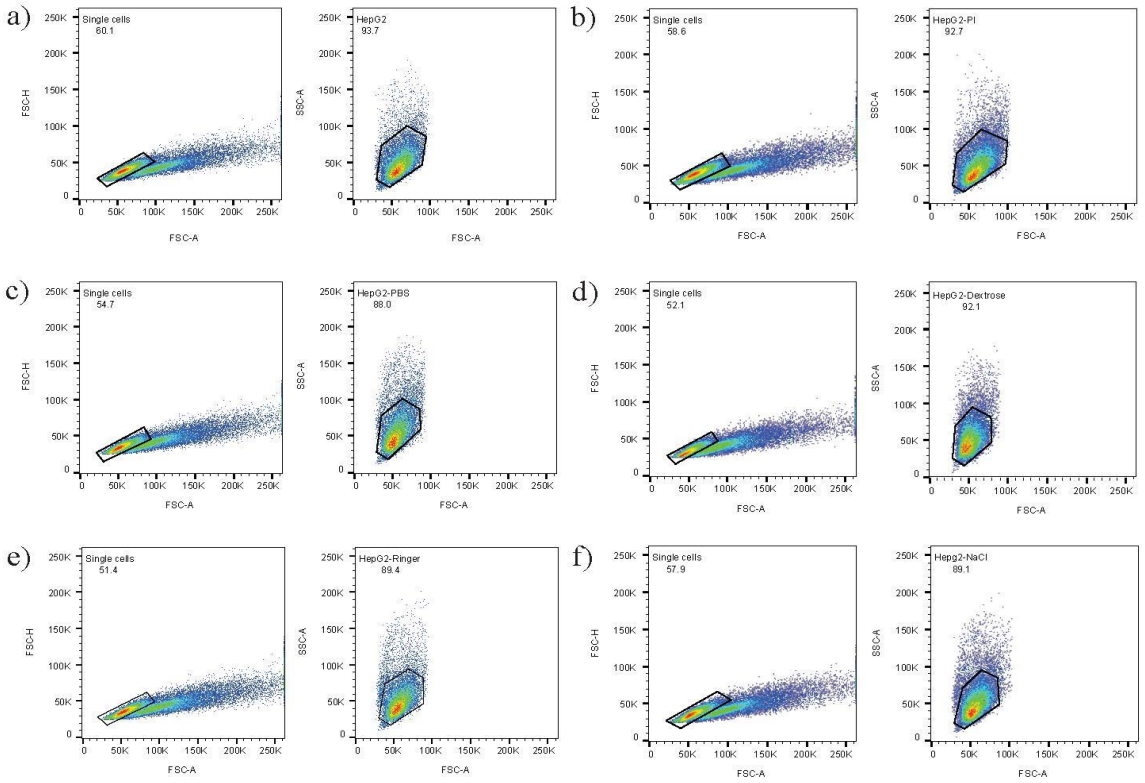

Figure 4.4.9. Forward scatter (FCS) vs. side scatter (SSC) data are depicted in the dot display mode, and the core population of the HepG2 cells is surrounded by a gate for confirming cell morphology changes in IV fluids. (a) The HepG2 cells without staining with PI and incubation in IV fluids. (b) The HepG2 cells with PI staining and without incubation in IV fluids. The HepG2 with PI staining and 15 minutes incubation in PBS (c), in Dextrose (d), in Ringer (e), in NaCl (f).

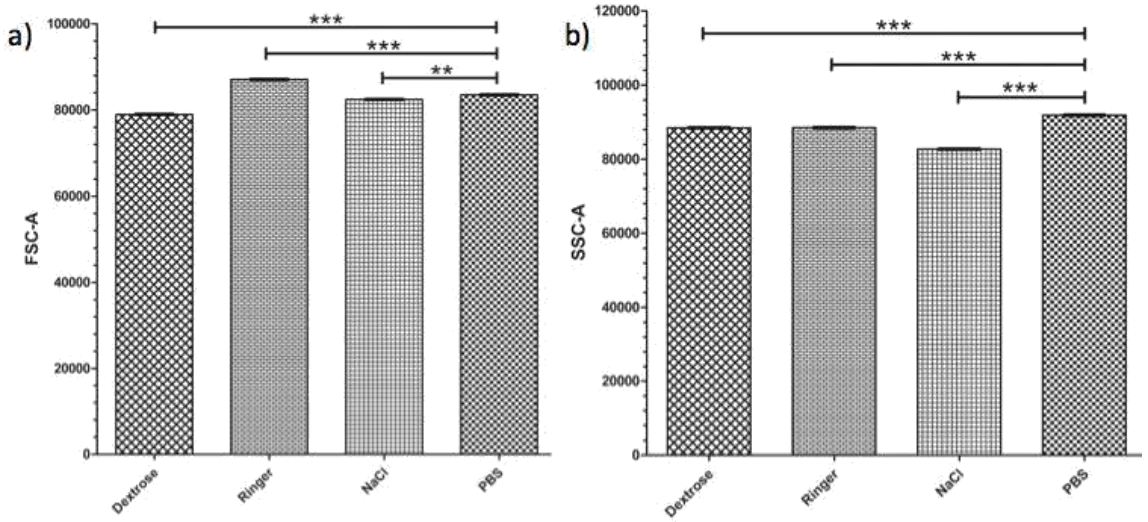

Figure 4.4.10. Student's t-test analysis for the HepG2 cells obtained in Figure S8, (a) Forward scatter, (b) Side Scatter comparison.

After incubating MCF7 cells in IVFS, Ringer solution significantly increased the viability of the MCF7 cells compared to other solutions; all IVFs increased the cellular area of the MCF7 cells (Figure 4.4.11). The plots for the analysis of the changes in the MCF7 cell nucleus-size with IVFs and the flow cytometry data can be found in Figure 4.4.2, Figure 4.4.12 and Figure 4.4.13.

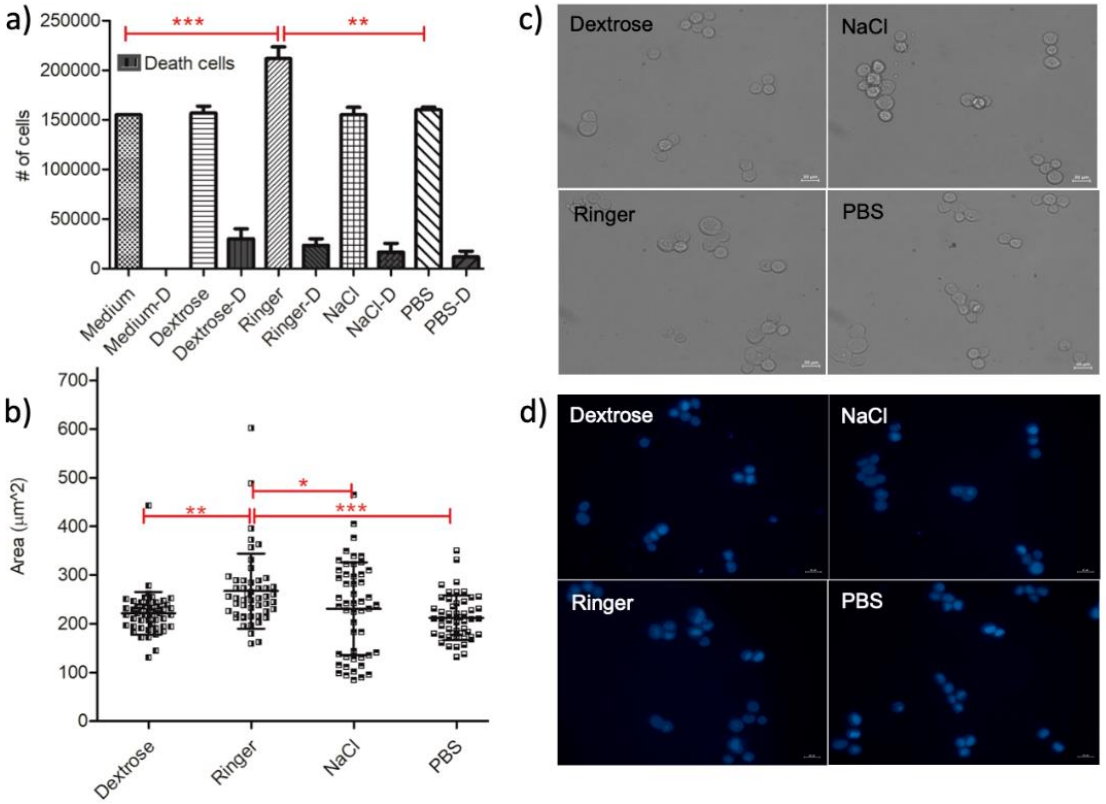

Figure 4.4.11. Plots and correlating microscopy images showing cell viability and cellular area of MCF7 cells. a) Cell viability graph of the macrophages showing the number of live and dead cells after incubation in IVF, medium and PBS for 15 minutes. One-way ANOVA Tukey's Multiple Comparison Test is applied; $p < 0.05$ is significant. b) Surface area measurements of the MCF7 presented upon IVF, medium and PBS incubations for 15 minutes. One-way ANOVA Tukey's Multiple Comparison Test is applied; $p < 0.05$ is significant. c) The phase images of macrophages are taken by inverted fluorescent microscopy after 15-minute incubation in PBS, Dextrose, Ringer and NaCl with 12,5 ms exposure time. d) Fluorescence microscopy images of the DAPI stained MCF7 cells, exposure time: 300 ms. The scale bar shows 20 µm. Data are representative of three independent experiments and the values are expressed in mean ± s.d.

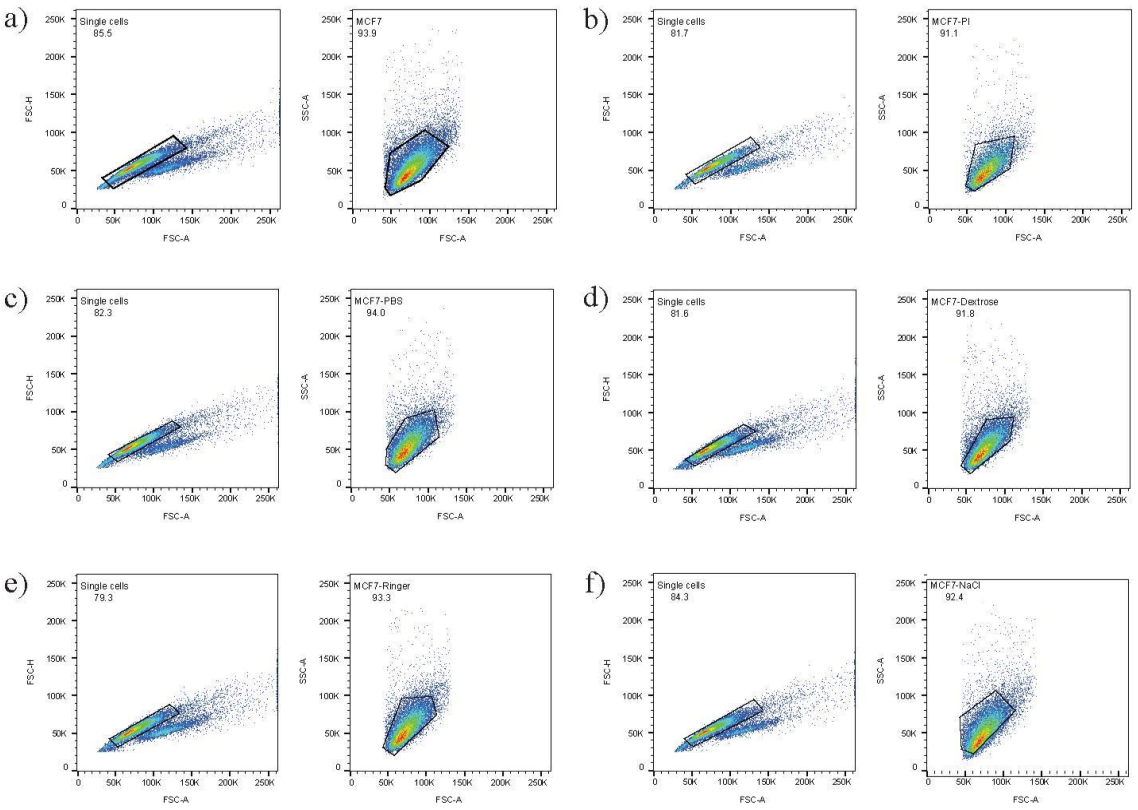

Figure 4.4.12. Forward scatter (FCS) vs. side scatter (SSC) data are depicted in the dot display mode, and the core population of the MCF7 cells is surrounded by a gate for confirming cell morphology changes in IV fluids. (a) The MCF7 cells without staining with PI and incubation in IV fluids. (b) The MCF7 cells with PI staining and without incubation in IV fluids. The MCF7 with PI staining and 15 minutes incubation in PBS (c), in Dextrose (d), in Ringer (e), in NaCl (f).

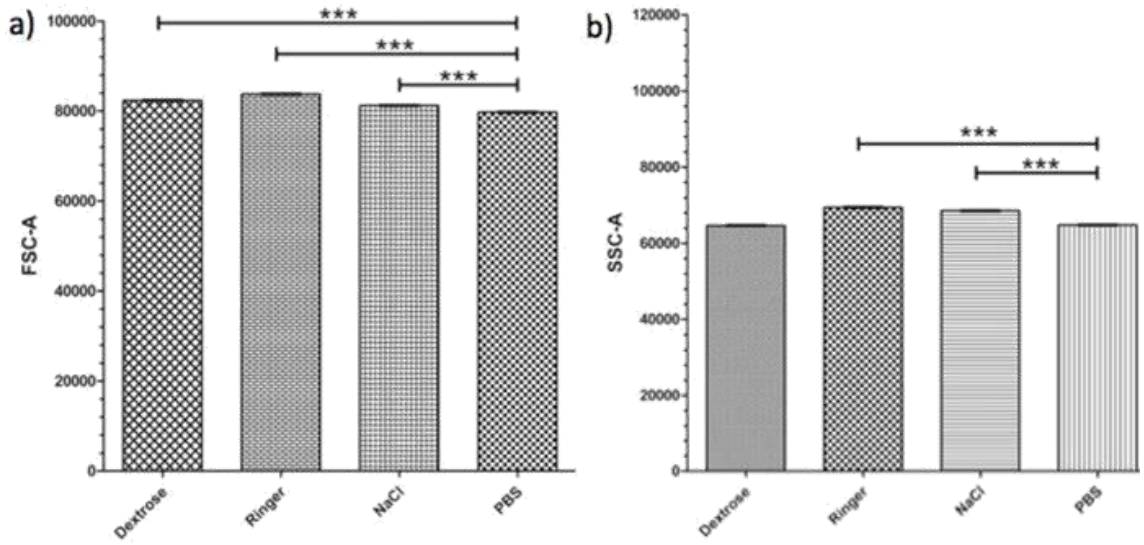

Figure 4.4.13. Statistical t-test analysis for the MCF7 cells obtained in Figure S11, (a) Forward scatter, (b) Side Scatter comparison.

According to the One-way ANOVA Tukey's Multiple Comparison Test, we listed the response of U937 monocyte, U937-differentiated macrophage, HepG2, and MCF7 cells in Table 4.4.2 and Table 4.4.3. Our single-cell analysis outcomes revealed that the viability of the immune cells decreased more than that of cancer cells when they were incubated in IVFs (Table 4.4.2). The statistical analysis of the forward and side scatter data obtained using flow cytometry can be found in Table 4.4.4 and Table 4.4.5.

Viability	**Dextrose**	**Ringer**	**NaCl**	**Medium**
U937 Monocyte	ns	***	***	ns
U937-differentiated Macrophage	***	**	***	ns
HepG2	ns	ns	***	ns
MCF7	ns	**	ns	ns

Table 4.4.2. One-way ANOVA Tukey's Multiple Comparison Test results for the viability of U937 monocytes, macrophages, HepG2, and MCF7 cells in IVF relative to PBS. $p < 0.05$ is significant.

	Dextrose		**Ringer**		**NaCl**	
Area measurements	Surface	Nucleus	Surface	Nucleus	Surface	Nucleus
U937 Monocyte	***	*	*	ns	***	*
U937-differentiated Macrophage	*	**	***	***	***	***
HepG2	***	ns	***	ns	ns	*
MCF7	ns	ns	***	*	ns	ns

Table 4.4.3. One-way ANOVA Tukey's Multiple Comparison Test results for the cellular area and nuclear area measurements of the U937 monocytes, macrophages, HepG2, and MCF7 cells in IVF relative to PBS. $p < 0.05$ is significant.

Cell Lines	Dextrose	Ringer	NaCl
Monocyte	*** (p< 0.0001)	*** (p< 0.0001)	*** (p< 0.0001)
Macrophage	*** (p< 0.0001)	*** (p< 0.0001)	*** (p< 0.0001)
HepG2	*** (p< 0.0001)	*** (p< 0.0001)	** (p=0.0013)
MCF7	*** (p< 0.0001)	*** (p< 0.0001)	*** (p< 0.0001)

Table 4.4.4. Student's t-test results based on forward scatter comparison using flow cytometry data.

Cell Lines	Dextrose	Ringer	NaCl
Monocyte	*** (p< 0.0001)	*** (p< 0.0001)	*** (p< 0.0001)
Macrophage	*** (p< 0.0001)	ns (p=0.2188)	*** (p< 0.0001)
HepG2	*** (p< 0.0001)	*** (p< 0.0001)	*** (p< 0.0001)
MCF7	ns (p<0.6259)	*** (p< 0.0001)	*** (p< 0.0001)

Table 4.4.5. Student's t-test results based on side scatter comparison using flow cytometry data.

Among IVFs used in treatments, dextrose solution is one of the most frequently applied diluents in clinics. Nevertheless, new investigations have disclosed an increasing concern over the safety of dextrose solution [171]. This is because dextrose is a form of glucose, which might change cellular capability to maintain ion and water balance, intracellular homeostasis. Hence, dextrose solution might **s**plinter the plasma membrane, leading to cytoplasm leakage into the extracellular environment [172]. Our outcomes demonstrated that dextrose solution decreased the viability of the U937-differentiated macrophage cells (Fig. 4.4.5a and Table 4.4.2). Cellular and nuclear area of macrophage cells increased in dextrose solution, but it did not significantly influence MCF7 cells (Fig. 4.4.5b, Fig. 4.4.6, Fig. 4.4.7, Fig. 4.4.11b and Table 4.4.3).

The NaCl diluent is another fundamental diluent in clinics; still, it has been proclaimed that it might cause hyperchloremia, metabolic acidosis, acute kidney injury

and renal vasoconstriction [171]. Thus, our results of the viability experiments with diminishing number of cells after exposure to NaCl solution, with the exclusion of MCF7 cells, are backed due to the NaCl solution making the medium hypertonic [173]. Our outcomes showed that NaCl significantly decreased viability of U937 monocytes, macrophages and HepG2 cells (Fig. 4.4.1a, Fig. 4.4.5a, Fig. 4.4.8a and Table 4.2). Moreover, neither the cellular nor the nuclear areas of the MCF7 cells were altered in NaCl diluent, whereas others were affected (Fig. 4.4.1b, Fig. 4.4.2, Fig. 4.4.5b, Fig. 4.4.8b 4.4.11b and Table 4.4.3).

As reported by intensive care units, in spite of NaCl and dextrose being the fundamental crystalloid fluids for revival, the usage of lactated Ringer has elevated lately [174][175][176]. Dr. Brown and co-worker's argument concerning the results of the treatment diluent suggested balanced crystalloids like lactated Ringer solution since their chemical composition is harmless for the acid-base status and organ function of a patient [171][177]. In our research, the viability of immune related cells, U937 monocytes and U937-differentiated macrophages, diminished while the viability of breast cancer cells elevated in Ringer solution (Fig. 4.4.1a, Fig. 4.4.5a, Fig. 4.4.8a, Fig. 4.4.11a and Table 4.2). Cellular and nuclear areas of the cells expanded in the Ringer solution, with the exclusion of U937 monocyte cells whose cellular size became smaller, and nuclear size was not significantly changed (Fig. 4.4.1b, Fig. 4.4.2, Fig. 4.4.5b, Fig. 4.4.8b 4.4.11b and Table 4.4.3).

In this investigation, we detected that IVFs lowered the viability of immune cells more than cancer cells (Fig. 4.4.1a, Fig. 4.4.5a, Fig. 4.4.8a and Table 4.2). Also, we showed that IVFs alter cellular or nuclear areas of the cells (Fig. 4.4.1b, Fig. 4.4.2, Fig. 4.4.5b, Fig. 4.4.8b 4.4.11b and Table 4.4.3). Kadota et al. expressed that the nuclear diameter of the cells is one of the independent predictive elements for bad reactions when they conducted extensive pathological analysis in lung squamous cell carcinoma [178]. Cell morphology and surface are important biomechanical features for main cellular actions such as adhesion, spread and migration [179][180]. Based on our results, IVF might also cause to diversity of nuclear diameter when patients are given medication with IVFs. Especially, for the lactated Ringer diluent, a previous research conducted by Bonuccelli et al., in which MCF7 cells were used in a co-culture environment,

demonstrated a risk of advanced metastasis in cancer patients [175]. Hence, the utility of IVFs should be investigated to dispose of the spreading doubt over its safety and benefits.

Distinctly, in this research, we examined the surface areas of cells and their nuclei performing image analysis on microscopy images as well [181]. Still, the number of cells was relatively low for image analysis; thus, we performed flow cytometry analysis as mentioned above (Fig. 4.4.3, Fig. 4.4.4, Fig. 4.4.6, Fig. 4.4.7, Fig. 4.4., Fig. 4.4.10, Fig. 4.4.12, Fig. 4.4.13, Table 4.4.4 and Table 4.4.5). However, our work has an important limitation which is that this study shows *in vitro* behavior of cell lines with IVFs that do not represent completely the interactions in the human body when the medicine is given with IVFs.

Chapter 5

CONCLUSION AND FUTURE WORK

In this thesis, novel microfluidic cell culturing platforms and a microfluidic gradient generator were designed, fabricated and tested using mammalian cancer and immune system cell lines after initial testing for feasibility with food dyes. First, a microfluidic cell culturing chip and a microfluidic gradient generator allowing the analysis of cells in flow, and microscopy imaging was enabled thanks to the transparency of the PDMS mold. These devices were tested with MCF7 cells and different concentrations of SDS as a drug representative providing a way to evaluate the efficacy of a drug on a single type or different types of cells through microfluidic platforms. The cell culturing chip and the microfluidic gradient generator can be utilized for personalized medicine through the application of different concentrations of a drug with the gradient generator and examination of the response of cells to the stimuli inside the culturing chambers. However, there were problems in the experiments due to bubble formation during cell loading. Hence, a new and plain microfluidic cell culturing chip was designed, fabricated and used to investigate the behavior of HepG2 liver cancer cells. To this device, as distinct from the previous devices, an inlet tip and an outlet tip for medium exchange were inserted providing stable fluid flow through height differences between tips. HepG2 cells were grown both at population-level using batch culture and at single-cell level using our microfluidic-microscopy system. After overnight incubation of cells, some of the cells inside the petridish remained circular while other cells generated pseupodium. However,

in our microfluidic device we did not observe any pseupodium. Cells without pseupodium could not attach to the surface of the glass and grow. Our experiment demonstrated the difference in the behavior of liver cells in our microfluidic device compared to their behavior in a macroscopic petridish. This variation in the action of liver cells involving the presence or absence of pseupodium growth is caused by cell heterogeneity. This study showed that a better understanding of liver cell heterogeneity is needed. In order to achieve this goal, new standardized microdevices can be developed allowing single-cell analysis with high throughput and high content analysis. In this way, new knowledge about the behaviors of liver cells and their heterogeneity in response to their microenvironments can be obtained and novel liver cancer treatments can be developed.

After examining a single type of cell per a microfluidic platform, a microfluidic co-culturing platform was designed, fabricated and tested with U87 brain cancer cells with U937 macrophages differentiated from U937 monocytes. This chip, as different from our previous devices, was used to investigate the invasiveness of the U87 cells. The preliminary results that were obtained showed that U937 macrophages were moving towards U87 cells.

Shifting focus to a better understanding of cell behavior, the influences of IVF on U937 monocytes, U937-differentiated macrophages, HepG2, and MCF7 cancer cells were examined *in vitro* by exposing the cells to IVF for 15 minutes since patients are given IVFs for 15 minutes. This inquiry revealed that viability of the monocytes and macrophages significantly decreased compared to those of breast and liver cancer cells. Additionally, differences in the nuclear and cellular area of cells were brought in with IVF. Our conclusions should be elucidated carefully because our results exhibit in vitro behavior with IVF in cell lines that do not represent exactly the interactions in the human body when medication is delivered via IVF. Still, our work demonstrates the urgent need for more precise investigation of IVF at high resolution and more physiologically relevant human body mimicking models. As future work, 3D organs-on-a-chip studies might be conducted which might provide a better understanding of biokinetics, signaling between cells and clinical insights [37]. Currently, organotypic culture studies are also in their infancy and there is an urgent need for their improvement to achieve in vivo likeness with a better practical usage in clinical studies [38].

Finally, it was noticed that the cell growth rates in our microfluidic cell cultures are several orders of magnitude less than those of the tested conventional cell cultures. This aspect has enormous potential for further researching these types of microfluidic cell cultures, or for studies which deal with the effects of physical parameters such as shear flow and geometry on cell growth, signaling, and other vital cellular interactions.

REFERENCES

[1] Hudu, S. A., Alshrari, A. S., Syahida, A., & Sekawi, Z. (2016). Cell Culture, Technology: Enhancing the Culture of Diagnosing Human Diseases. *Journal of clinical and diagnostic research: JCDR*, *10*(3), DE01-5.

[2] Khalili, A. A., & Ahmad, M. R. (2015). A Review of Cell Adhesion Studies for Biomedical and Biological Applications. *International journal of molecular sciences*, *16*(8), 18149-84.

[3] Valente, K. P., Khetani, S., Kolahchi, A. R., Sanati-Nezhad, A., Suleman, A. & Akbari, M. (2017). Microfluidic technologies for anticancer drug studies. *Drug Discovery Today*, *22*(11),1654-1670.

[4] Seoane, J. (2017). Division hierarchy leads to cell heterogeneity. *Nature, 549*, 164–166.

[5] Tehranirokh, M., Kouzani, A. Z., Francis, P. S., & Kanwar, J. R. (2013). Microfluidic devices for cell cultivation and proliferation. *Biomicrofluidics*, *7*(5), 51502.

[6] Sung M. H. (2013). A checklist for successful quantitative live cell imaging in systems biology. *Cells*, *2*(2), 284-93.

[7] Mata, A., Fleischman, A. J., & Roy, S. (2005). Characterization of Polydimethylsiloxane (PDMS) Properties for Biomedical Micro/Nanosystems. *Biomedical Microdevices*, *7*(4), 281-293.

[8] Torino, S., Corrado, B., Iodice, M., & Coppola, G. (2018). PDMS-Based Microfluidic Devices for Cell Culture. *Inventions*, *3*(3), 65.

[9] Ambrose, C. T. (2016). An amended history of tissue culture: Concerning Harrison, Burrows, Mall, and Carrel. *J Med Biogr*.

[10] Duval, K., Grover, H., Han, L. H., Mou, Y., Pegoraro, A. F., Fredberg, J., & Chen, Z. (2017). Modeling Physiological Events in 2D vs. 3D Cell Culture. *Physiology (Bethesda, Md.)*, *32*(4), 266-277.

[11] H-M Wu, T-A Lee, P-L Ko, H-J Chiang, C-C Peng, & Y-C Tung. (2018). Review of microfluidic cell culture devices for the control of gaseous microenvironments *in vitro. J. Micromech. Microeng.*, *28* (4).

[12] Dangi-Garimella S, Krantz SB, Barron MR, Shields MA, Heiferman MJ, Grippo PJ, Bentrem DJ, Munshi HG. Three-dimensional collagen I promotes gemcitabine resistance in pancreatic cancer through MT1-MMP-mediated expression of HMGA2. Cancer Res 71: 1019–1028, 2011

[13] Nagaprashantha LD, Vatsyayan R, Lelsani PCR, Awasthi S, Singhal SS. The sensors and regulators of cell-matrix surveillance in anoikis resistance of tumors. Int J Cancer 128: 743–752, 2011

[14] Bloom, A. B., & Zaman, M. H. (2014). Influence of the microenvironment on cell fate determination and migration. *Physiological genomics*, *46*(9), 309-14.

[15] Warrick, J. W., Murphy, W. L., & Beebe, D. J. (2008). Screening the cellular microenvironment: a role for microfluidics. *IEEE reviews in biomedical engineering*, *1*(1), 75-93.

[16] Barthes, J., Özçelik, H., Hindié, M., Ndreu-Halili, A., Hasan, A., & Vrana, N. E. (2014). Cell microenvironment engineering and monitoring for tissue engineering and regenerative medicine: the recent advances. *BioMed research international*, *2014*, 921905.

[17] Yang, J., Duan, Y., Zhang, X., Wang, Y., & Yu, A. (2016). Modulating the cellular microenvironment with disulfide-containing nanoparticles as an auxiliary cancer treatment strategy. *Journal of Materials Chemistry B, 4*(22), 3868-3873.

[18] Satyam A, Kumar P, Fan X, et al. (2014). Macromolecular crowding meets tissue engineering by self-assembly: a paradigm shift in regenerative medicine. *Advanced Materials*, *26*(19), 3024–3034.

[19] Fiore, A. P., Ribeiro, P. D., & Bruni-Cardoso, A. (2018). Sleeping Beauty and the Microenvironment Enchantment: Microenvironmental Regulation of the Proliferation-Quiescence Decision in Normal Tissues and in Cancer Development. *Frontiers in Cell and Developmental Biology*, *6*.

[20] Fouad, Y. A., & Aanei, C. (2017). Revisiting the hallmarks of cancer. *American journal of cancer research, 7*(5), 1016-1036.

[21] Primary, Adaptive, and Acquired Resistance to Cancer Immunotherapy.*Sharma P, Hu-Lieskovan S, Wargo JA, Ribas A Cell. 2017 Feb 9; 168(4):707-723.*

[22] Barton, M.K. (2015). Daily aspirin may reduce mortality from prostate cancer with risk of high recurrence. *CA Cancer J Clin, 65*(2):83-4.

[23] World Health Organization. (2018, September 12). *Latest global cancer data: Cancer burden rises to 18.1 million new cases and 9.6 million cancer deaths in 2018*. Retrieved from https://www.iarc.fr/featured-news/latest-global-cancer-data-cancer-burden-rises-to-18-1-million-new-cases-and-9-6-million-cancer-deaths-in-2018/

[24] Zhang, H., & Chen, J. (2018). Current status and future directions of cancer immunotherapy. *Journal of Cancer, 9*(10), 1773-1781.

[25] Fiedler, E.C., & Hemann, M.T. (2019). Aiding and Abetting: How the Tumor Microenvironment Protects Cancer from Chemotherapy and Michael T. *Annual Review of Cancer Biology, 3*(1), 409-428.

[26] Yuan, Y., Jiang, Y., Sun, C., & Chen, Q. (2016). Role of the tumor microenvironment in tumor progression and the clinical applications (Review). *Oncology Reports, 35*(5), 2499-2515.

[27] Foster, D.S., Jones, R.E., Ransom, R.C., Longaker, M.T., & Norton, J.A. (2018). The evolving relationship of wound healing and tumor stroma. JCI Insight, 3(18), e99911.

[28] Thompson, S. L., & Compton, D. A. (2011). Chromosomes and cancer cells. Chromosome research: an international journal on the molecular, supramolecular and evolutionary aspects of chromosome biology, 19(3), 433–444.

[29] Fitzgerald, K. A., M. Malhotra, C. M. Curtin, F. J. O' Brien, and C. M. O' Driscoll. (2015). Life in 3D is never flat: 3D models to optimise drug delivery. *Journal of Controlled Release, 215,* 39–54.

[30] Rollin, B.E. (2003). Toxicology and new social ethics for animals. *Toxicologic Pathology, 31*(1), 128–131.

[31] Doke, S. K., & Dhawale, S. C. (2015). Alternatives to animal testing: A review. *Saudi Pharmaceutical Journal, 23*(3), 223-229.

[32] Ponce De León-Rodríguez, M.D.C., Guyot, J.P., & Laurent-Babot, C. (2018). Intestinal in vitro cell culture models and their potential to study the effect of food components on intestinal inflammation. *Critical Reviews in Food Science and Nutrition,* 1-19.

[33] Baker, M. (2016). 1,500 scientists lift the lid on reproducibility. *Nature, 533,* 452–454.

[34] Muelas, M.W., Ortega, F., Breitling, R., Bendtsen, C., & Westerhoff, H.V. (2018). Rational cell culture optimization enhances experimental reproducibility in cancer cells. *Scientific Reports, 8*(1).

[35] Haverty, P.M., Lin, E., Tan, J., Yu, Y., Lam, B., Lianoglou, S., Neve, R.M., Martin, S., Settleman, J., Yauch, R.L., & Bourgon, R. (2016). Reproducible pharmacogenomic profiling of cancer cell line panels. *Nature, 533*(7603), 333-337.

[36] Coluccio, M.L., Perozziello, G., Malara, N., Parrotta, E., Zhang, P., Gentile, F., Limongi, T., Raj, P.M., Cuda, G., Candelore, P., & Fabrizio, E.D. (2019). Microfluidic platforms for cell cultures and investigations. *Microelectronic Engineering, 208,* 14-28.

[37] Y. Choi, J. Hyun, J. Seo, C. Blundell, H. C. Kim, E. Lee, S. H. Lee, A. Moon, W. K. Moon and D. Huh, Lab Chip, 2015, 15, 3350–3357

[38] Young, E.W., & Beebe, D. J. (2010). Fundamentals of microfluidic cell culture in controlled microenvironments. *Chemical Society reviews, 39*(3), 1036-48.

[39] Huang, S.B., Wang, S.S., Hsieh, C.H., Lini, Y.C., Lai, C.S., & Wu., M.H. (2013). An integrated microfluidic cell culture system for high-throughput perfusion three-dimensional cell culture-based assays: effect of cell culture model on the results of chemosensitivity assays. *Lab Chip, 13*(2013), 1133-1143.

[40] Xu, B.Y., Hu, S.W., Qian, G.S., Xu, J.J. & Chen, H.Y. (2013). A novel microfluidic platform with stable concentration gradient for on chip cell culture and screening assays. *Lab Chip, 13*(18), 3714-3720.

[41] Munoz-Berbel, X., Rodriguez, R., Vigues, N., Demming, S., Mas, J., Buttenbach, S., Verpoorte, E., Ortiz, P., & Llobera A. (2013). Monolithically integrated biophotonic lab-on-a-chip for cell culture and simultaneous pH monitoring. *Lab Chip, 13*(21), 4239-4247.

[42] Zhu, Q., Heon, M., Zhao, Z., & He, M. (2018). Microfluidic engineering of exosomes: Editing cellular messages for precision therapeutics. *Lab on a Chip, 18*(12), 1690-1703.

[43] Zheng, Y., Chen, J., Craven, M., Choi, N.W., Totorica, S., Diaz-Santana, A., Kermani, P., Hempstead, B., Fischbach-Teschl, C., Lopez, J.A., & Stroock, A.D. In vitro microvessels for the study of angiogenesis and thrombosis. *Proc. Natl. Acad. Sci. U. S. A.*, *109*(24), 9342-9347.

[44] Esch, M.B., Prot, J.M., Wang, Y.I., Miller, P., Lamas-Vidales, J.R., Naughton, B.A., Applegate, D.R. & Shuler M.L. (2015). Multi-cellular 3D human primary liver cell culture elevates metabolic activity under fluidic flow. *Lab on a Chip, 15(10), 2269-2277.*

[45] Zór, K., Heiskanen, A., Caviglia, C., Vergani, M., Landini, E., Shah, F., Carminati, M., Martinez-Serrano, A., Moreno, T.R., Kokaia, M., Benayahu, D., Keresztes, Z., Papkovsky, D., Wollenberger, U., Svendsen, W.E., Dimaki, M., Ferrari, G., Raiteri, R., Sampietro, M., Dufva, M. & Emnéus, J. (2014). A compact multifunctional microfluidic platform for exploring cellular dynamics in real-time using electrochemical detection. *RSC Adv.*, *4*(109), 63761-63771.

[46] Tse, H. T., Weaver, W.M., & Di Carlo, D. (2012). Increased asymmetric and multi-daughter cell division in mechanically confined microenvironments. *PloS one, 7*(6), e38986.

[47] Barthes, J., Özçelik, H., Hindié, M., Ndreu-Halili, A., Hasan, A., & Vrana, N. E. (2014). Cell microenvironment engineering and monitoring for tissue engineering and regenerative medicine: the recent advances. *BioMed research international*, *2014*, 921905.

[48] Yamazoe, H., Sugiyama, Y., Omri, A. E., Hagihara, Y., & Okada, T. (2014). Facile immunostaining and labeling of nonadherent cells using a microfluidic device to entrap the cells. *Journal of Bioscience and Bioengineering, 117*(3), 375-378.

[49] Liberale, C., Cojoc, G., Bragheri, F., Minzioni, P., Perozziello, G., La Rocca, R., Ferrara, L., Rajamanickam, V., Di Fabrizio, E., & Cristiani, I. (2013). Integrated microfluidic device for single-cell trapping and spectroscopy. *Scientific reports, 3*, 1258.

[50] Ono, T., Suzuki, Y., Kato, Y., Fujita, R., Araki, T., Yamashita, T., et al. (2014). A Single-Cell and Feeder-Free Culture System for Monkey Embryonic Stem Cells. *PLoS ONE, 9*(2), e88346.

[51] Lo, S., & Yao, D. (2015). Get to Understand More from Single-Cells: Current Studies of Microfluidic-Based Techniques for Single-Cell Analysis. *International Journal of Molecular Sciences, 16*(8), 16763-16777.

[52] Wang, B.L., Ghaderi, A., Zhou, H., Agresti, J., Weitz, D.A., Fink, G.R., & Stephanopoulos, G. (2014). Microfluidic high-throughput culturing of single cells for selection based on extracellular metabolite production or consumption. *Nature Biotechnology, 32*(5), 473-478.

[53] Simone, G., Malara, N., Trunzo, V., Renne, M., Perozziello, G., Fabrizio, E.D., & Manz, A. (2014). Galectin-3 coats the membrane of breast cells and makes a signature of tumours. *Mol. BioSyst.,10*(2), 258-265.

[54] Simone, G., Malara, N., Trunzo, V., Perozziello, G., Neuzil, P., Francardi, M., Roveda, L., Renne, M., Prati, U., Mollace, V., Manz, A., & Fabrizio, E. D. (2013). Protein-Carbohydrate Complex Reveals Circulating Metastatic Cells in a Microfluidic Assay. *Small, 9*(12), 2152-2161.

[55] Breslin, S., & O'Driscoll, L. (2013). Three-dimensional cell culture: The missing link in drug discovery. *Drug Discovery Today, 18*(5-6), 240-249.

[56] Weltin, A., Slotwinski, K., Kieninger, J., Moser, I., Jobst, G., Wego, M., . . . Urban, G. A. (2014). Cell culture monitoring for drug screening and cancer research: A transparent, microfluidic, multi-sensor microsystem. Lab Chip, 14(1), 138-146.

[57] Breslin, S., & O'Driscoll, L. (2013). Three-dimensional cell culture: The missing link in drug discovery. *Drug Discovery Today, 18*(5-6), 240-249.

[58] Krausz, E., Hoogt, R. D., Gustin, E., Cornelissen, F., Grand-Perret, T., Janssen, L., Vloemans, N., Wuyts, D., Frans, S., Axel, A., Peeters, P.J., Hall, B., & Cik, M. (2013). Translation of a Tumor Microenvironment Mimicking 3D Tumor Growth Co-culture Assay Platform to High-Content Screening. *Journal of Biomolecular Screening, 18*(1), 54-66.

[59] Lovitt, C., Shelper, T., & Avery, V. (2014). Advanced Cell Culture Techniques for Cancer Drug Discovery. *Biology, 3*(2), 345-367.

[60] Macown, R.J., Veraitch, F.S., & Szita N. Robust, microfabricated culture devices with improved control over the soluble microenvironment for the culture of embryonic stem cells. (2014). *Biotechnology Journal, 9*(9), 1223-1223.

[61] Yang, K., Han, S., Shin, Y., Ko, E., Kim, J., Park, K. I., Chung S., & Cho, S.W. (2013). A microfluidic array for quantitative analysis of human neural stem cell self-renewal and differentiation in three-dimensional hypoxic microenvironment. *Biomaterials, 34*(28), 6607-6614.

[62] Metto, E. C., Evans, K., Barney, P., Culbertson, A. H., Gunasekara, D. B., Caruso, G., Hulvey, M.K., Frascassi de Silva, J.A., Lunte, S.M., & Culbertson, C. T. (2013). An Integrated Microfluidic Device for Monitoring Changes in Nitric Oxide Production in Single T-Lymphocyte (Jurkat) Cells. *Analytical Chemistry, 85*(21), 10188-10195.

[63] Krull, R., & Peterat, G. (2016). Analysis of reaction kinetics during chemostat cultivation of *Saccharomyces cerevisiae* using a multiphase microreactor. *Biochem. Eng. J., 105*, 220-229.

[64] Marques, M.P.C., & Szita, N. (2017). Bioprocess microfluidics: applying microfluidic devices for bioprocessing. *Curr. Opin. Chem. Eng., 18*, 61-68

[65] Hubert, C. G., Rivera, M., Spangler, L. C., Wu, Q., Mack, S. C., Prager, B. C., Couce, M., McLendon, R.E., Sloan, A.E., & Rich, J. N. (2016). A Three-Dimensional Organoid Culture System Derived from Human Glioblastomas Recapitulates the Hypoxic Gradients and Cancer Stem Cell Heterogeneity of Tumors Found In Vivo. *Cancer Research, 76*(8), 2465-2477.

[66] Edmondson, R., Broglie, J.J., Adcock, A.F., & Yang L.J. (2014). Three-dimensional cell culture systems and their applications in drug discovery and cell-based biosensors. *Assay Drug Develop. Technol., 12*(14), 207-218.

[67] Matsusaki, M., Case, C.P., Akashi, M. (2014). Three-dimensional cell culture technique and pathophysiology. *Adv. Drug Deliv. Rev., 74*, 95-103.

[68] Graf, B. W., & Boppart, S. A. (2010). Imaging and analysis of three-dimensional cell culture models. Methods in molecular biology (Clifton, N.J.), 591, 211–227.

[69] Joshi, P., Datar, A., Yu, K., Kang, S., & Lee, M. (2018). High-content imaging assays on a miniaturized 3D cell culture platform. Toxicology in Vitro, 50, 147-159.

[70] Hydrogels as extracellular matrix mimics for 3D cell culture.Tibbitt MW, Anseth KSBiotechnol Bioeng. 2009 Jul 1; 103(4):655-63

[71] Gurski L, Petrelli N, Jia X, Farach-Carson M: Three-dimensional matrices for anti-cancer drug testing and development. Oncol Issues 2010; 25:20–25

[72] Mishra DK, Sakamoto JH, Thrall MJ, et al. : Human lung cancer cells grown in an ex vivo 3D lung model produce matrix metalloproteinases not produced in 2D culture. PLoS One 2012; 7:e45308.

[73] Yamada KM, Cukierman E: Modeling tissue morphogenesis and cancer in 3D. Cell 2007;130:601–610

[74] Elitas, M., Sadeghi, S., Karamahmutoglu, H., Gozuacik, D., & Turhal, N. S. (2017). Microfabricated platforms to quantitatively investigate cellular behavior under the influence of chemical gradients. *Biomedical Physics & Engineering Express, 3*(3), 035023.

[75] Hande Karamahmutoglu, Metin Çetin, Tamer Yağcı, and Meltem Elitaş "Behavior of HepG2 liver cancer cells using microfluidic-microscopy: a preliminary study", Proc. SPIE 10491, Microfluidics, BioMEMS, and Medical Microsystems XVI, 104910Y (19 February 2018)

[76] Shutherland R L, Hall R E and Taylor I W 1983 Cell proliferation kinetics of MCF-7 human mammary carcinoma cells in culture and effects of tamoxifen on exponentially growing and plateau-phase cells *Cancer Res.* **43** 3998–4006

[77] Jeon N L et al 2000 Generation of solution and surface gradients using microfluidic systems Langmuir**16** 8311–6

[78] Dertinger S K W, Chiu D T, Jeon N K and Whitesides G M 2001 Generation of gradients having complex shapes using microfluidic networks Anal. Chem. **73** 1240–6

[79] Toh A G G, Wang Z P, Yang C and Nguyen N T 2014 Engineering microfluidic concentration gradient generators for biological applications Microfluid. Nanofluid. **16** 1–18

[80] Beta C and Bodenschatz E 2011 Microfluidic tools for quantitative studies of eukaryotic chemotaxis Eur. J. Cell Biol. **90** 811–6

[81] Whitesides G M, Ostuni E, Takayama S, Jiang X and Ingber D E 2001 Soft lithography in biology and biochemisty *Annu. Rev. Biomed. Eng.* **3** 335–73

[82] Huabert K, Drier T and Beebe D 2006 PDMS bonding by means of portable, low-cost corona system *Lab Chip* **6** 1548–9

[83] Sadeghi, S & Elitas, M. (2017). A simple, bubble-free cell loading technique for culturing mammalian cells on lab-on-a-chip devices. Chips and Tips.

[84] Smereka, M., & Dulęba, I., International Journal of Applied Mathematics and Computer Science, 18(1), (2008).

[85] Basiji, D. A., Ortyn, W. E., Liang, L., Venkatachalam, V., & Morrissey, P. (2007). Cellular Image Analysis and Imaging by Flow Cytometry. Clinics in Laboratory Medicine, 27(3), 653-670.

[86] Peiris, T. H., García-Ojeda, M. E., & Oviedo, N. J. (2016). Alternative flow cytometry strategies to analyze stem cells and cell death in planarians. Regeneration, 3(2), 123-135.

[87] Maestre-Batlle, D., Pena, O. M., Hirota, J. A., Gunawan, E., Rider, C. F., Sutherland, D., . . . Carlsten, C. (2017). Novel flow cytometry approach to identify bronchial epithelial cells from healthy human airways. Scientific Reports, 7(1).

[88] Shutherland R L, Hall R E and Taylor I W 1983 Cell proliferation kinetics of MCF-7 human mammary carcinoma cells in culture and effects of tamoxifen on exponentially growing and plateau-phase cells *Cancer Res.* **43** 3998–4006

[89] Waters, J. C, Methods in Cell Biology Digital Microscopy, 125-150, (2013).

[90] Cadena-Herrera, D., Lara, J. E., Ramírez-Ibañez, N. D., López-Morales, C. A., Pérez, N. O., Flores-Ortiz, L. F., & Medina-Rivero, E. (2015). Validation of three viable-cell counting methods: Manual, semi-automated, and automated. Biotechnology Reports, 7, 9-16. doi:10.1016/j.btre.2015.04.004

[91] Smereka, M., & Dulęba, I., International Journal of Applied Mathematics and Computer Science, 18(1), (2008).

[92] Ebrahimpour, R., Rasoolinezhad, R., Hajiabolhasani, Z., & Ebrahimi, M. (2012). Vanishing point detection in corridors: Using Hough transform and K-means clustering. *IET Computer Vision, 6*(1), 40. doi:10.1049/iet-cvi.2010.0046

[93] Liu, J., Dang, H., & Wang, X. W. (2018). The significance of intertumor and intratumor heterogeneity in liver cancer. *Experimental & Molecular Medicine, 50*(1). doi:10.1038/emm.2017.165

[94] Xiaohui C., Xiaoyue F., Qing X., Hua G., Ning Z. and Mingyue D., "Observation of liver cells in scanning probe acoustic microscope: A preliminary study," Proc. SPIE 9790, 97901T (2016)

[95] Cobb, L. (2013). Cell Based Assays: The Cell Cycle, Cell Proliferation and Cell Death. *Materials and Methods, 3*. doi:10.13070/mm.en.3.172

[96] Jevtic, V., Kindle, P., & Avilov, S. V. (2018). SYBR Gold dye enables preferential labelling of mitochondrial nucleoids and their time-lapse imaging by structured illumination microscopy. *Plos One, 13*(9). doi:10.1371/journal.pone.0203956

[97] Dendrophthoe pentandra Induced Apoptosis and Cell Cycle Arrest at G1/S in Human Breast Adenocarcinoma Cells, MCF-7 via Up- Regulation of p53. (2018). *Journal of Applied Pharmaceutical Science, 8*(9), 130-141. doi:10.7324/japs.2018.8919

[98] Sharma P, Allison JP. Immune checkpoint targeting in cancer therapy: toward combination strategies with curative potential. *Cell* 2015; **161**: 205–214.

[99] Hu, C., Liu, J., Chen, H., & Nie, F. (2017). Microfluidic Platforms for Gradient Generation and its Applications. Biochemistry & Analytical Biochemistry, 06(02). doi:10.4172/2161-1009.1000320

[100] Mirbagheri, M., Adibnia, V., Hughes, B. R., Waldman, S. D., Banquy, X., & Hwang, D. K. (2019). Advanced cell culture platforms: A growing quest for emulating natural tissues. *Materials Horizons, 6*(1), 45-71. doi:10.1039/c8mh00803e

[101] J.H. Kang, S. Krause, H. Tobin, A. Mammoto, M. Kanaathipillai, D.E. Ingber. A combined micromagnetic-microfluidic device for rapid capture and culture of rare circulating tumor cells. Lab Chip, 12 (2012), pp. 2175-2181

[102] F. Abeille, F. Mittler, P. Obeid, M. Huet, F. Kermarrec, M.E. Dolega, F. Navarro, P. Pouteau, B. Icard, X. Gidrol, V. Agache, N. Picollet-D'hahan. Continuous microcarrier-based cell culture in a benchtop microfluidic bioreactor. Lab Chip, 14 (2014), pp. 3510-3518

[103] A. Amman, M. Zwierzina, G. Gamerith, M. Bitsche, J.M. Huber, G.F. Vogel, M. Blumer, S. Koeck, E.J. Pechriggl, J.M. Kelm, W. Hilbe, H. Zwierzina. Development of an innovative 3D cell culture system to study tumour – stroma interactions in non-small cell lung cancer cells. PLoS One, 9 (2014)

[104] V.N. Goral, C.F. Zhou, F. Lai, P.K. Yuen. A continuous perfusion microplate for cell culture. iiLab Chip, 13 (2013), pp. 1039-1043

[105] W.H. Minhass, P. Pop, J. Madsen, M. Hemmingsen, P. Skafte-Pedersen, M. Dufva. Cell culture microfluidic biochips: Experimental throughput maximization. IEEE, 11 (2011)

[106] P. Skafte-Pedersen, H. Hemmingsen, D. Sabourin, F.S. Blaga, H. Bruus, M. Dufva. A self-contained, programmable microfluidic cell culture system with real-time microscopy access. Biomed. Microdevices, 14 (2012), pp. 385-399

[107] F.F. Tao, X. Xiao, K.F. Lei, I.C. Lee. Paper-based cell culture microfluidic system. Biochip J., 9 (2015), pp. 97-104

[108] R. Li, X. Li, M. Hasan, J. Xu, X. Zhang, K. Qin, J. Wang, D. Zhou, Y. Deng. A rapidly fabricated microfluidic chip for cell culture. J. Chromatogr. Sci., 54 (2016), pp. 523-530

[109] D. Sabourin, P. Skafte-Pedersen, M.J. Soe, M. Hemminsen, M. Alberti, V. Coman, J. Petersen, J. Emneus, J.P. Kutter, D. Snakenborg, F. Jorgensen, C. Clausen, K. Holmstrom, M. Dufva, et al. J. Lab. Autom., 18 (2013), pp. 212-218

[110] T.S. Salameh, T.T. Le, M.B. Nichols, E. Bauer, J. Cheng, I.G. Camarillo. An ex vivo co-culture model system to evaluate stromal-epithelial interactions in breast cancer. Int. J. Cancer, 132 (2013), pp. 288-296

[111] N. Jaccard, R.J. Macown, A. Super, L.D. Griffin, F.S. Veraitch, N. Szita. Automated and online characterization of adherent cell culture growth in a microfabricated bioreactor. J. Lab. Autom., 19 (2014), pp. 437-443

[112] A.D. van der Meer, V.V. Orlova, P. ten Dijke, A. van der Berg, C.L. Mummery. Three-dimensional co-cultures of human endothelial cells and embryonic stem cell-derived pericytes inside a microfluidic device. Lab Chip, 13 (2013), pp. 3562-3568

[113] K. Funamoto, I.K. Zervantonakis, Y.C. Liu, C.J. Ochs, C. Kim, R.D. Kamm. A novel microfluidic platform fo-high resolution imaging of a three-dimensional cell culture under controlled hypoxic environment. Lab Chip, 12 (22) (2012), pp. 4855-4963

[114] M.K. Conway, M.J. Gerger, E.E. Balay, R. O'Connell, S. Hanson, N.J. Daily, T. Wakatsuki. Scalable 96-well plate based iPSC culture and production using a robotic liquid handling system. ttJ. Vis. Exp., 14 (99) (2015), Article e52755

[115] D. Paull, A. Sevilla, H. Zhou, A.K. Hahn, H. Kim, C. Napolitano, A. Tsankov, L. Shang, K. Krumholz, P. Jagadesan, C.M. Woodard, B. Sun, T. Vilboux, M. Zimmer, E. Forero, D.N. Moroziewicz, H. Martinez, M.C. Malicdan, K.A. Weiss, L.B. Vensad, C.R. Dusenberry, H. Polus, K.T. Sy, D.J. Kahler, W.A. Gahl, S.L. Solomon, S. Chang, A. Meissner, K. Eggan, S.A. Noggle. Automated, high-throughput derivation, characterization and differentiation of induced pluripotent stem cells. Nat. Methods, 12 (2015), pp. 885-892

[116] E. Cimetta, D. Sirabella, K. Yeager, K. Davidson, J. Simon, R.T. Moon, G. Vunjak-Novakovic. Microfluidic bioreactor for dynamic regulation of early mesodermal commitment in human pluripotent stem cells. Lab Chip, 13 (2013), pp. 355-364

[117] P. Occhetta, M. Centola, B. Tonnarelli, A. Redaelli, I. Martin, M. Rasponi. High-throughput microfluidic platfomr for 3D cultures of mesenchymal stem cells, towards engineering developmental processes. Sci. Rep., 5 (2015), p. 10288

[118] M. Amit, J. Chebath, V. Margulets, I. Laevsky, Y. Miropolsky, K. Shariki, M. Peri, I. Blais, G. Slutsky, M. Revel, J. Itskovitz-Eldor. Suspension culture of undifferetiated human embryonic and induced pluripotent stem cells. Stem Cell Rev., 6 (2010), pp. 248-259

[119] A. Bolic, H. Larsson, S. Hugelier, A. Eliasson Lantz, U. Kruhne, K.V. Gernaey. A flexible well-mixed milliliter-scale reactor with high oxygen transfer rate for microbioal cultivations. Chem. Eng. J., 303 (2016), pp. 655-666

[120] C.G. Sip, N. Bhattacharjee, A. Folch. Microfluidic transwell inserts for generation of tissue culture-friendly gradients in well plates. Lab Chip, 14 (2014), pp. 302-314

[121] R.M. Huval, O.H. Miller, J.L. Curley, Y. Fan, B.J. Hall, M.J. Moore. Microengineered peripheral nerve-on-a-chip for preclinical physiological testing. Lab Chip, 15 (2015), pp. 2221-2232

[122] I. Mashmeyer, A.K. Lorenz, K. Chimek, T. Hasenberg, A.P. Ramme, J. Hubner, M. Lindner, C. Drewell, S. Bauer, A. Thomas, N.S. Sambo, F. Sonntag, R. Lauster, U. Marx. A four-organ-chip for interconnected long-term co-culture of human intestine, liver, skin and kidney equivalents. Lab Chip, 15 (2015), pp. 2688-2699

[123] K. Rennert, S. Steinborn, M. Groger, B. Ungerbock, A.M. Jank, J. Ehgartner, S. Nietzsche, J. Dinger, M. Kiehntopf, H. Funke, F.T. Peters, A. Lupp, C. Gartner, T. Mayr, M. Bauer, O. Huber, A.S. Mosig. A microfluidically perfused three dimensional human liver model. Biomaterials, 71 (2015), pp. 119-131

[124] A. Marsano, C. Conficconi, M. Lemme, P. Occhetta, E. Gaudiello, E. Votta, G. Cerino, A. Redaelli, M. Rasponi. Beating heart on a chip: a novel microfluidic platform to generate functional 3D cardiac microtissues. Lab Chip, 16 (2016), pp. 599-610

[125] M.D. Nguyen, J.P. Tinney, F.P. Yuan, T.J. Roussel, A. El-Baz, G. Giridharan, B.B. Keller, P. Sethu. Cardiac cell culture model as a left ventricle mimic for cardiac tissue generation. Anal. Chem., 85 (2013), pp. 8773-8779

[126] C. Gartner, B. Ungerbock, I. Schultz, T. Jahn, A. Mosig, T. Mayr, H. Becker. Sensor enhanced microfluidic devices for cell based assays and organs on chip. Smart Biomed. Physiol. Sensor Technol., 9487 (2015)

[127] A. Blin, A. Le Goff, A. Magniez, S. Poirault-Chassac, B. Teste, G. Sicot, K.A. Nguyen, F.S. Hamdi, M. Reyssat, D. Baruch. Microfluidic model of the platelet-generating organ: beyond bone marrow biomimetics. Sci. Rep., 6 (2016)

[128] J. Zhang, H. Wu, H.F. Li, Q.S. Chen, J.M. Lin. An in vitro liver model on microfluidic device for analysis of capecitabine metabolite using mass spectrometer as detector. Biosens. Bioelectron., 68 (2015), pp. 322-328

[129] H.E. Abaci, R. Devendra, Q. Smith, S. Gerecht, G. Drazer. Design and development of microbioreactors for long-term cell culture in controlled oxygen microenvironments. Biomed. Microdevices, 14 (2012), pp. 145-152

[130] Y.H. Kato, K. Kamei, T. Tsuchiya, O. Tabata. Microfluidic device to interconnect multiple organs via fluidic circulation: towards body-on-a-chip. Transducers (2015), pp. 1549-1552

[131] K. Schimek, A. Markhoff, F. Sonntag, M. Blechert, R. Lauster, U. Marx, G. Lindner. Integrating skin and vasculature in a multi-organ-chip platform. BMC Proc., 9 (2015)

[132] V.N. Goral, S.H. Au, R.A. Faris, P.K. Yuen. Methods for advanced hepatocyte cell culture in microwells utilizing air bubbles. Lab Chip, 15 (2015), pp. 1032-1037

[133] G. Perozziello, J. Mollenbach, S. Laursen, E. Di Fabrizio, K. Gernaey, U. Kruhne. Lab on a chip automates in vitro cell culturing. Microelectron. Eng. (2012), pp. 655-658

[134] H. Tazawa, K. Sato, A. Tsutiya, M. Tokeshi, E.R. Ohtani-Kaneko. A microfluidic cell culture system for monitoring of sequential changes in endothelial cells after heat stress. Thromb. Res., 136 (2015), pp. 328-334

[135] S.M. Ju, H.J. Jang, K.B. Kim, J. Kim. High-throughput cytotoxicity testing system of acetaminophen using a microfluidic device (Mfd) in Hepg2 cells. J. Toxicol. Environ. Health, 78 (2015), pp. 1063-1072

[136] P.F. Song, W.Z. Zhang, A. Sobolevski, K. Bernard, S. Hekimi, X.Y. Liu. A microfluidic device for efficient chemical testing using Caenorhabditis elegans. Biomed. Microdevices, 17 (2015)

[137] Y.L. Chen, D. Gao, H.X. Liu, S. Lin, Y.Y. Jiang. Drug cytotoxicity and signaling pathway analysis with three-dimensional tumor spheroids in a microwell-based microfluidic chip for drug screening. Anal. Chim. Acta, 898 (2015), pp. 85-92

[138] A. Skardal, M. Devarasetty, S. Soker, A.R. Hall. In situ patterned micro 3D liver constructs for parallel toxicology testing in a fluidic device. Biofabrication, 7 (2015). 031001

[139] B. Hong, P. Xue, Y. Wu, J. Bao, Y.J. Chuah, Y. Kang. A concentration gradient generator on a paper-based microfluidic chip coupled with cell culture microarray for high-throughput drug screening. Biomed. Microdevices, 18 (2016)

[140] A. Mathur, P. Loskill, K.F. Shao, N. Huebsch, S. Hong, S.G. Marcus, N. Marks, M. Mandegar, B.R. Conklin, L.P. Lee, K.E. Healy. Human iPSC-based cardiac microphysiological system for drug screening applications. Sci. Rep., 5 (2015)

[141] J. Bai, T.Y. Yu, C. Kim, J.P. Thiery, R.D. Kamm. Identification of drugs as single agents or in combination to prevent carcinoma dissemination in a microfluidic 3D environment. Oncotarget, 6 (2015), pp. 36603-36614

[142] B. Patra, C.C. Peng, W.H. Liao, C.H. Lee, Y.C. Tung. Drug testing and flow cytometry analysis on a large number of uniform sized tumor spheroids using a microfluidic device. Sci. Rep., 6 (2016)

[143] E. Kondo, K.I. Wada, K. Hosokawa, M. Maeda. Cryopreservation of adhered mammalian cells on a microfluidic device: toward ready-to-use cell-based experimental platforms. Biotechnol. Bioeng., 113 (2016), pp. 237-240

[144] E. Berthier, D.J. Guckenberger, P. Cavnar, A. Huttenlocher, N.P. Keller, D.J. Beebe. Kit-on-a-lid-assays for accessible self-contained cell assays. Lab Chip, 13 (2013), pp. 424-431

[145] Carrel A 1912 Pure cultures of cells *J. Exp. Med.* **16** 165–8

[146] Huang P J, Lee P J, Sabounchi P, Lin R and Lee L P 2004 Continuous perfusion microfluidic cell culture array for high-throughput cell-based assays *Biotechnol. Bioeng.* **89** 1–8

[150] Woodruff K and Maerkl S J 2016 A high-throughput microfluidic platform for mammalian cell transfection and culturing *Sci. Rep.* **6** 23937

[151] Mehling M and Tay S 2014 Microfluidic cell culture *Curr. Opin. Biotechnol.* **25** 95–102

[152] Beebe D J, Ingber D E and Toonder den J 2013 Organs on chip *Lab Chip* **13** 3447–8

[153] Barbulovic-Nad I, Au S H and Wheeler A R 2010 A microfluidic platform for complete mammalian cell culture *Lab Chip* **10** 1536–42

[154] Jeon N L *et al* 2000 Generation of solution and surface gradients using microfluidic systems *Langmuir***16** 8311–6

[155] Toh A G G, Wang Z P, Yang C and Nguyen N T 2014 Engineering microfluidic concentration gradient generators for biological applications *Microfluid. Nanofluid.* **16** 1–18

[156] Beta C and Bodenschatz E 2011 Microfluidic tools for quantitative studies of eukaryotic chemotaxis *Eur. J. Cell Biol.* **90** 811–6

[157] Berthier, E., Surfus, J., Verbsky, J., Huttenlocher, A., & Beebe, D. (2010). An arrayed high-content chemotaxis assay for patient diagnosis. Integrative Biology, 2(11-12), 630-638.

[158] Self, W. H. et al. Balanced Crystalloids versus Saline in Noncritically Ill Adults. Lancet. 378, 819-828, DOI: https://doi.org/10.1056/NEJMoa1711586 (2018).

[159] Bihari, S., Ou, J., Holt, A.W. & Bersten, A.D. Inadvertent sodium loading in critically ill patients. Crit Care Resusc. 14, 33-37, (2012).

[160] Brown, R.M., Stollings, J.L. & Semler, M.W. Making the medicine go down: Salt or sugar? Crit Care Medicine. 46, 1370–1371, DOI: https://doi.org/10.1097/CCM.0000000000003229 (2018).

[161] Magee C. A. et al. Insidious harm of medication diluents as a contributor to cumulative volume and hyperchloremia: A perspective, open-label, sequential period pilot study. Crit Care Med. 46, 1217-1223, DOI: https://doi.org/10.1097/CCM.0000000000003191 (2018).

[162] Semler, M. W. et al. Insidious harm of medication diluents as a contributor to cumulative volume and hyperchloremia: A perspective, open-label, sequential period pilot study. N Engl J Med. 378, 829-839, DOI: https://doi.org/10.1056/NEJMoa1711584 (2018).

[163] Shields, C.J et al. Hypertonic saline impedes tumor cell-endothelial cell interaction by reducing adhesion molecule and laminin expression. Surgery. 136, 76-83, DOI: https://doi.org/10.1016/j.surg.2003.11.011 (2004).

[164] Sato, Y. et al. Effect of Plasma-Activated Lactated Ringer's Solution on Pancreatic Cancer Cells In Vitro and In Vivo. Ann Surg Oncol. 25, 299-307, DOI: https://doi.org/10.1245/s10434-017-6239-y (2018).

[165] Chen, S.L. et al. Hypertonic saline protects brain endothelial cells against hypoxia correlated to the levels of estimated glomerular filtration rate and interleukin-1β. Medicine. 96, e5786, DOI: https://doi.org/10.1097/MD.0000000000005786 (2017).

[166] Stubblefield, E. & Mueller, G.C. Effects of Sodium Chloride Concentration on Growth, Biochemical Composition, and Metabolism of HeLa Cells. Cancer Research. 20, 1646-1655, (1960).

[167] Yurinskaya, V.E et al. Dual Response of Human Leukemia U937 Cells to Hypertonic Shrinkage: Initial Regulatory Volume Increase (RVI) and Delayed Apoptotic Volume Decrease (AVD). Cell Physiol Biochem. 20, 964-973, DOI: https://doi.org/10.1159/000341473 (2012).

[168] Tchounwou, C. K., Yedjou, C. G., Farah, I., & Tchounwou, P. B. D-Glucose-Induced Cytotoxic, Genotoxic, and Apoptotic Effects on Human Breast Adenocarcinoma (MCF-7) Cells. Journal of cancer science & therapy, 6, 156-160. DOI: https://doi.org/10.4172/1948-5956.1000265 (2014).

[169] Fleisher, T. A., & Oliveira, J. B. (2019). Flow Cytometry. In *Clinical Immunology: Principles and Practice* (5th ed., pp. 1239-1251). Elsevier.

[170] Samsel, L., Dagur, P. K., Raghavachari, N., Seamon, C., Kato, G. J., & Mccoy, J. P. (2013). Imaging flow cytometry for morphologic and phenotypic characterization of rare circulating endothelial cells. *Cytometry Part B: Clinical Cytometry, 84*(6), 379-389. doi:10.1002/cyto.b.21088

[171] Brown, R.M., Stollings, J.L. & Semler, M.W. Making the medicine go down: Salt or sugar? Crit Care Medicine. 46, 1370–1371, DOI: https://doi.org/10.1097/CCM.0000000000003229 (2018).

[172] Zhao, Y., Wieman, H.L., Jacobs, S.R. & Rathmell, J.C. Two Mechanisms and Methods in Glucose Metabolism and Cell Death, Programmed Cell Death, General Principles For Studying Cell Death, Part A. Methods in Enzymology. 442, 439-457, DOI: https://doi.org/10.1016/S0076-6879(08)01422-5 (2008).

[173] Self, W. H. et al. Balanced Crystalloids versus Saline in Noncritically Ill Adults. Lancet. 378, 819-828, DOI: https://doi.org/10.1056/NEJMoa1711586 (2018).

[174] Frazee, E.N., Leedahl, D.D. & Kashani, K.B. Key Controversies in Colloid and Crystalloid Fluid Utilization. Hospital Pharmacy. 50, 446-453, DOI: https://doi.org/10.1310/hpj5006-446 (2015).

[175] Bonuccelli, G. et al. Ketones and lactate "fuel" tumor growth and metastasis. Cell Cycle. 9, 3506-3514, DOI: https://doi.org/10.4161/cc.9.17.12731 (2010).

[176] Guidet, B. et al. A balanced view of balanced solutions. Critical Care. 14, 325, DOI: https://doi.org/10.1186/cc9230 (2010).

[177] Magee C. A. et al. Insidious harm of medication diluents as a contributor to cumulative volume and hyperchloremia: A perspective, open-label, sequential period pilot study. Crit Care Med. 46, 1217-1223, DOI: https://doi.org/10.1097/CCM.0000000000003191 (2018).

[178] Kadota, K. et al. Comprehensive pathological analyses in lung squamous cell carcinoma: single cell invasion, nuclear diameter, and tumor budding are independent prognostic factors for worse outcomes. J. Thorac Oncol. 9, 1126-1139, DOI: https://doi.org/10.1097/JTO.0000000000000253 (2004).

[179] Shields, C.J et al. Hypertonic saline impedes tumor cell-endothelial cell interaction by reducing adhesion molecule and laminin expression. Surgery. 136, 76-83, DOI: https://doi.org/10.1016/j.surg.2003.11.011 (2004).

[180] Seyfried, T.N. & Huysentruyt, L.C. Tumor expressing macrophage characteristics. On the origin of cancer matestasis. Crit Rev Oncog. 18, 43-73, DOI: https://doi.org/10.1615/CritRevOncog.v18.i1-2.40 (2013).

[181] Pincus, Z. & Theriot J.A. Comparison of quantitative methods for cell-shape analysis. Journal of Microscop. 227, 140-156, DOI: https://doi.org/10.1111/j.1365-2818.2007.01799.x (2007).